4.2.8. Azimuthal direction determination.

In section **(4.2.4)** it was shown that the azimuthal direction **(θ)** of an earthquake, which generates an electrical field, in respect to the location of the monitoring site, is given from the equation:

$$(\theta) = \arctan(V_{NS}/V_{EW}) \qquad (4.2.8.1)$$

where: V_{NS} and V_{EW} are the normalized to the trigonometric circle values of the **NS** and **EW** components of the registered, electric field.

It is evident that the V_{NS} and V_{EW} values must represent solely the "anomalous" electric field. Consequently, a stage of detrending operation of the normalized, registered signal must precede the application of the equation **(4.2.8.1).**

The entire procedure is presented in the following figures. In figure **(4.2.8.1)** a sample of a short period, of a few minutes, signal, is presented at its **EW** and **NS** components.

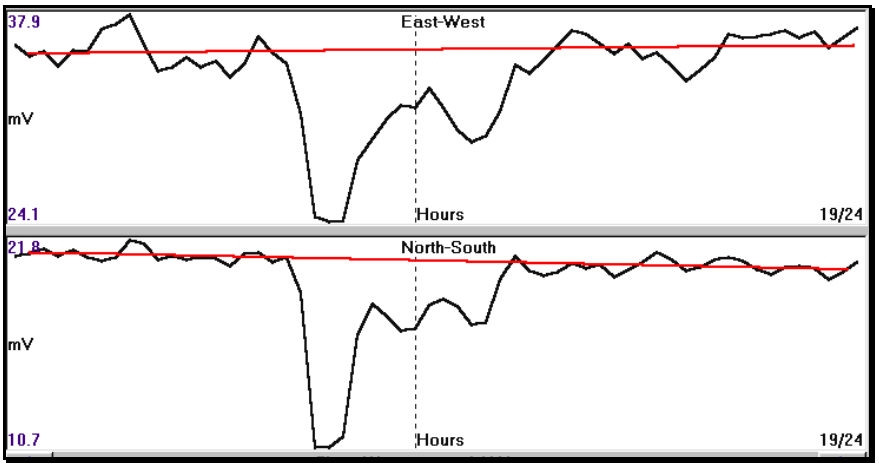

Fig. 4.2.8.1. Raw data (solid black line) and assumed trend (solid red line). Time span of the recording is 58 minutes, while the signal spans for about 16 minutes. **HIO** monitoring site, date of recording 15th April 2007, time span from 17.32 to 18.30.

The **EW** component of the signal is superimposed on a DC level of almost 35 mV, while the **NS** component is superimposed on a DC level of about 20mV. Obviously, any attempt to calculate azimuthal direction, based on these signals would end into erroneous results. In the following figure **(4.2.8.2)** the detrended components are presented after having subtracted the corresponding trend from the original normalized values.

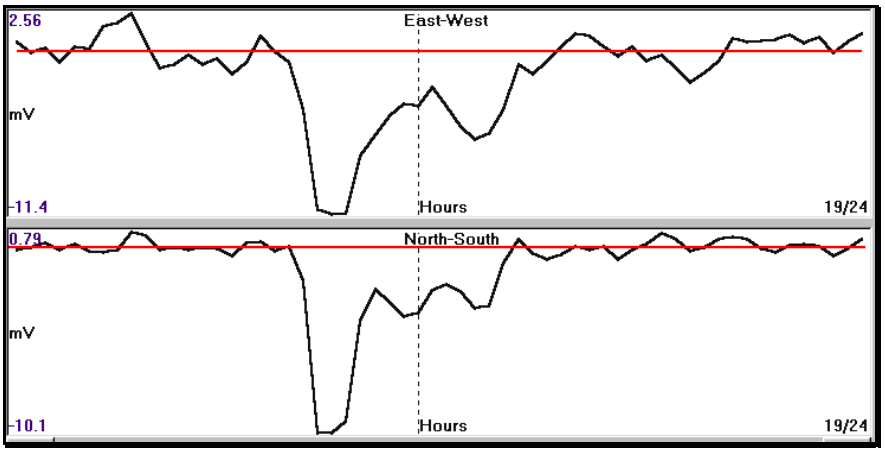

Fig. 4.2.8.2. "Clean" electrical signal, obtained after detrending, to be used for azimuthal determination. The red solid line indicates the "zero reference" level of the electrical signal.

The next step is to assign a certain time and to apply equation (**4.2.8.1)** on the corresponding **EW** and **NS** values of the detrended signal. This operation is presented in the following figure **(4.2.8.3).**

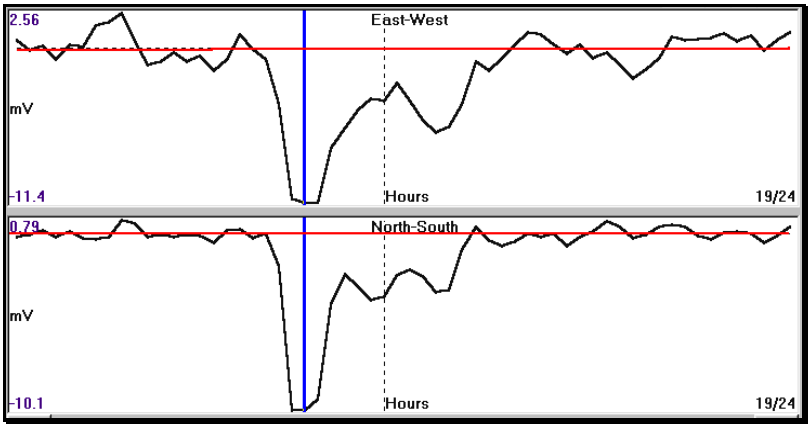

Fig. 4.2.8.3. The values of the **EW** and **NS** components, which correspond to time **(17.53)** and are indicated, by the solid blue line, are used in equation **(4.2.8.1)** to calculate the anomalous intensity vector of the Earth's electric field.

The calculated value of **θ** is:

$$\theta = 3.89 \text{ rad} \qquad (4.2.8.2)$$

counter clockwise from east towards north. Although this "counting" methodology is not used in any geological procedure, it, largely, facilitates the related, trigonometric calculations and the presentations of the azimuthal direction.

In the following figure **(4.2.8.4),** the result, presented by **(4.2.8.2)** along with the location of **HIO** monitoring site, is superimposed on the map of Greece**.**

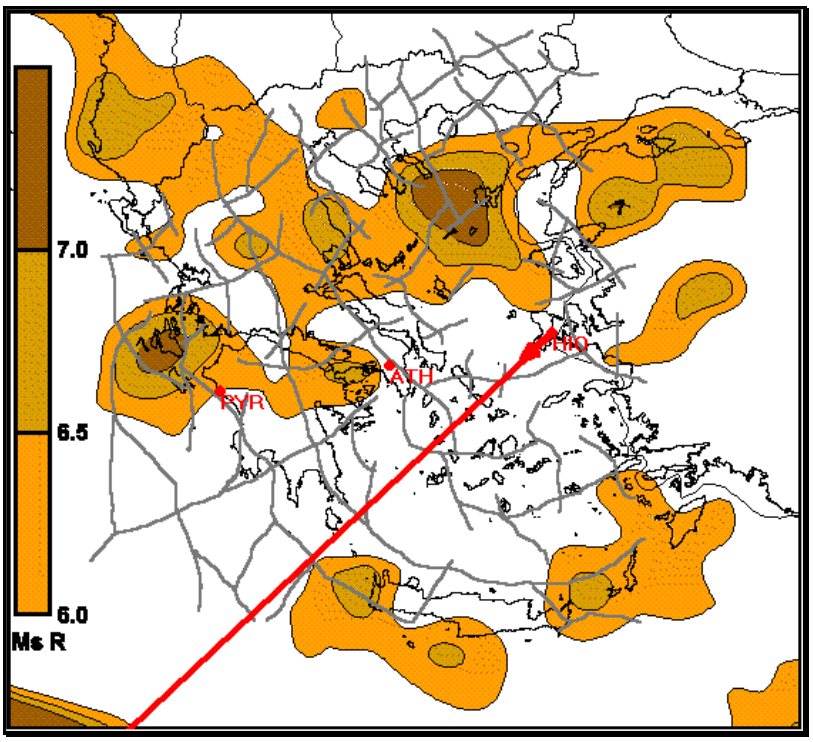

Fig. 4.2.8.4. Azimuthal direction (red line and arrow) calculated for the maximum amplitude time of the electrical signal indicated in figure **(4.2.8.3)**.

The colored map of Greece will be described in detail in the section of magnitude determination, while the gray thick lines indicate the location of the major fracturing of the lithosphere.

Although the selection of the maximum amplitude of the signal has a merit in the azimuthal calculation, it is worth to obtain an average value of it along its time span.

Consequently, the equation **(4.2.8.1)** is applied allover the time span (at each data point in turn) of the corresponding electrical field recording, presented, in figure **(4.2.8.3).** The obtained results are presented on a trigonometric circle. The center of this circle represents the location of **HIO** monitoring site. The latter is illustrated in the following figure **(4.2.8.5).**

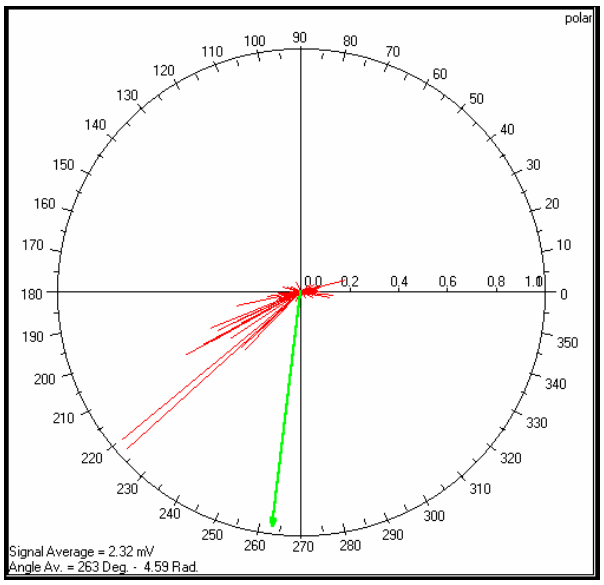

Fig. 4.2.8.5. Azimuthal direction of the intensity vector of the Earth's anomalous field, calculated, for all data points along the previous registration. The red lines indicate the individual, calculated directions, while the green arrow indicates their average value. The center of the circle represents the location of **HIO** monitoring site.

What is observed, at the first glance, is that the average value of the calculated, azimuthal direction **(4.59 rad)**, deviates, a lot, from the one, which has been calculated at the maximum of the signal (single value). This discrepancy is due to the random noise which is present in the recording and the fact that these noisy, data points have been taken into account in the calculation of the average value. This problem can be solved in two ways. The first one is to confine the recording length only to the anomalous signal extent itself. In other words the length of recording which is assumed to contain only noise is excluded from this operation. The second method is to use a threshold level for the signal amplitude, above which calculations of the azimuthal direction are allowed. These two operations are presented in the following figures.

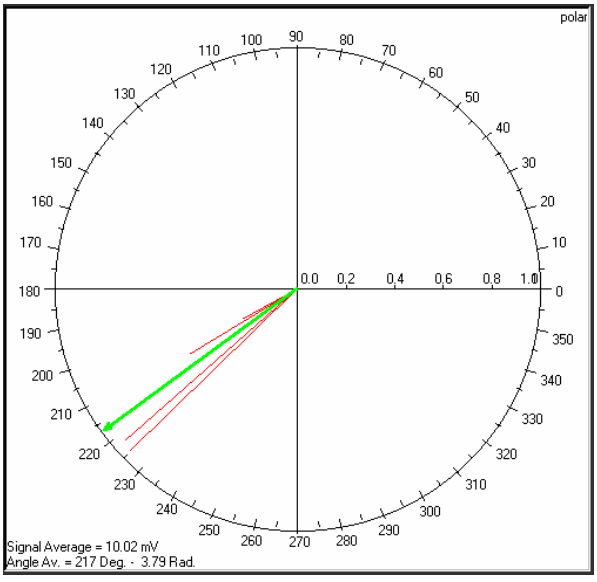

Fig. 4.2.8.6. Azimuthal average direction value **(θ = 3.79 rad)** for the **signal span only**, using a threshold level of 0.2 of the maximum signal amplitude.

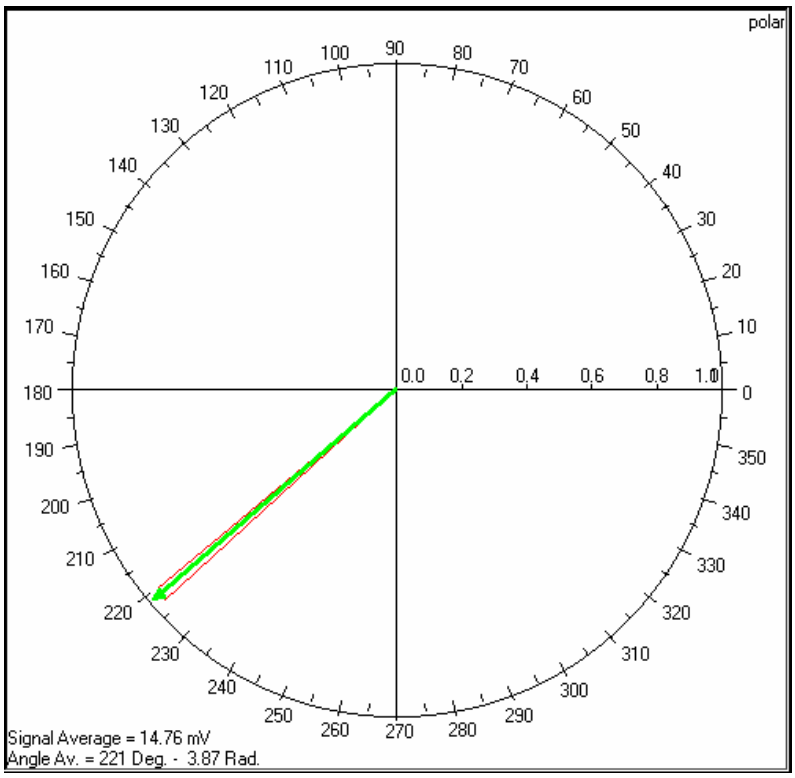

Fig. 4.2.8.7. Azimuthal average value **(θ = 3.87 rad)** calculation along the entire recording, using a threshold of 0.6 of its maximum magnitude amplitude.

The three azimuthal values which were calculated in the aforementioned cases are presented in the map of Greece, figure **(4.2.8.8),** in order to facilitate their comparison.

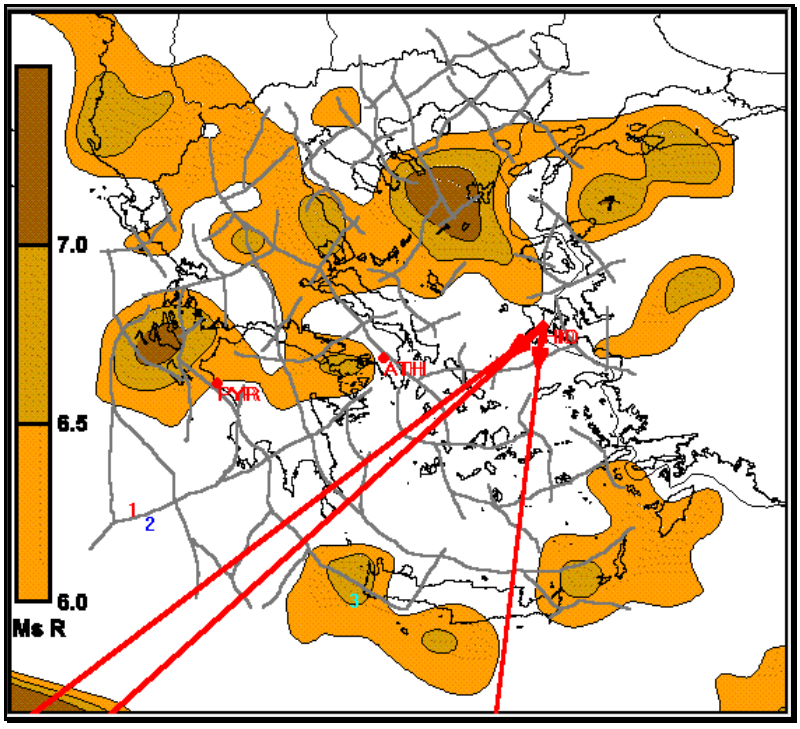

Fig. 4.2.8.8. The obtained, three azimuthal values are, simultaneously, presented.

In case the data have been used without any signal length (in time) constraint or signal amplitude threshold level, this leads to false results. On the contrary, the calculated azimuthal values are almost identical, for the two constrained cases.

The same procedure has been applied on an anomalous signal that lasts for a longer period (almost two days). The original signal is presented in the following figure **(4.2.8.9)**. The red line indicates the assumed trend that must be subtracted before any operation is performed.

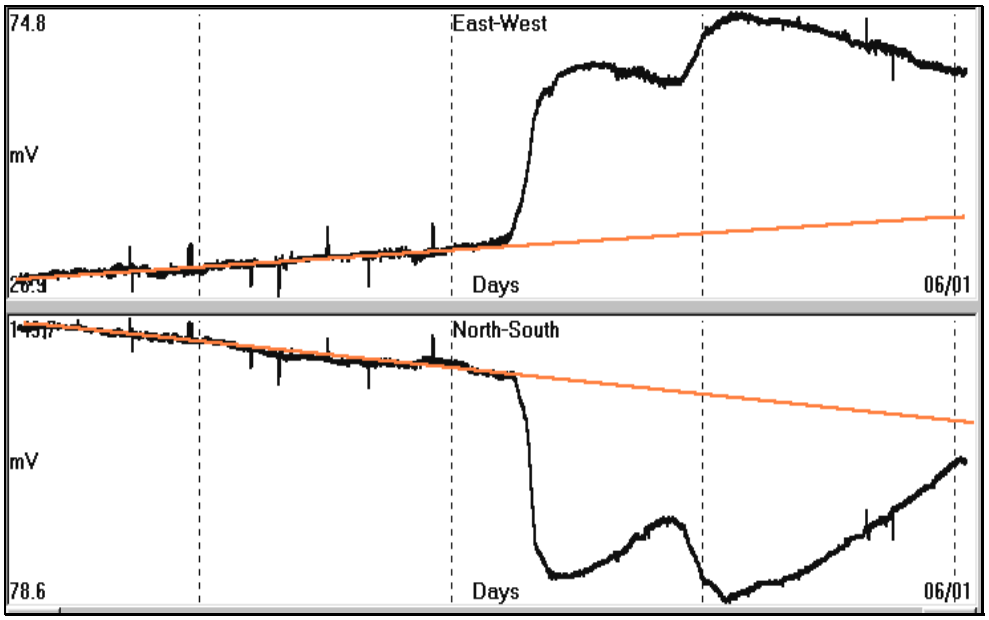

Fig. 4.2.8.9. Raw data (background level and anomalous electrical signal) registered, during the recording period of 200601020654 – 200601060103 (in yyymmddhhmm mode), by Pyrgos **(PYR)** monitoring site. The solid red line indicates the assumed linear trend to be subtracted.

After subtraction of the assumed trend the registration takes the form which is presented in the following figure **(4.2.8.10).**

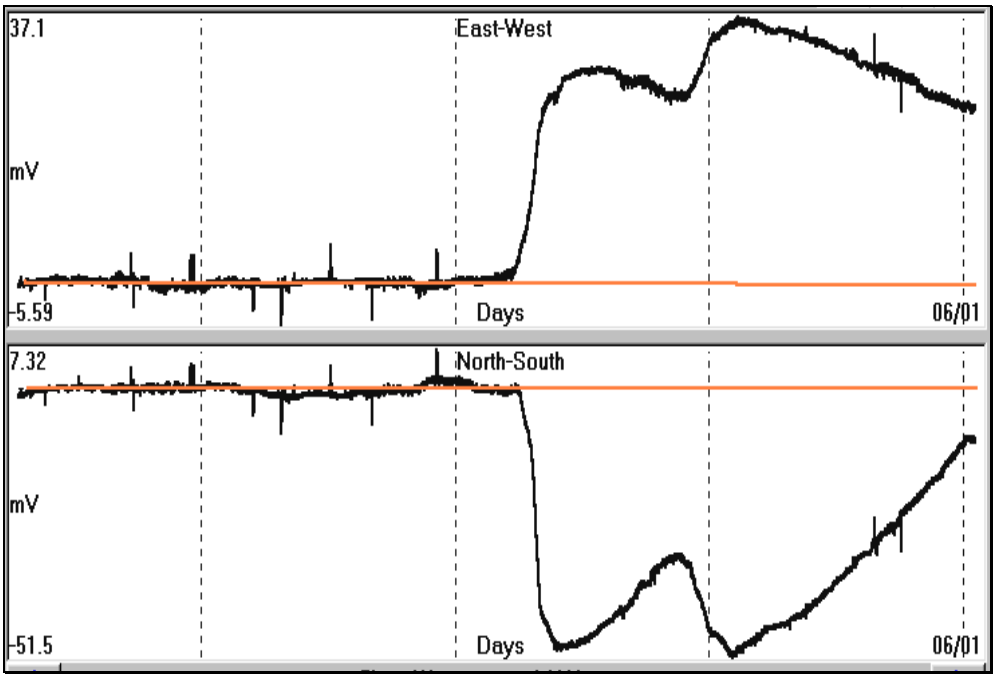

Fig. 4.2.8.10. Detrended, electric potential that resulted from the previous registration, after having subtracted the assumed trend (red line)

At first, the azimuthal, polar diagram is constructed for the entire data set, without applying any constraint. This is shown in the following figure **(4.2.8.11).**

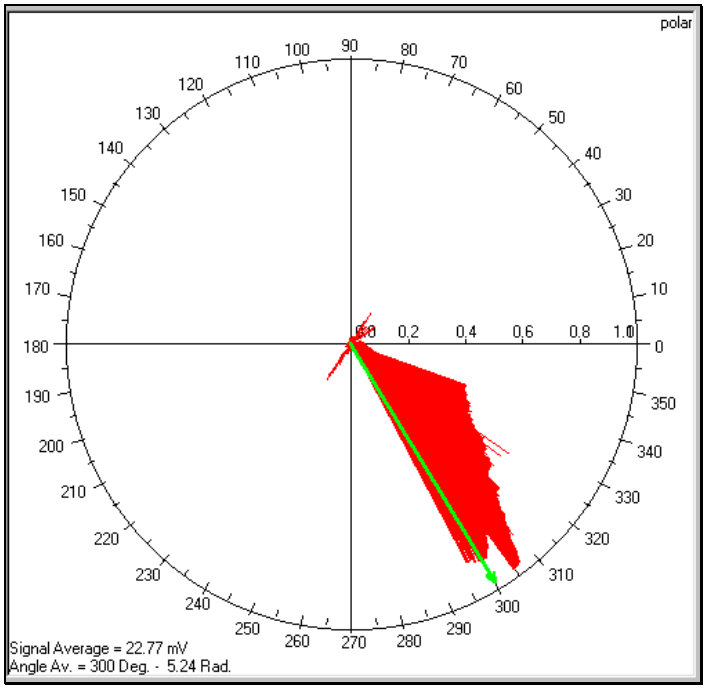

Fig. 4.2.8.11. Polar diagram which indicates the calculated azimuthal direction (red lines) from the entire data set. The green arrow represents the average value of the calculated azimuths. No threshold level was used in this presentation.

The spurious directions, shown with small red lines, almost normal to the average direction, are due to the noise which is present in the non-signal part of the recording. In the next figure **(4.2.8.12)** a threshold level of **0.2** was used and therefore the average value which is indicated by the green arrow is representative of the signal itself.

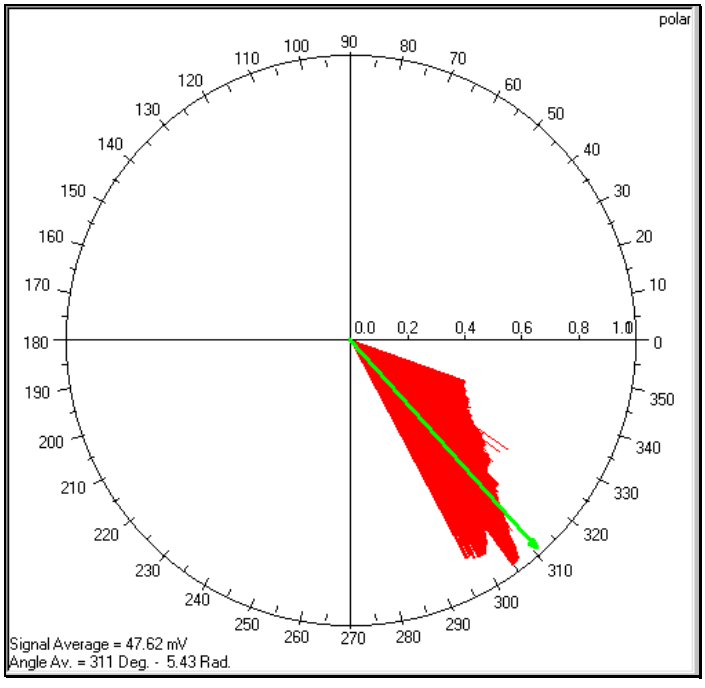

Fig. 4.2.8.12. Azimuthal direction, calculated, for all the data set, by using a threshold level of **0.2**

Both directions which are calculated and presented in the previous figures are superimposed on the map of Greece. This is demonstrated in the following figure **(4.2.8.13).**

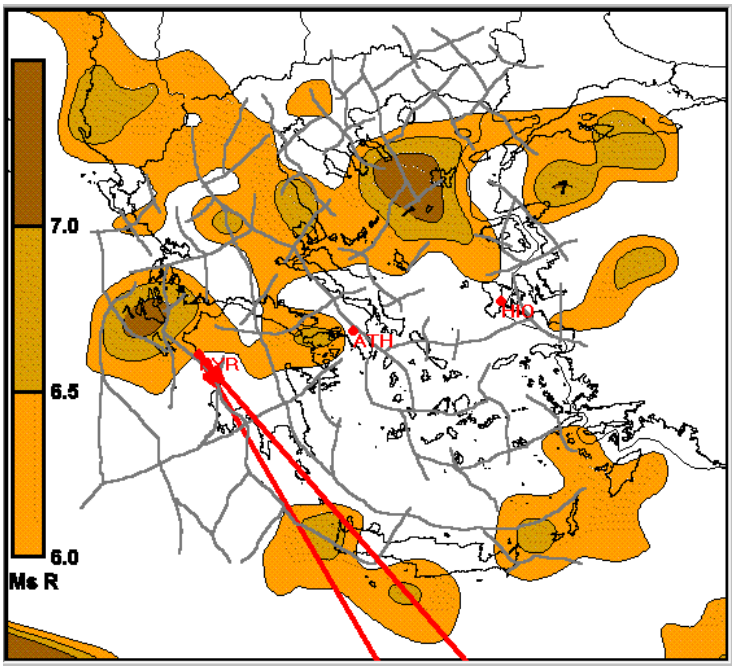

Fig. 4.2.8.13. Map of Greece, superimposed, by the average azimuthal vectors which were presented in figures **(4.2.8.11)** and **(4.2.8.12).**

The case of an oscillating monochromatic signal **(T = 24 hours)** is treated in a very similar way. Since the two (**NS** and **EW**) components of the signal oscillate, the same happens with its azimuthal direction and scalar value too. Consequently, if different times are selected for the, specific, azimuthal direction calculation, it will end up with completely different azimuthal directions. The latter is demonstrated in the following figures **(4.2.8.14, 4.2.8.15, 4.2.8.16, 4.2.8.17).**

In figure **(4.2.8.14)** are presented the oscillating monochromatic **EW** and **NS** components of the Earth's electric field. This recording was obtained during 20070412 – 20070415 period of time by Athens **(ATH)** monitoring site. In practice, this recording is obtained after having filtered the corresponding raw data by a "band-pass" filter **(FFT)** with a bandwidth of 24 hours. The idea, behind this kind of frequency selection, is to make an attempt to identify signals that have their origin in the corresponding, same frequency (diurnal) of the lithospheric oscillation.

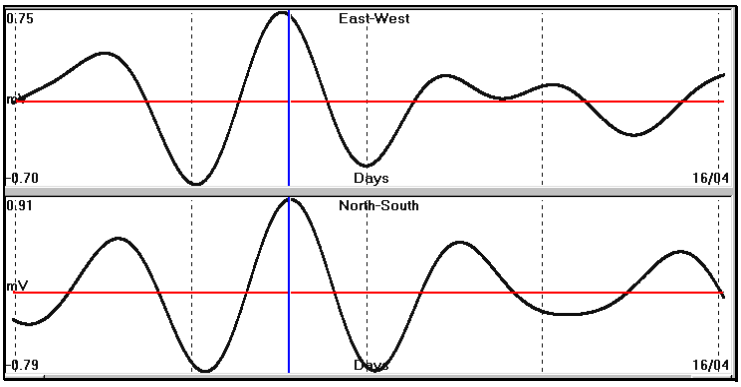

Fig. 4.2.8.14. The oscillating monochromatic **EW** and **NS** components of the Earth's electric field are presented. Red line indicates the zero reference level of the electric field, while the blue vertical line indicates the time when the azimuthal calculation will be performed.

As time, for the azimuthal calculation, was selected the one, when the signal amplitude is maximum. The resulted, azimuthal direction is presented in the following figure **(4.2.8.15).**

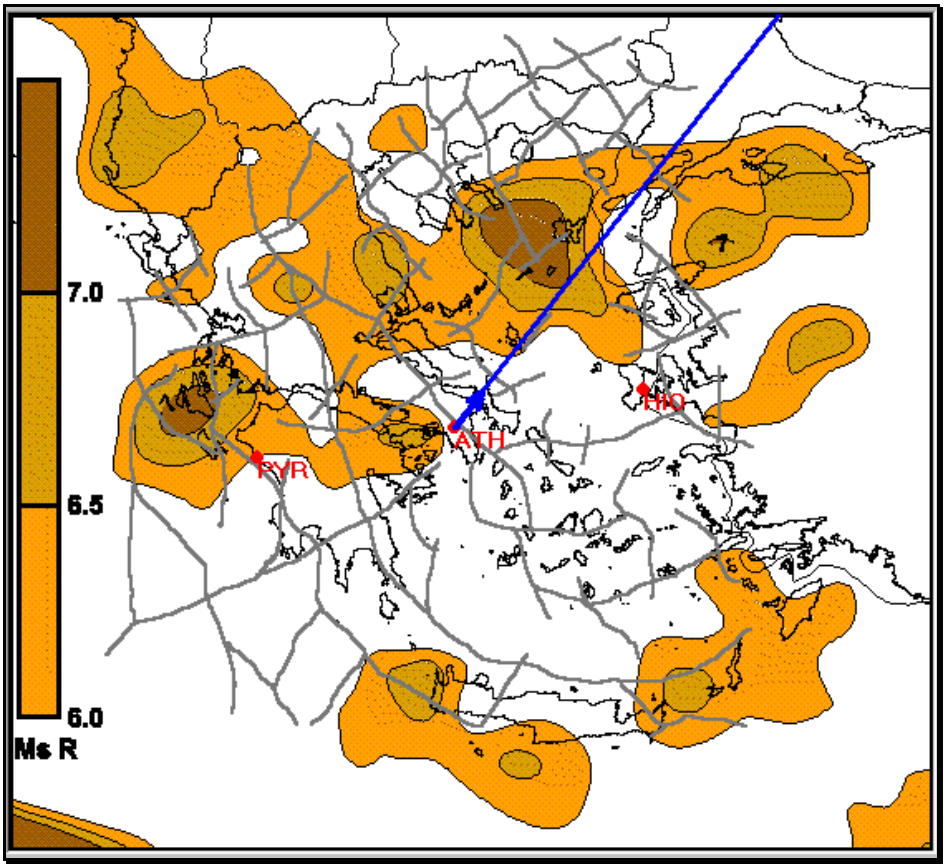

Fig. 4.2.8.15. Azimuthal direction (θ = 0.91 rad, blue line), calculated, from the electrical field which is presented in figure **(4.2.8.14),** in relation to the location of the **ATH** monitoring site.

The dependence of the calculated, azimuthal direction on the selected time is presented by the following two figures **(4.2.8.16)** and **(4.2.8.17).** In this case a negative peak of the oscillating field was chosen for the utilization of the azimuthal direction.

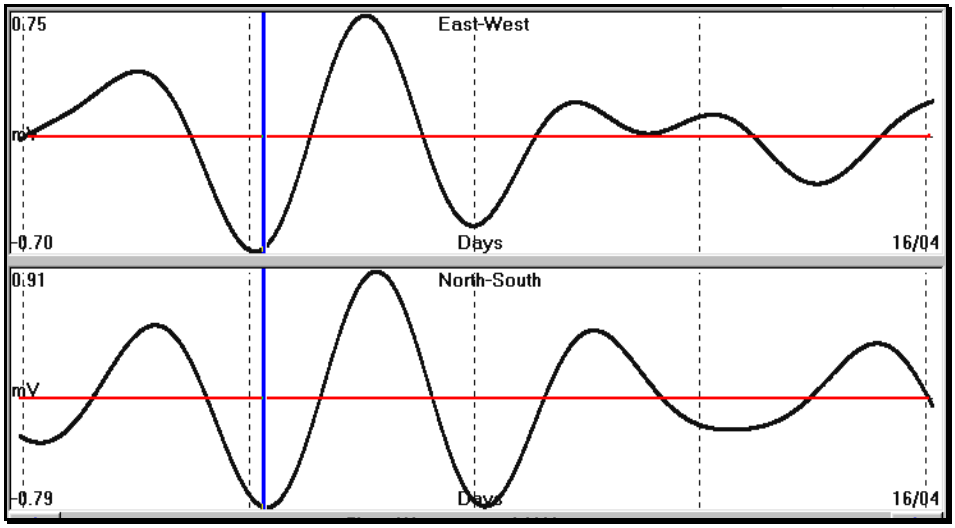

Fig. 4.2.8.16. Oscillating monochromatic EW and NS components of the Earth's electric field are presented. The red line indicates the zero reference level of the electric field, while the blue vertical line indicates the time when the azimuthal calculation will be performed.

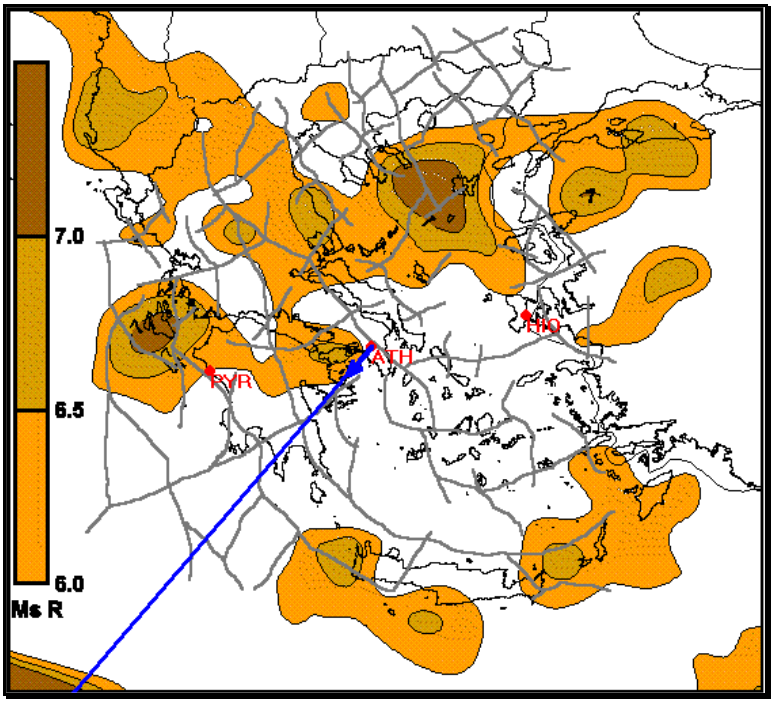

Fig. 4.2.8.17. Azimuthal direction (θ = 3.99 rad, blue line), calculated from the electrical field which is presented in figure **(4.2.7.23)** in relation to the location of the **ATH** monitoring site.

The fact that the azimuthal direction, in the case of an oscillating electric field, is a function of time, dictates the necessity to study it, as such, for the entire length of the presented recording. Moreover, the calculated, azimuthal direction time function could be correlated to the seismicity that occurred in the same time period. In this way, a preliminary test is made, regarding the correlation of the oscillating, electrical field to the synchronous, in time, seismicity of Greek territory.

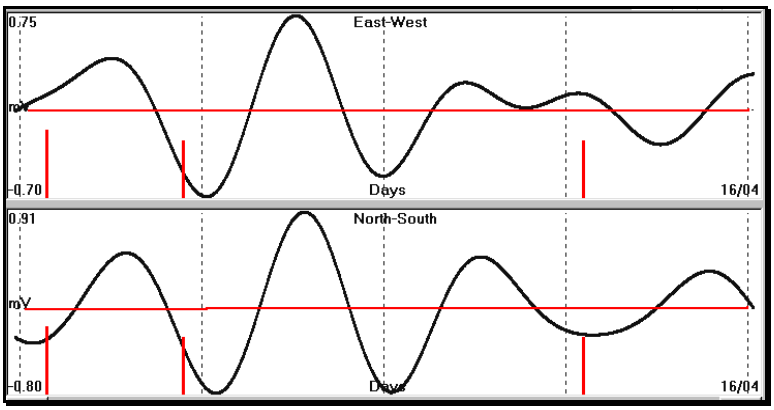

Fig. 4.2.8.18. Oscillating monochromatic **EW** and **NS** components, of the Earth's electric field, are presented. The red lines indicate the time of occurrence of earthquakes with a minimum threshold level of 4.5 R.

The azimuthal direction was calculated for each minute (data sampling rate) along the time span and was presented in the trigonometric circle. This is illustrated in the following figure **(4.2.8.19).** The center of the circle coincides with the location of **ATH** monitoring site. The green lines indicate the observed, maximum, scalar values of the Earth's electrical field intensity vector. Different colors facilitate to indicate different, local, maxims scalar values of the intensity

vector, in time. It is assumed that these values are due to the increase of the electric field, which resulted by the stress-load of a seismic focal area.

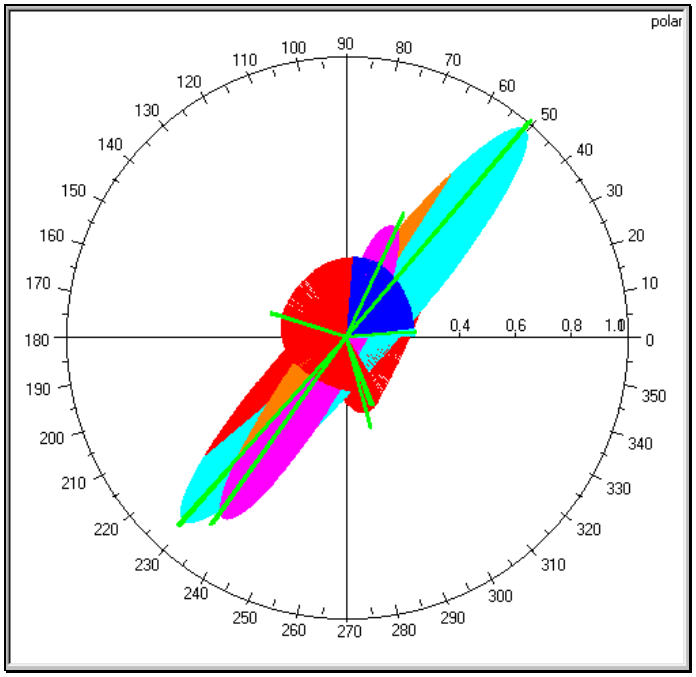

Fig. 4.2.8.19. Azimuthal direction and scalar amplitude of the electric signal as a function of time is presented. The green lines indicate the observed, maximum scalar values of the Earth's electrical field intensity vector. Different colors facilitate to indicate different, local maxims in time scalar values of the intensity vector.

The calculated azimuthal directions are compared with the seismicity (M => 4.5R) of Greece in the same period. This is presented in the following figure **(4.2.8.20).**

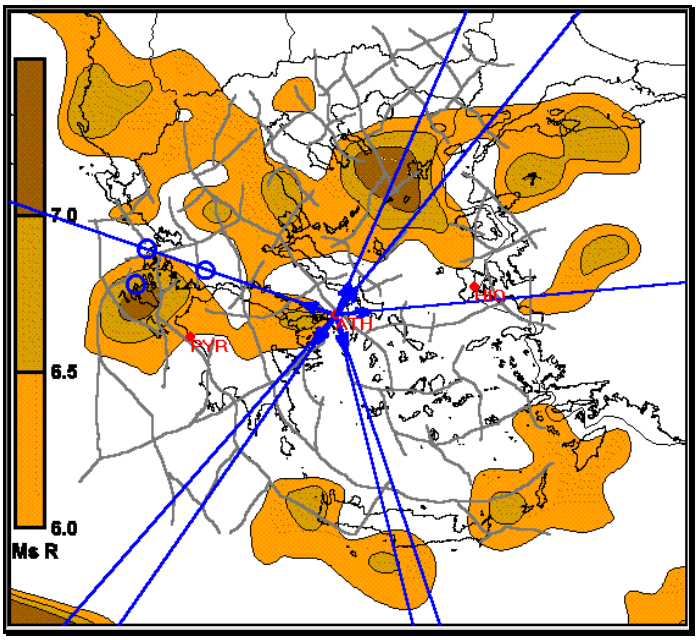

Fig. 4.2.8.20. Azimuthal directions (blue lines) of maxims of the calculated, electrical field intensity vector superimposed, on the map of Greece. The earthquakes (threshold minimum magnitude M = 4.5R) that occurred in this time period are represented in blue circles.

It is quite interesting the fact that, the three earthquakes, which occurred during this time period, coincide quite well with the direction which is indicated in figure **(4.2.8.20)**. The other groups of directions, present in the same figure, will be explained in section **(4.2.9)** to follow.

4.2.9. Multidirectional, oscillating, electrical field analysis.

During the overall seismic activation of a larger, seismic, prone area, it is understood that smaller areas may be activated in different periods of time. These small areas generate electrical signals which interfere with each other. Consequently, the registration of the Earth's electrical field corresponds to the total field which results from this interference.

The important fact is that, each time a focal area generates a strong signal. This signal prevails on all others and consist the main component of the electrical field to be analyzed. Therefore, its characteristic parameters will be mainly described in the analysis of the total electrical field.

4.2.9.1. The theoretical model.

Let us recall the equation:

$$\theta = \arctan(V_{NS}/V_{EW}) \qquad (4.2.9.1.1)$$

Equation **(4.2.9.1.1)** will be studied, in particular, for the case of an oscillating electrical field. In the case of an oscillating current source the current takes the form of:

$$I = I_0 \sin(kt) \qquad (4.2.9.1.2)$$

and therefore the equation that expresses the potential **V, ($V = I_0 R / 4\pi r$),** due to a current source **(I_0),** at a distance **(r),** in a medium of resistivity **(R),** is transformed into:

$$V = I_0 \sin(kt)\, r^{-1}\, R / (4*pi) \qquad (4.2.9.1.3)$$

From equation **(4.2.9.1.3)** it is easily obtained that V_{EW} and V_{NS} take the form of:

$$V_{EW} = V_1 \sin(kt) \text{ and } V_{NS} = V_2 \sin(kt) \qquad (4.2.9.1.4)$$

where V_1 and V_2 are:

$$V_1 = I_0 \sin(kt)\cos(\theta)\, r^{-1}\, R / (4\pi) \qquad (4.2.9.1.5)$$

$$V_2 = I_0 \sin(kt)\sin(\theta)\, r^{-1}\, R / (4*\pi) \qquad (4.2.9.1.6)$$

From equations **(4.2.9.1.4)**, **(4.2.9.1.5)**, **(4.2.9.1.6)** results that:

$$\text{Angle } (\theta) = \arctan(V_2 / V_1) \qquad (4.2.9.1.7)$$

it is the same equation which is valid for the non-oscillating field. The scalar value **(V_t)** of the electrical field intensity vector at time **(t)** takes the form of:

$$V_t = \sin(kt)(V^2_1 + V^2_2)^{1/2} \qquad \textbf{(4.2.9.1.8)}$$

Thus, indicating that the intensity vector of the electric field oscillates along an axis **(fig. 4.2.9.1.1)** that forms an angle **(θ)** to the **EW** direction, calculated by the equation **(4.2.9.1.7).**

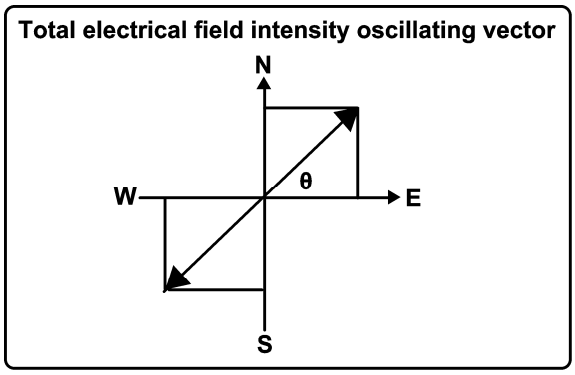

Fig. 4.2.9.1.1. V_t oscillates at an angle **(θ)** along the double black arrow.

Generally, when an external, oscillating, electrical field interferes with the initial one, the equation **(4.2.9.1.2)** takes the form of:

$$I = I_0 \sin(k_0)\sin[(k+k_1)t] \qquad \textbf{(4.2.9.1.9)}$$

Where: **(K_0)**, **(k)** and **(k_1)** are different angular velocities. As a result, angle **(θ)** is not anymore constant but becomes a function **(F)** of **(k_0, k, k_1),** as well as **(V_t)** is, too.

$$(\theta) = F(k_0, k, k_1) \text{ and } V_t = f(k_0, k, k_1). \qquad \textbf{(4.2.9.1.10)}$$

In this case **(V_t)** does not oscillate along a line but it generally prescribes an ellipse **(fig. 4.2.9.1.2).**

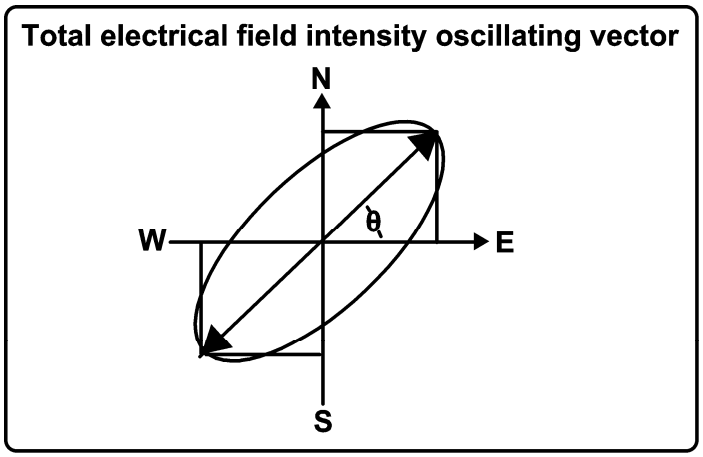

Fig. 4.2.9.1.2. V_t oscillates and prescribes an ellipse.

The following cases are representative examples of the latter analysis.

4.2.9.2 Electrical field orthogonal components which were generated by different current sources.

In this case, the calculated angle **(θ)** varies in random since there is no correlation between the observed two components. The recorded, two signals (Mares, 1984) are shown in figure **(4.2.9.2.1)**. The corresponding, calculated electrical field intensity vectors are presented in figure **(4.2.9.2.2)**.

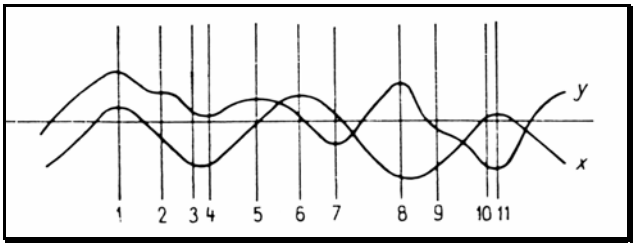

Fig.4.2.9.2.1. Uncorrelated, orthogonal, electrical field components (after Mares, 1984).

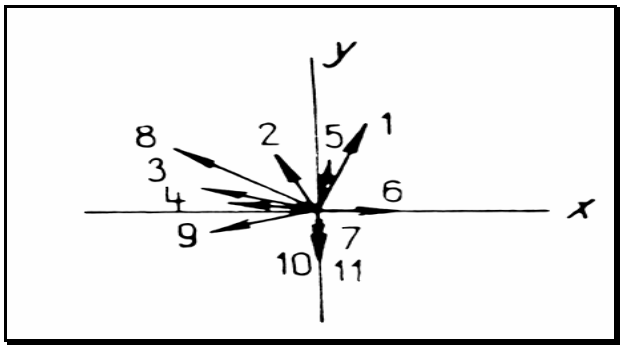

Fig.4.2.9.2.2. Vectorgram azimuthal values calculated for the observed, uncorrelated, electrical, orthogonal components (after Mares, 1984).

4.2.9.3. Electrical field, orthogonal components, which were generated by the same current source.

In this case, the previous mathematical analysis is valid and can be applied on the obtained data. The two orthogonal components (Telford et al. 1976) are shown in figure **(4.2.9.3.1)**, while the corresponding polarization ellipse is presented in figure **(4.2.9.3.2)**.

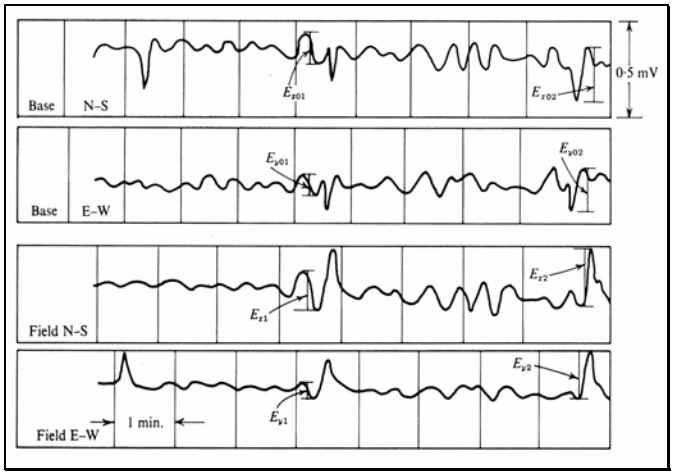

Fig. 4.2.9.3.1. Orthogonal components of the electrical field observed, that corresponds to a single, current source (after Telford et al. 1976).

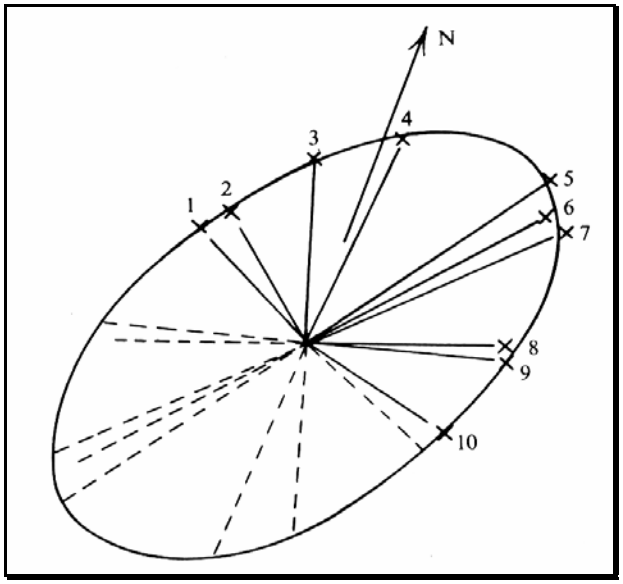

Fig. 4.2.9.3.2. Azimuthal values calculated, for the observed, correlated, electrical, orthogonal components (after Telford et al. 1976).

4.2.9.4 Electrical field orthogonal components which were generated by the same current source and correspond to a local electrical field anomaly.

The very same analysis was applied over data which correspond to a single anomaly of the electrical field, superimposed, over a larger, regional field (Patra and Mallick, 1980). The orthogonal components **(E_x)** and **(E_y),** are presented, in figure **(4.2.9.4.1).**

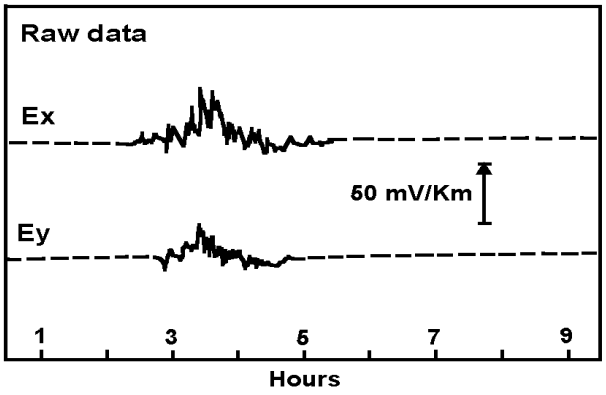

Fig. 4.2.9.4.1. Electrical field, orthogonal components (after Patra and Mallick, 1980) generated by the same, current source that corresponds to a local, electrical field anomaly.

It is obvious, as it appears from the data, that high frequency noise has interfered with the original data. Therefore, the corresponding ellipse was calculated, **(a)** for the original data as it is, **(b)** after having applied some "low-pass" and **(c)** "band-pass" filtering. This operation is shown in figure **(4.2.9.4.2)**.

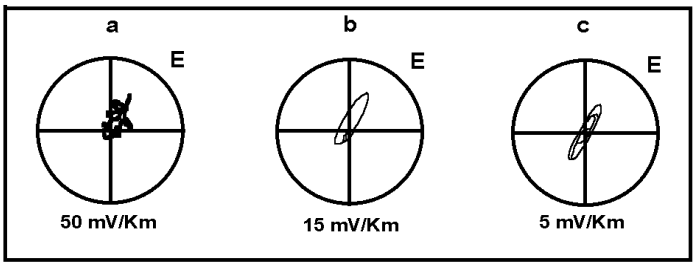

Fig. 4.2.9.4.2. Azimuthal values calculated, (after Patra and Mallick, 1980) for the observed, correlated, electrical, orthogonal components. Case (a) = raw data, (b) = 5^{th}-harmonic synthesis, (c) = band-pass filtered / T_0 = 10000 sec.

4.2.9.5 Electrical field orthogonal components which are generated by the interference of more than one current source.

Let us consider now the case of more than one current source, which affect the electrical field recorded by a monitoring site.

As an example, is studied the case of three current sources. In figure **(4.2.9.5.1)** is presented the location of three current sources **(EQ1, 2, 3)** in relation to the location of the monitoring site along with the expected, theoretical, equipotential lines.

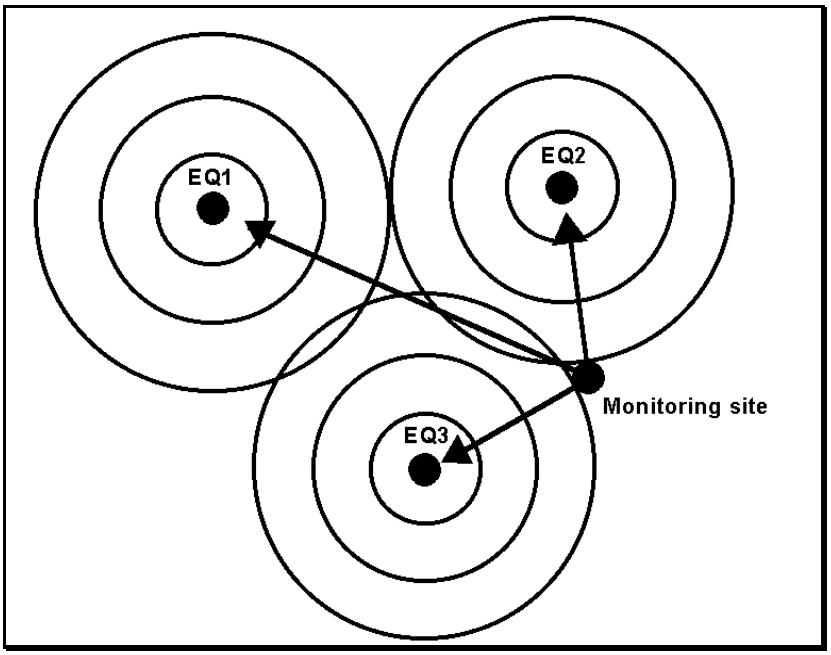

Fig. 4.2.9.5.1. Location of the **EQ1, 2, 3** current sources is presented, in respect to the location of the monitoring site.

An ellipse is generated **(fig. 4.2.9.5.2)** for each current source. Its major axis indicates the azimuthal direction of the Earth's oscillating, electric field, current source origin location, in relation to the location of the monitoring site.

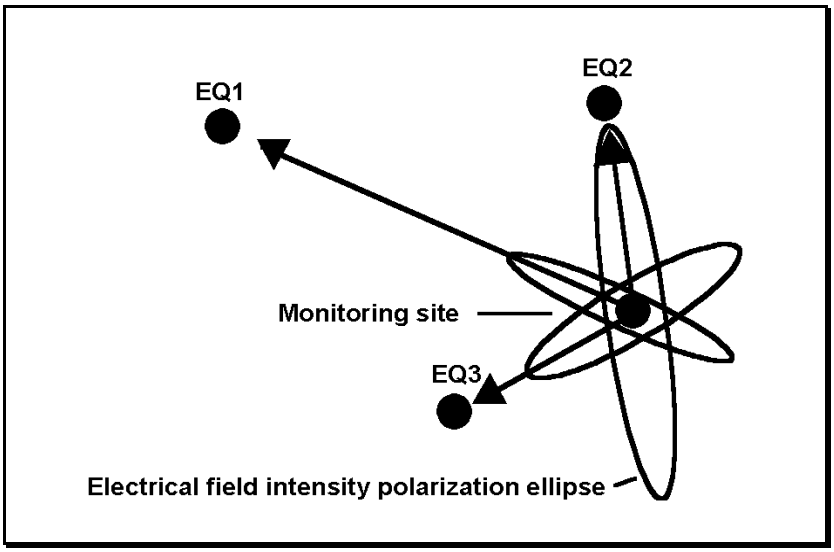

Fig. 4.2.9.5.2. Corresponding ellipses and electrical field intensity vector presentation for each current source **(EQ1, 2, 3)**.

If we take into account that the **EQ1, 2, 3** current sources do not evolve, in time, simultaneously, it is made clear that a sequential, in time, registration of the orthogonal components of the electric field, will result in a successive peaking, towards the corresponding direction of the **(V_t)** value, and each time, a discrete, current source prevails, to form the registered total electrical field.

The latter analysis was applied to the electrical signals which were observed during seismically active periods of time in the Greek territory. The epicentral (focal) areas which were activated seismically were considered as the current sources.

The working hypothesis is as follows:

If the seismically, activated, regional focal areas emit such electrical signals, then the continuous recording of the two orthogonal components of the oscillating electrical field, at a monitoring site, must reveal the preferential, azimuthal directions of the intensity vectors, in relation to the monitoring site location. This will coincide with the corresponding areas which have already been activated seismically.

4.2.9.6. Real data analysis.

The already presented analysis was applied on the data which were obtained by Volos **(VOL)** monitoring site (collaboration with Tsatsaragos, 2002). These data were analyzed with the same procedure by Thanassoulas and Klentos (2003). A brief presentation with actual examples follows. The two orthogonal components of the electric field were registered continuously, in a digital form, at a sampling interval of one minute.

The oscillating component of the electrical field is obtained by applying Fast Fourier Transform **(FFT)** and "band-pass" digital filtering to the recorded raw data. The center period of the band-pass filter is set at T = 24 hours.

A sample of raw data, as it is recorded, is shown in the following figure **(4.2.9.6.1)** while its filtered result is shown in figure **(4.2.9.6.2).**

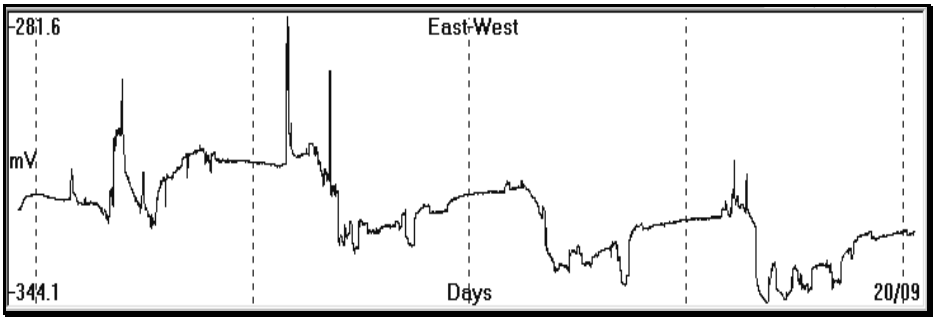

Fig. 4.2.9.6.1. A sample of raw data, as it is recorded.

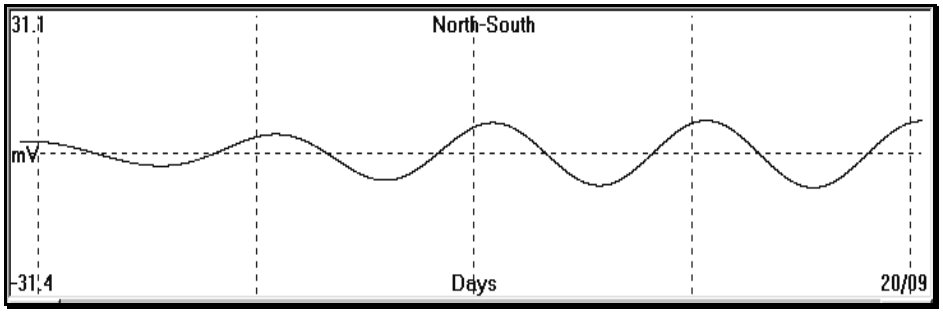

Fig. 4.2.9.6.2. Filtered data are presented, as a result of "band-pass" filtering operation.

4.2.9.6.a Determination of the azimuthal direction of a specific period of time, electrical field recording vs. concurrent seismicity.

A real application of the methodology is presented as follows:

- Time span – recorded orthogonal components.

The data which are used in this example extend from 18/06/2002 to 21/06/2002. A total recording of 4 days, whose oscillating component, of the electrical field registered, is presented in fig. **(4.2.9.6.a.1)**.

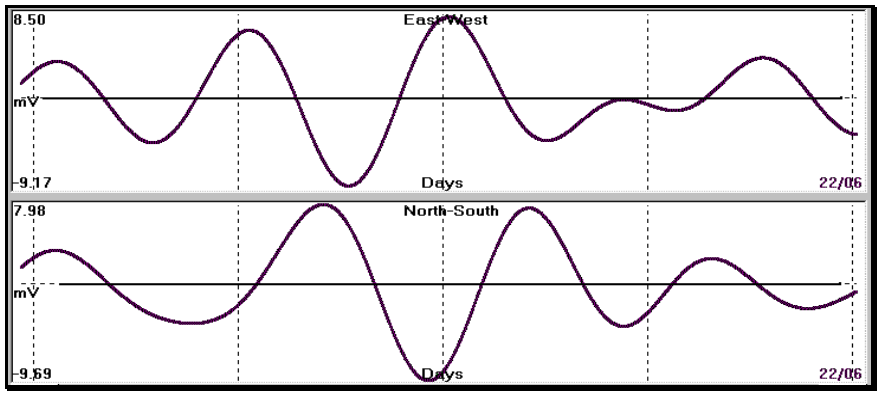

Fig. 4.2.9.6.a.1. Orthogonal, oscillating components, of the Earth's electric field are shown. The recording period extends from 18/06/2002 to 21/06/2002.

- Polar diagram construction.

The azimuthal direction of the electrical field intensity vector was calculated for the same time period at 1-minute intervals, and is presented in figure **(4.2.9.6.a.2)**. This calculation is performed by a specific software package constructed for this purpose. Its main feature is the detection of the maximum values of the calculated intensity vector, along the time axis of the recording, and the location, in a polar diagram, of its azimuthal direction. Each time a maximum value was identified the corresponding vector color changed, so that it facilitated the visual follow-up of this processing. The detected, successive peaks indicate the azimuthal directions of the consecutive, seismically, activated areas.

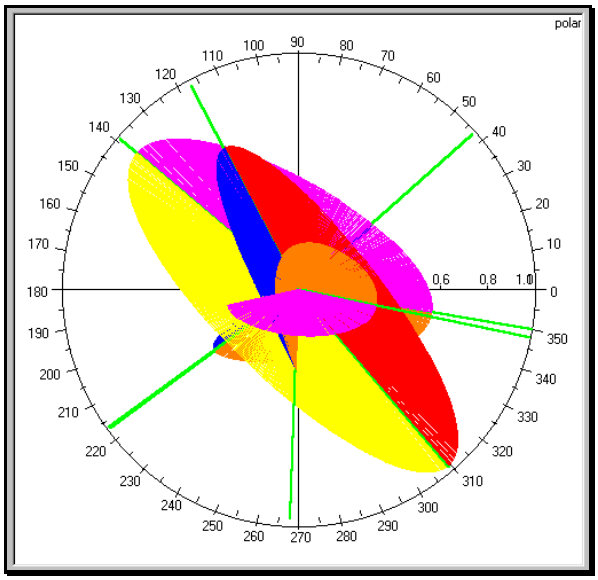

Fig. 4.2.9.6.a.2**.** Polar diagram of the azimuthal direction changes of the calculated, electrical field intensity vector along the same registration period of time.

- Seismicity map compared with the calculated polar diagram.

Finally, the azimuthal directions which were calculated from the maxims of the electrical field intensity vectors, are superimposed **(fig. 4.2.9.6.a.3)** on the map of the location of the corresponding earthquakes that occurred during this period of time.

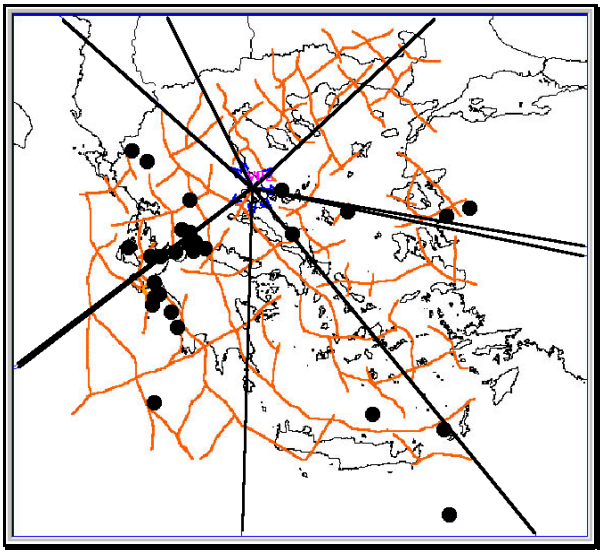

Fig. 4.2.9.6.a.3. Calculated azimuthal directions (solid black lines) compared with the location of the earthquakes (Ms>3R) of the same period of time.

It is obvious that the majority of the EQs are located along the calculated already azimuthal directions. The observed, discrepancy for some of the earthquakes or azimuthal directions will be discussed later on.

4.2.9.6.b. Other examples.

Some more examples, that foster the validity of the methodology, follow. The figures are presented in the same order as: oscillating signal, corresponding, polar diagram and correlation map of azimuthal directions with EQs location. At each case, the low-level threshold magnitude of the compared EQs, is presented, too.

<u>Example – 1</u>

Time period: 2002/03/16-18
Detected EQs low magnitude threshold Ms = 4R

Signal recorded.

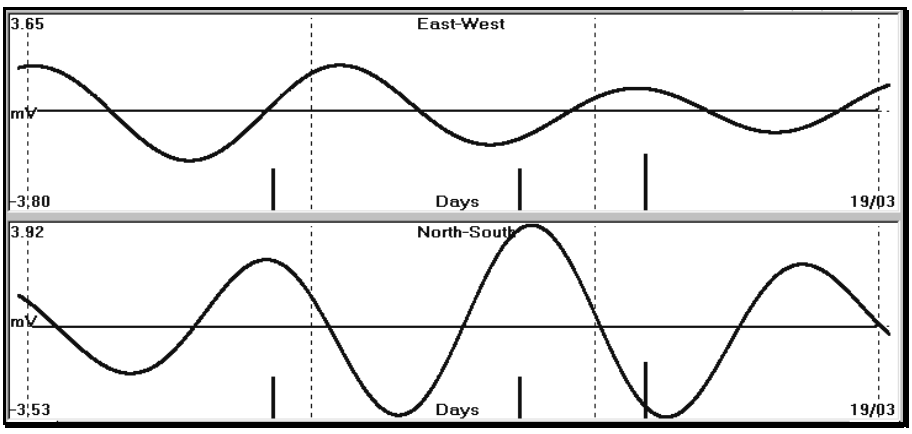

Corresponding, polar diagram.

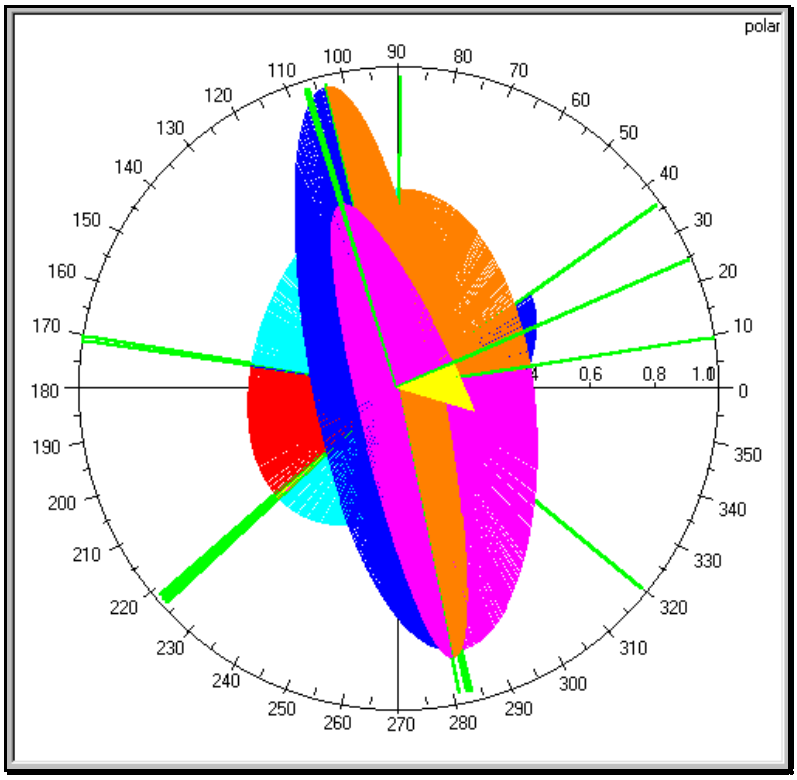

Correlation map of azimuthal directions to EQs location.

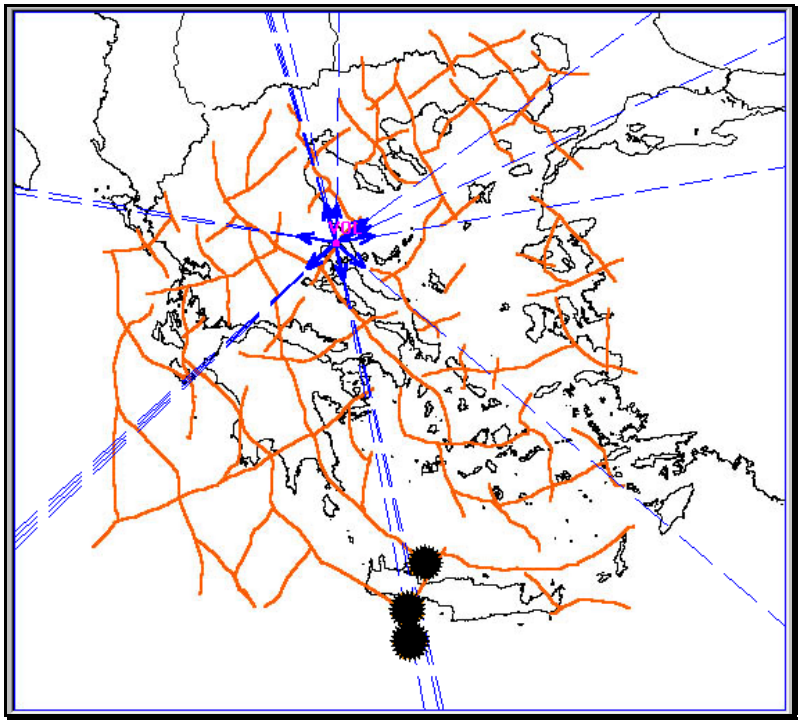

Example – 2

Time period: 2002/04/18-21
Detected EQs magnitude-low threshold Ms = 4.5R

Signal recorded.

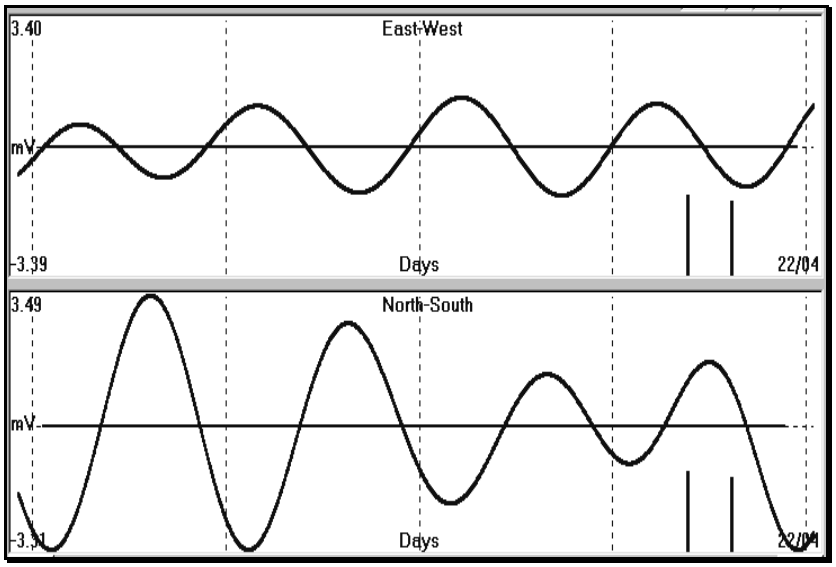

Corresponding, polar diagram.

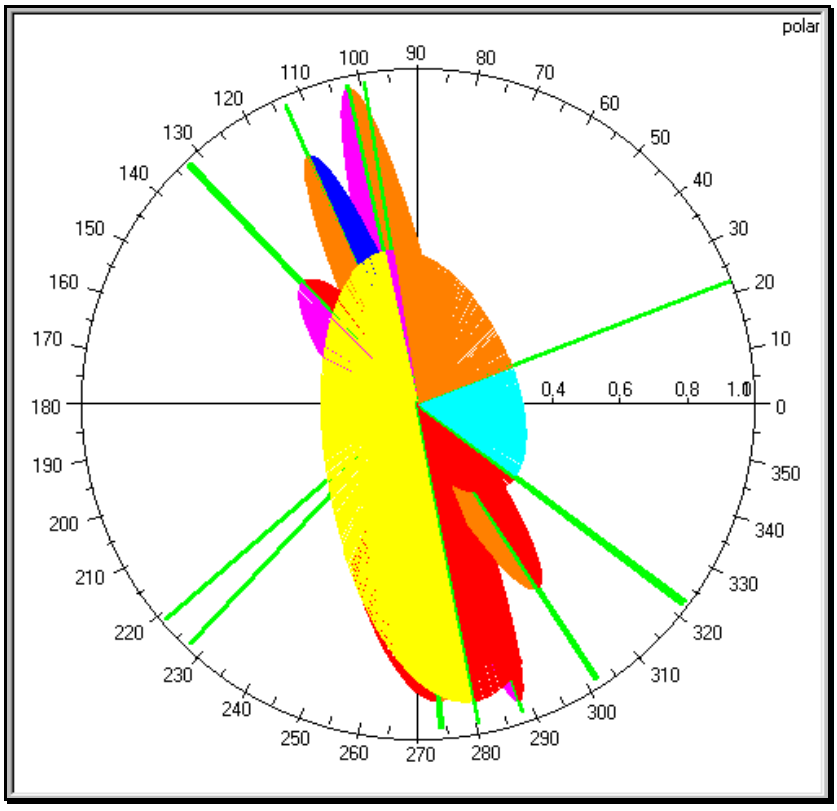

Correlation map of azimuthal directions to EQs location.

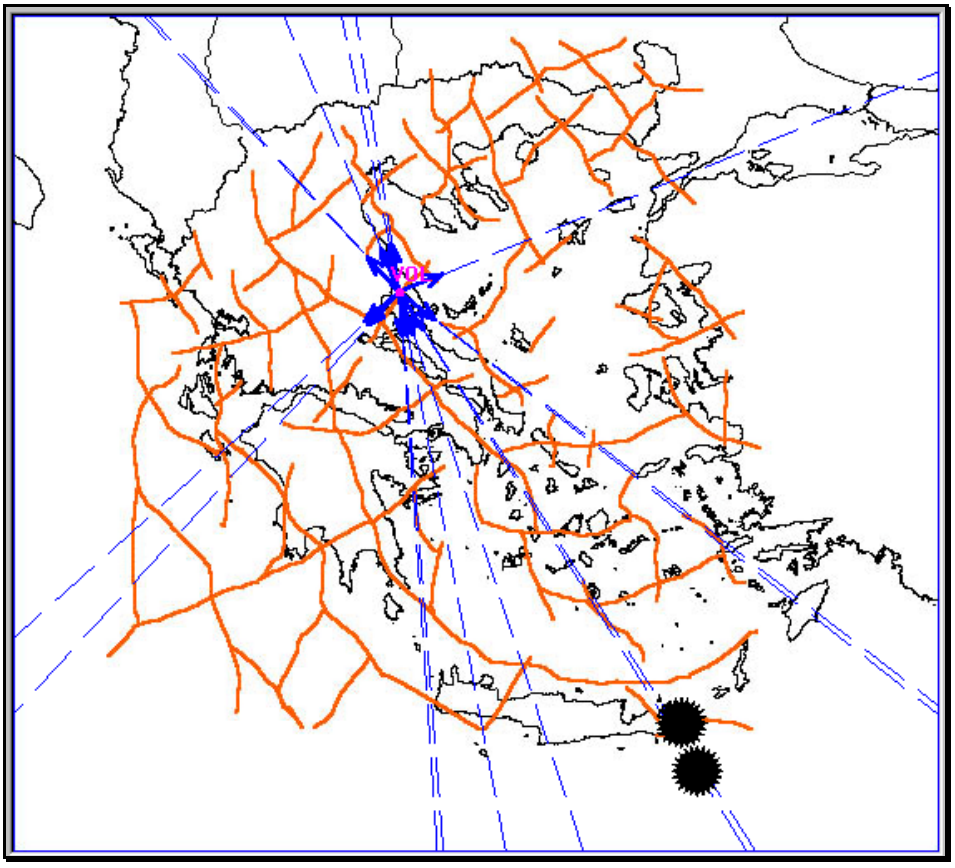

Example – 3

Time period: 2002/07/23-26
Detected EQs magnitude-low threshold Ms = 3R

Signal recorded.

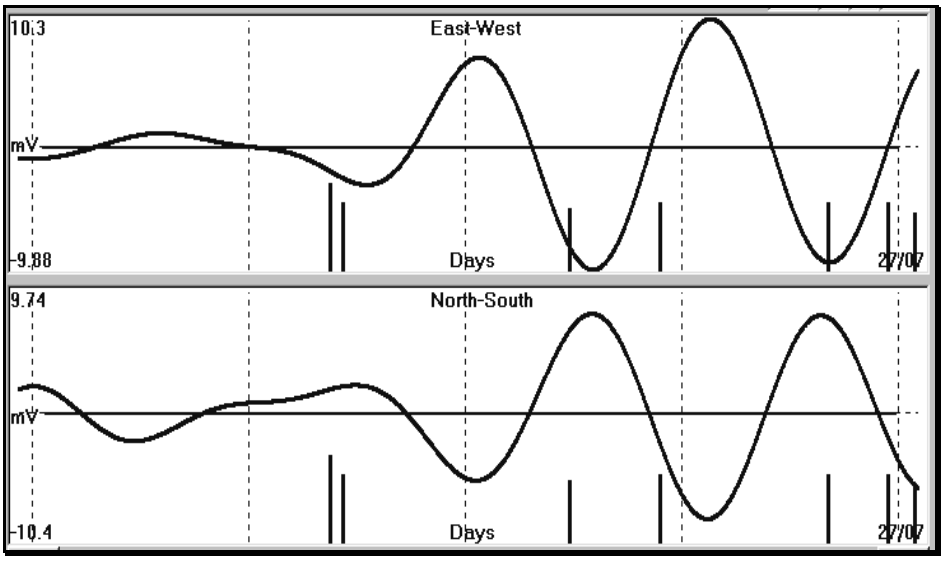

Polar diagram.

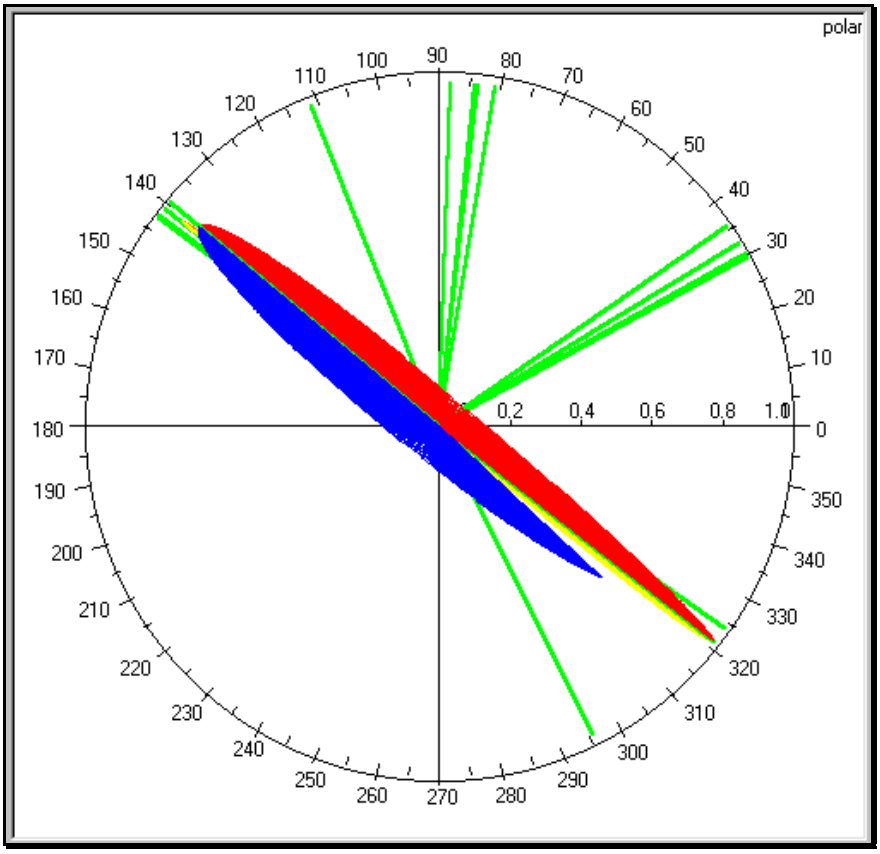

Correlation map of azimuthal directions to EQs location.

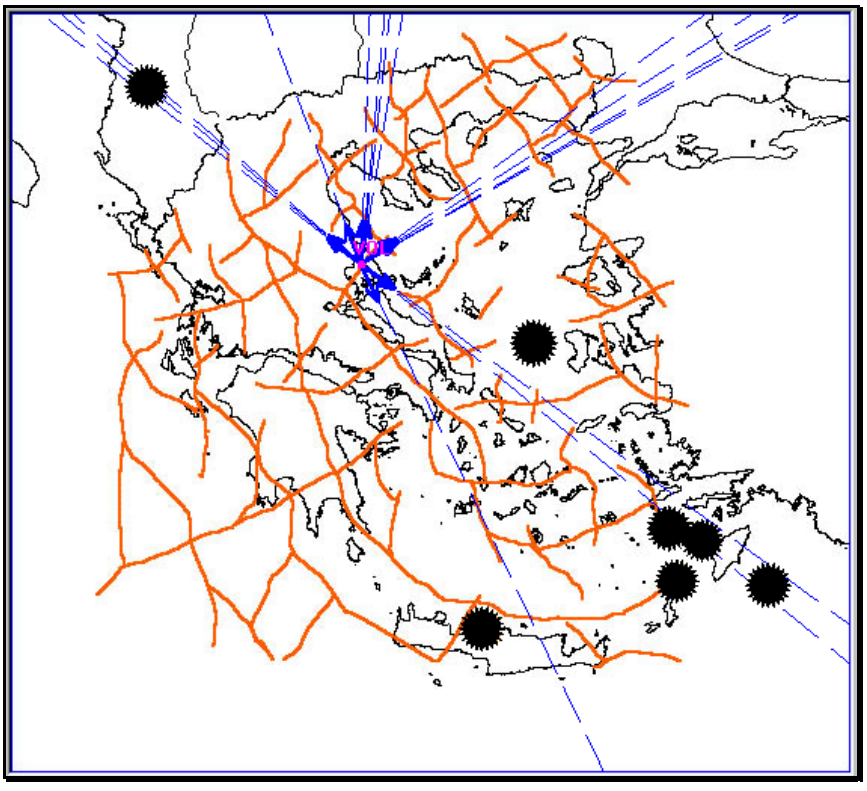

Example – 4

Time period: 2002/09/03-05
Detected EQs magnitude-low threshold Ms = 4R

Signal recorded.

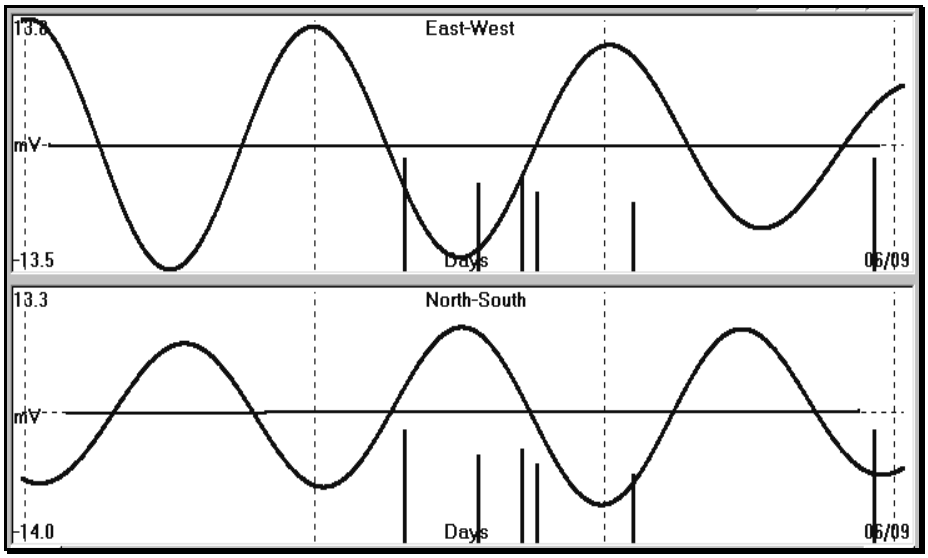

Polar diagram.

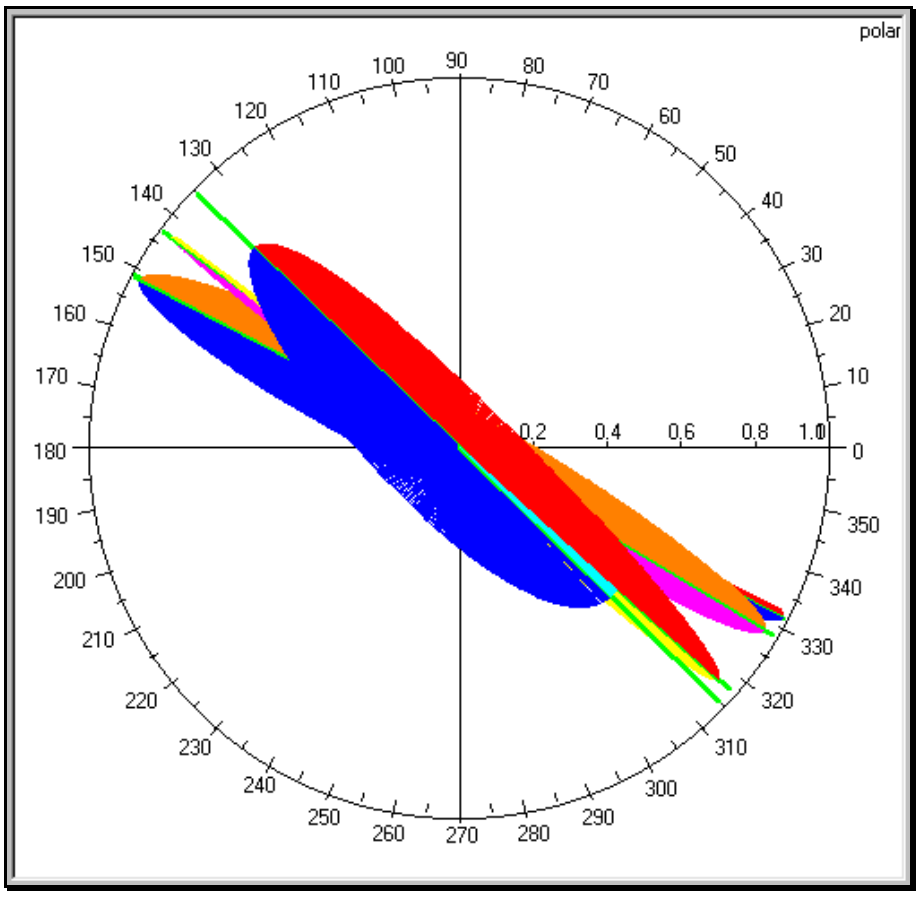

Correlation map of azimuthal directions to EQs location.

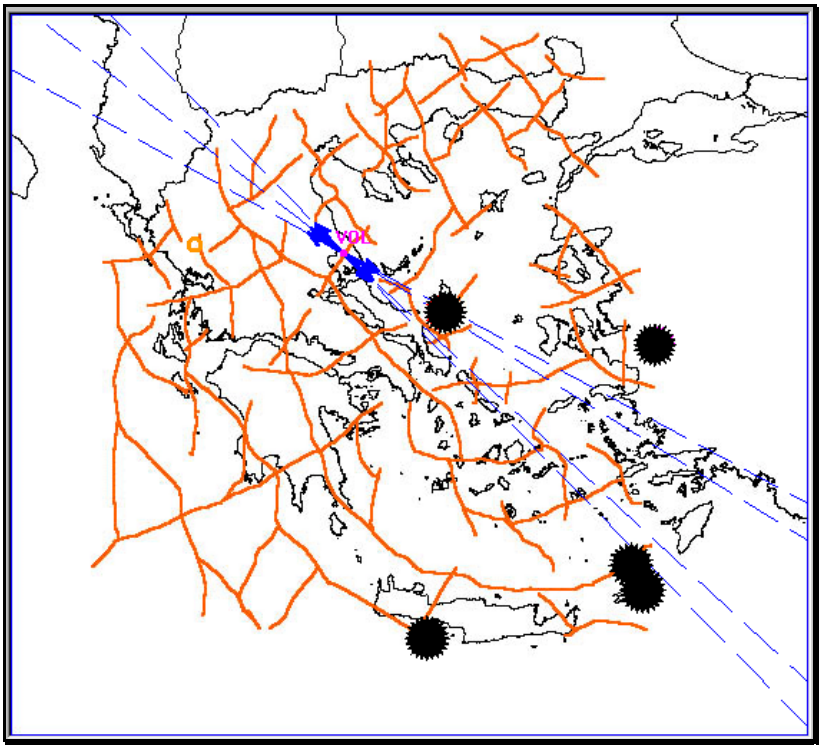

So far, the calculated, electrical field intensity vectors are distinguished into two groups.

The first one, generally, does not correlate with any known azimuthal direction, in relation to the monitoring site, of the EQs that occurred during the period of time of the study.
This group of vectors is clustered in narrow azimuthal bands, in contrast to an expected, normal, random, azimuthal direction distribution which reflects a random process. The later, probably indicates that, some seismogenic areas were excessively stress-loaded but didn't end up to the occurrence of any EQ.

The second group of vectors, in all the presented cases, exhibits a very good fit of azimuthal directions of calculated vectors and EQs. Comparing this group with the various magnitude levels of the EQs, it correlates very well, some times even down to magnitudes of M=3 R.

The latter shows not only the high sensitivity of the used method, but indicates very well that the generated, electrical field, at the focal area, can be detected at large distances from it. This can be explained by the highly resistant crustal seismogenic layer where the electrical dissipation of the transmitted electrical energy is either negligible or very small.

In conclusion, this analysis shows that, because of the applied stress load, the seismically, activated areas, generate electrical signals that can be used for the calculation of their (seismically activated areas) azimuthal direction, in relation to a monitoring site.

This methodology opens up the possibility for the "seismic electrical potential status" of a largely extended seismogenic region to be monitored **"a priori" in real time, even if there is no seismological, preseismic evidence at all,** by installing a network of monitoring sites, evenly distributed, over a large, seismogenic area (i.e. Greece),

4.2.10. Triangulation of preseismic electrical signals.

What was presented, so far, is the "homogeneous" ground, Earth model and the way it responds to the propagation of the electrical fields in it, the various, generating mechanisms that

are triggered in the seismogenic area and account for the existence of the preseismic, electric signals and the way these signals are conditioned, in order to be used for azimuthal direction determination of the current source. The latter is assumed that coincides with the focal area of the pending strong earthquake.

At the present time, the term "preseismic", referring to the electrical signals that are generated before the occurrence of an earthquake, can be ignored, since **we have adopted the assumption that "all the recorded electrical signals" are of seismic origin.**

In seismology, the determination of the epicenter area of an earthquake is performed by triangulating the calculated distances of the observed earthquake from the different seismic monitoring sites, which were determined from the difference between the first arrival times of the seismic **P** and **S** waves at each seismic observatory.

A rather similar technique is used in triangulating the "azimuthal directions" of the calculated intensity vector of the Earth's electric field, which is observed at each monitoring site. The latter is, schematically, presented in the following figure **(4.2.10.1).**

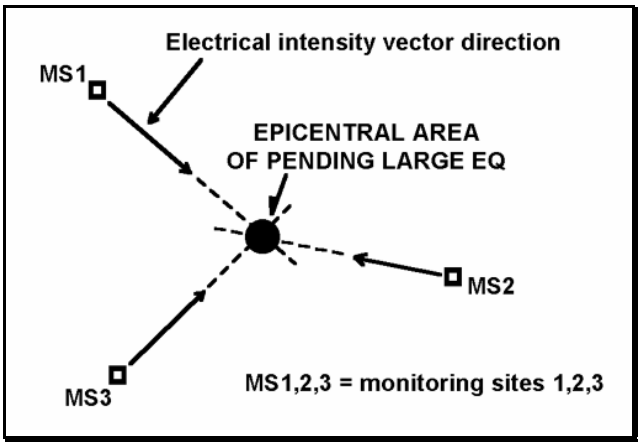

Fig. 4.2.10.1. Triangulation of the electrical field intensity vectors (black arrows) calculated by **MS1**, **2, 3** monitoring sites. A solid large black circle indicates the epicenter area.

It is very interesting, at this point, to examine the azimuthal behavior of electrical signals that are not related to imminent earthquakes (null hypothesis).

Let us hypothesize that three monitoring sites register at the same time some **random signal.** The application of the latter method, since the determined azimuths are of random value, will result in **random intersection sites**, which are calculated from all the electrical vector pairs by all monitoring sites. In such a case (using on line, real time software) this signal will be rejected.

Consequently the following question arises:

What is the probability to hit, by chance, a convergence site of azimuths, using a random, non-preseismic, electric signal?

This is analyzed as follows:

The entire **(360^0)** azimuthal circle is considered as being divided in **(20)** sectors of **(18^0)** degrees each (could be less).

The probability to hit, by chance, the correct, azimuthal direction, which is calculated by a random, electrical signal, for the following number of monitoring sites, is as follows:

<u>Let us assume that an observer is asked to select, in random, the azimuthal direction of an earthquake that will occur in the near future in relation to its location. The probability to select the correct direction is:</u>

for one (1) mon. site the probability (p) is: $p1 = p^1 = 1/20$ $(1/20)^1$

The predictive value, in terms of location of the epicenter, is still non-existent, even if the correct selection is made. Actually, the problem is, the inability to determine, the location of the epicentral area, through a single direction only. Moreover, the origin of the signal is still unknown. It might be of anthropogenic or ionospheric origin, presenting thus, no relation at all (only accidentally) to the pending earthquake.

The predictive value of the used scheme will become worse if two different "guesses" are made at two different, monitoring sites at different, distant locations. In such a case, the probability to select, the correct, azimuthal direction, in random, is even less as:

for two (2) mon. sites the probability (p) is: $p2 = p^2 = 1/400$ $(1/20)^2$

Accordingly, the calculated, azimuthal directions **of intensity vector of the Earth's electric field of random origin,** exhibit a lesser probability to point to the correct, epicentral area of an imminent earthquake. However, if two noise generators are present, each one in the vicinity of each monitoring site, then the azimuthal directions which are calculated at each monitoring station will generally intersect. This is due to the fact that two non-parallel lines in a plane generally intersect. In this case a "false" epicenter area is indicated. In the following figure **(4.2.10.2)** this case is presented schematically.

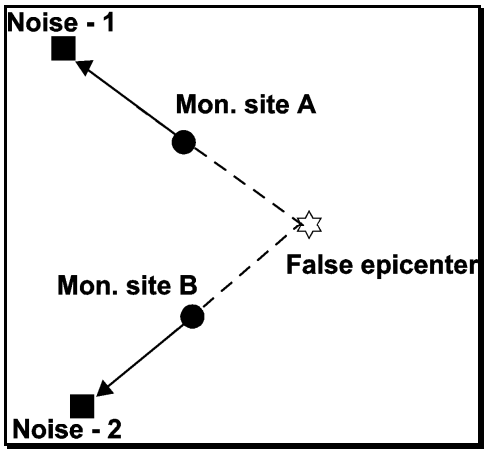

Fig. 4.2.10.2. Monitoring sites **A** and **B** (solid black circles) identify an electric signal, which is generated by two different noise sources (solid black squares), and detected by the monitoring network. The calculated, electrical field intensity vectors (black solid arrows) suggest a false, epicenter area (open star).

A quite different possibility may exist, when the two detected signals end up with electrical field intensity vectors of different polarity. In this case, it is evident that the current sources are different and cannot be interrelated at all. These signals are rejected. The latter is illustrated in the following figure **(4.2.10.3).**

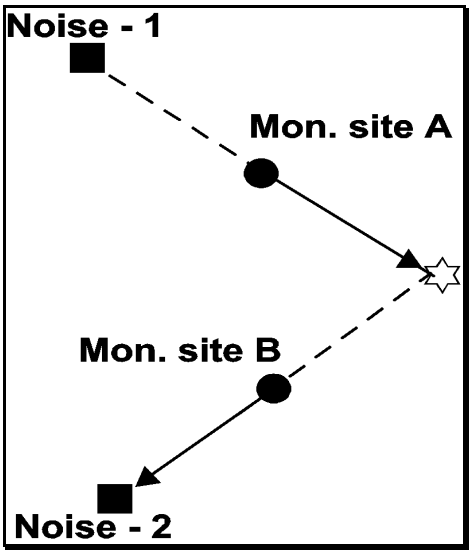

Fig. 4.2.10.3. The monitoring sites **A** and **B** (solid black circles) detect electrical signals of different polarity. Evidently, these intensity vectors of the electrical field (black arrows) cannot be correlated.

It has been made clear, from the latter two examples that, even if two monitoring sites are used, it is not good enough for the calculation of a justified epicentral area. Consequently, the next logical step is to increase the number of the monitoring sites which are used for the detection of the Earth's electric field. The probability for a "by chance" convergence of the electric field intensity vectors thus, decreases drastically. This case, in conjunction with the "same polarity" prerequisite property of the Earth's electric field intensity vector, has a very low probability value to succeed by "chance" as follows:

for three (3) mon. sites the probability (p) is: p3 = p^3 = 1/8000 $(1/20)^3$

If the number of the monitoring sites increases then the probability for a "random hit" of the epicentral area decreases by this method as follows:

for four (4) mon. sites the probability (p) is: p4 = p^4 = 1/160000 $(1/20)^4$

for five (5) mon. sites the probability (p) is: p5 = p^5 = 1/3200000 $(1/20)^5$

Therefore, having convergence, at the same location and same polarity, from at least three or even more monitoring sites, it must be considered rather as an acceptable fact that the signal under investigation, originates at the very same **(x, y)** location of current source, "focal area", and consequently, it may be considered as being related to an imminent earthquake that, most probably, will occur under **the epicenter area determined by using this method.**

The proposed test procedure of the electrical signal validity is demonstrated in the following figures **(4.2.10.4, 4.2.10.5, 4.2.10.6, 4.2.10.7).**

In this case the Earth's oscillating electric field will be used as it was registered (after **FFT** band-pass filtering) by three monitoring sites, which are in operation during the period 20070418 – 20070421 (mode = YYYYMMDD). The monitoring sites are **PYR, ATH** and **HIO** while their location is presented in figure **(4.2.10.7).**

The oscillating, electrical signals which are recorded by each monitoring site are presented as follows:

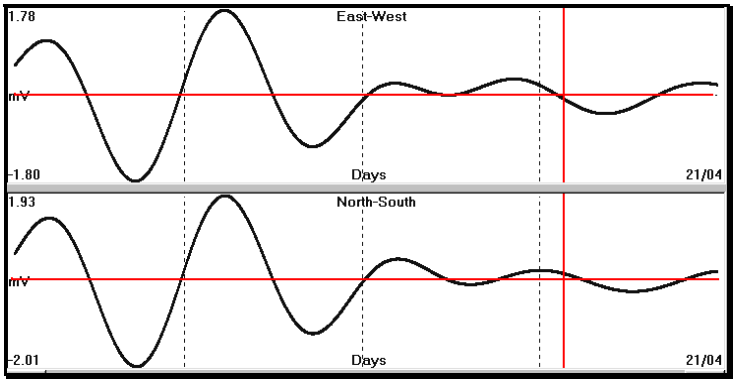

Fig. 4.2.10.4. Oscillating Earth's electric field (solid black line), registered by **PYR** monitoring site. A horizontal red line represents the zero-reference level. The time (03.16h) of azimuthal calculation is represented by a vertical red line.

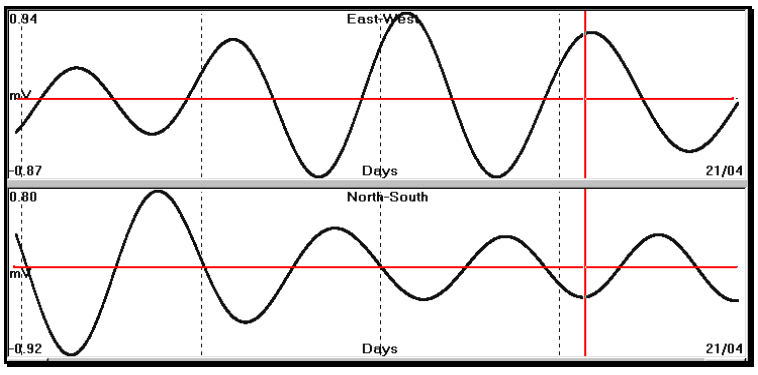

Fig. 4.2.10.5. Oscillating Earth's electric field (solid black line), registered by **ATH** monitoring site. A horizontal red line represents the zero-reference level. The time (03.16h) of azimuthal calculation is represented by a vertical red line.

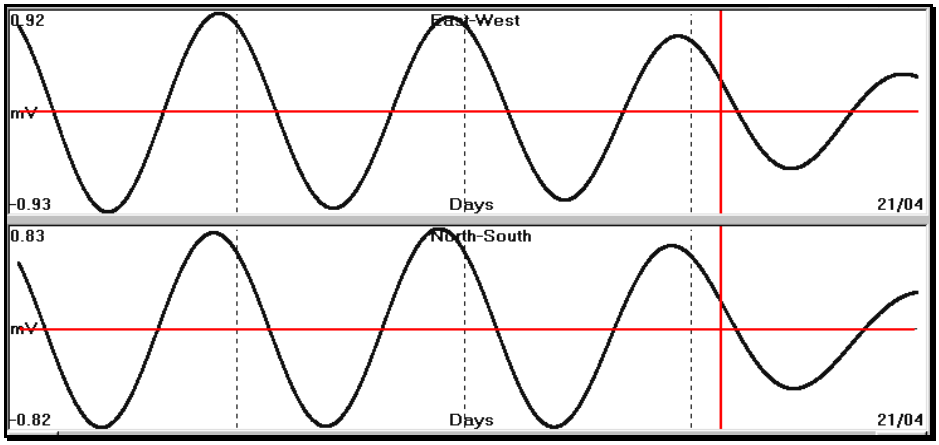

Fig. 4.2.10.6. Oscillating Earth's electric field (solid black line), registered, by **HIO** monitoring site. A horizontal red line represents the zero-reference level. The time (03.16h) of azimuthal calculation is represented by a vertical red line.

For the shake of the test, the azimuthal direction at the three monitoring sites will be utilized at time = 03.16 hours, 21st April 2007 that is indicated by a vertical red line in all three recordings. All the azimuthal directions that were calculated are, simultaneously, presented in a map **(fig. 4.2.10.7).**

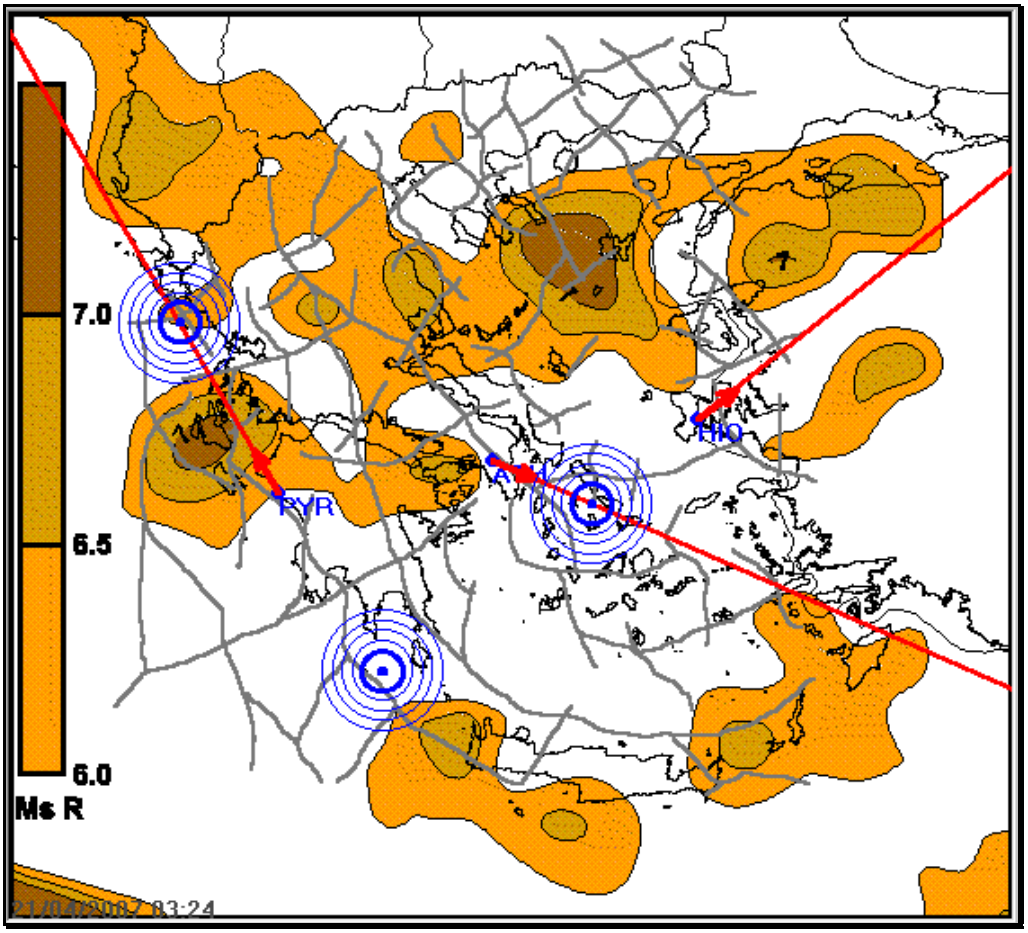

Fig. 4.2.10.7. Map of Greece indicating the location of the three monitoring sites **(PYR, ATH, HIO**) in blue capital letters. The azimuthal direction of the Earth's electric field which is calculated at each case, is shown in red vectors and lines, while multiple blue circles represent the corresponding azimuthal per pair intersections.

The analysis of this presentation shows the following:

1. The intensity vectors which are calculated for **PYR** and **HIO** intersect at the southern part of the map, while the polarity of the vectors is compatible with each other. There is a possibility that these intensity vectors might be generated by the same current source. However, what is still open in questioning in this case is, **whether these signals are due to different sources or not.**

2. **PYR** and **ATH** intensity vectors intersect at the **NW** part of the map. This case is immediately rejected, since the polarity of the intensity vectors, is not compatible.

3. The very same holds for the case of **ATH** and **HIO** monitoring sites.

The conclusion, about the kind of the signal that is registered at time 03.16 on 21st April 2007 is that it is not associated to any preseismic activity. The same procedure was followed for all the anomalous signals which were recorded by the monitoring network, no matter what their origin was. **It is obvious that only preseismic, electrical signals of common origin will pass this test successfully.**

The electrical, noisy signals, of anthropogenic origin, cannot pass this test, successfully, neither for the following main reasons:

a. Their content of frequency is higher than the one which is observed in the preseismic electric signals. Therefore, these signals will be attenuated faster in the ground and consequently, it is rather unlikely to be detected at large distances, where the different monitoring sites are located.

b. The energy injected, in the ground by the industrial activities, is not adequate to produce noisy signals which will be capable of being detected at large distances.

c. A direct result of this is that, these signals will be mostly detected by a single monitoring site at the vicinity of the noise current source only. Therefore, these signals will be rejected by the latter methodology and statistical “by chance” test.

4.2.11. Ionospherically induced noise rejection.

What remains to be discussed, is how the preseismic, electric signals can be discriminated against the signals, induced by the ionospheric currents.

An objection, often put against the seismic, electric, precursory signals, is that these signals may be generated by ionospheric and magnetic anomalies of the Earth’s normal field. This is partly correct, since induction currents, of variable amplitude, are observed in the ground. Moreover, these currents were used as a current source in some applied geophysical methods (magnetotellurics), aiming to the study of deep structure and tectonics of the subsurface of the Earth.

Consequently, the question that arises is: if it is possible, for any methodology that uses electrical signals, recorded, on ground surface, to discriminate between electrical signals, induced, by magnetic and ionospheric anomalies from the electrical signals that are generated at the focal area.

To this end, the methodology which is used so far is the calculation of the magnetotelluric impedance tensor **(T),** at the recording monitoring site, and the calculation of the signals which are induced either magnetically or ionospherically. The latter are subtracted from the original recordings and therefore, hopefully, is obtained a more "clean”, from extraterrestrial disturbances, signal.

Although, this methodology is theoretically correct, in practice it requires expensive and complicated equipment, while its results, as far as it concerns extraterrestrial disturbances elimination, is of a serious concern, regarding its effectiveness, due to the limited bandwidth of the available magnetotelluric recording hardware to date.

As far as it concerns the problem of the discrimination between signals of different origin (extra-terrestrial - seismic), the following procedure is applied to the data which were recorded by, the already in use, monitoring site.

As long as, the recorded signals, originate from a seismogenic area, which is located in the vicinity of the recording network, as a result, the calculated, electrical field intensity vectors will, theoretically, intersect over the seismogenic area.

In the case of an extraterrestrial, induced signal, since the induced field is of "far" origin, its effect will be the same on all monitoring sites, and therefore, the azimuthal direction of the calculated, electrical field intensity vector will be the same for all of them.

In this specific case, the calculated electrical field intensity vectors will all be parallel to each other.

An example of the application of this methodology is presented in the following figures. In fig. **(4.2.11.1, a, b)** the magnetic field for the period between 15-29/Jan/2004 is presented.

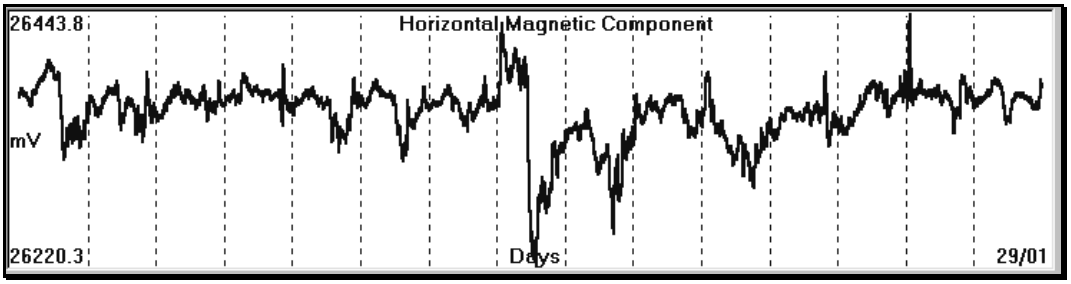

Fig. 4.2.11.1. The Horizontal, magnetic field, recorded by the Magnetic Observatory of Penteli **(MOP)**, Athens, Greece for the period between 15/01/04 - 29/01/04.

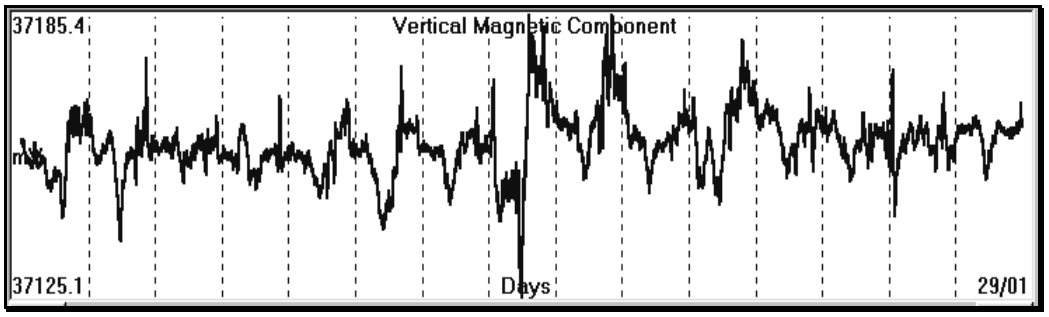

Fig. 4.2.11.1a. The Vertical, magnetic field, recorded by the Magnetic Observatory of Penteli **(MOP)**, Athens, Greece for the period between 15/01/04 - 29/01/04.

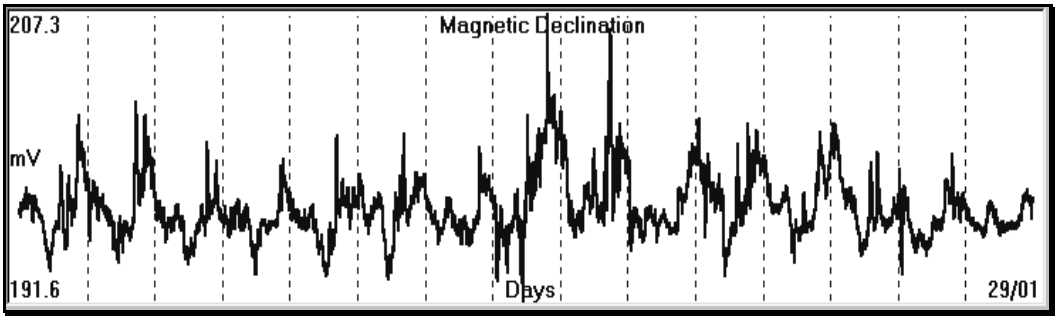

Fig. 4.2.11.1b. The Declination of the magnetic field recorded, by the Magnetic Observatory of Penteli **(MOP)**, Athens, Greece for the period between 15/01/04 - 29/01/04.

For the same period, the Earth's electrical field, recorded, by Athens **(ATH)** and Pyrgos **(PYR)** monitoring sites, is presented in the following figures **(4.2.11.2)** and **(4.2.11.3).**

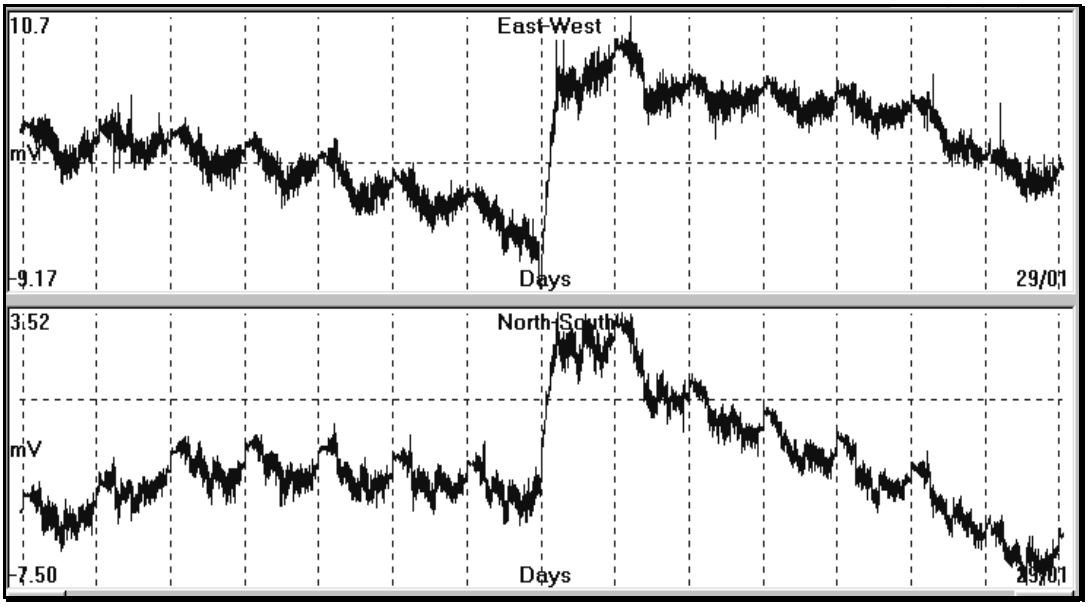

Fig. 4.2.11.2. The Earth's electric field recorded, by Athens **(ATH)** monitoring site, for the period from 15/01/04 to 28/01/04.

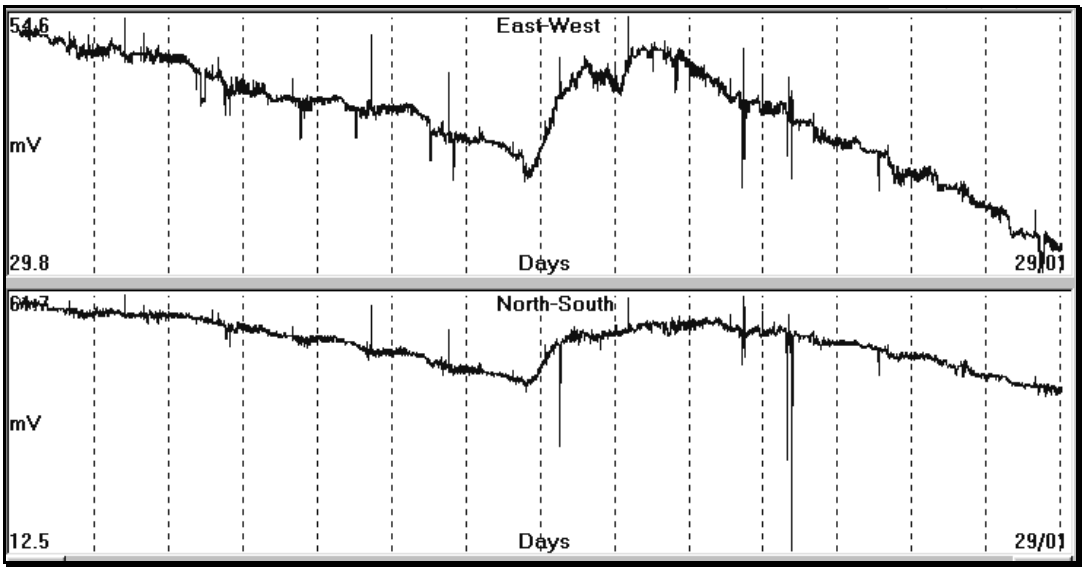

Fig. 4.2.11.3. The Earth's electrical field recorded, by Pyrgos **(PYR)** monitoring site, for the period from 15/01/04 to 28/01/04.

A comparison of figures **(4.2.11.1, a, b)** with figure **(4.2.11.2)** and figure **(4.2.11.3)** indicates that the magnetic storm which was recorded by the Magnetic Observatory of Athens **(MOP)**, induced an anomalous electrical field at both monitoring sites, **ATH** and **PYR**. This magnetic event took place between 21st and 22nd January 2004 and at the same period Very Large Period **(VLP)** signals were simultaneously recorded by both monitoring sites.

These electrical signals were, initially, considered, of seismic origin. The normal procedure, for the calculation of the azimuthal direction of the electrical field intensity vector, was applied to both of them. The obtained results are presented in the following figure **(4.2.11.4).**

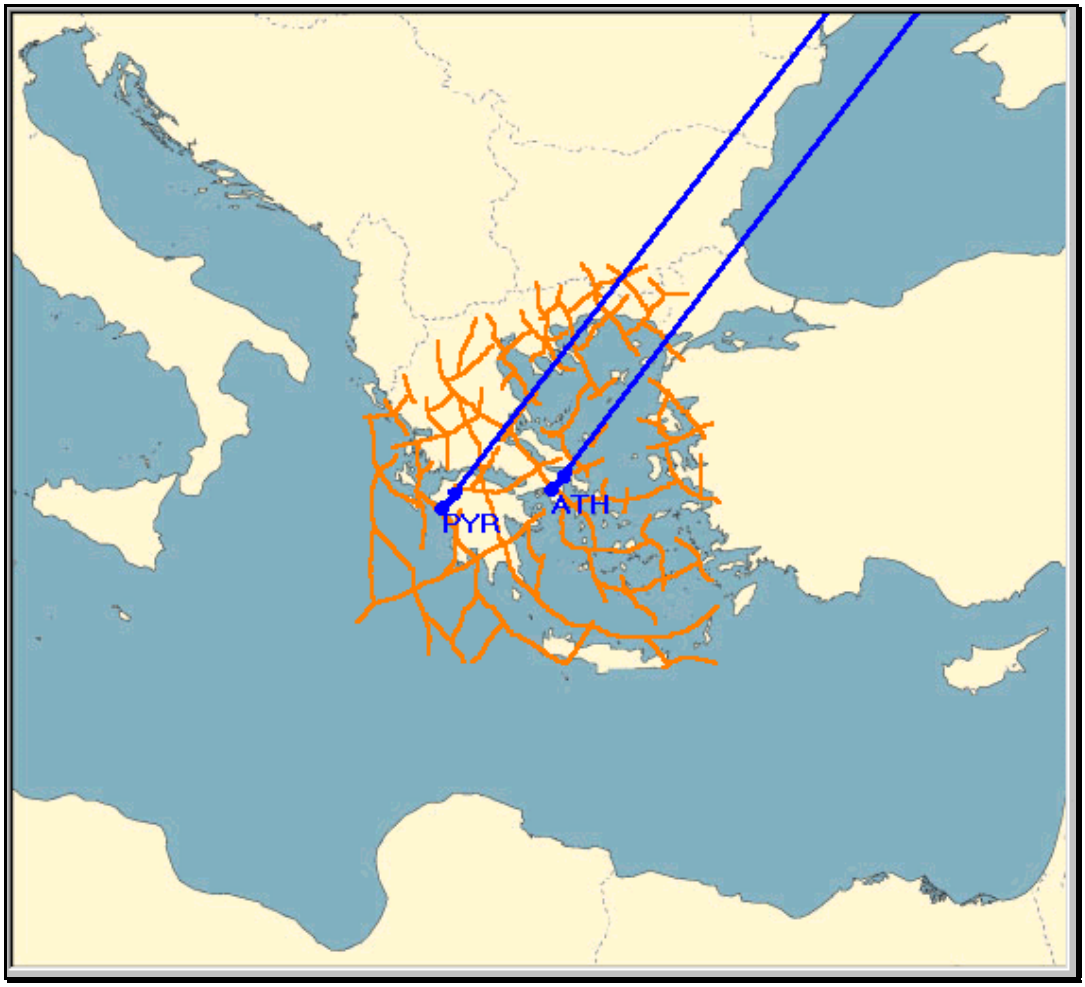

Fig. 4.2.11.4. Azimuthal direction (blue lines) of the Earth's electrical field intensity vector, calculated for the **ATH** and **PYR** monitoring sites, determined from the electrical signals which were induced by the magnetic storm on 21-22/01/04.

The parallel, calculated Earth's electrical field intensity, vectors suggest that these signals have a cause that is very distant, correlate very well with the observed magnetic storm and therefore, validate the postulated methodology.

It has been made clear from all the aforementioned examples that the postulated methodology, applied to the azimuthal direction calculations, for at least three monitoring sites, **rejects all signals that have no seismic origin,** provided that the latter were observed by three of them at least.

In case that a signal is recorded by only two monitoring sites with the correct polarity, the determined intersection is questionable as far as it concerns its predictive potential (the third monitoring site may have failed to detect the incoming, preseismic signal), therefore, it cannot be used for earthquake warning purposes.

4.2.12. Virtual epicenter area determination. The “Common Point Method - CPM”.

The Earth’s electric field, registered, by a monitoring site, can be treated in a quite different way, than the usual one, presented, earlier, in an attempt to calculate the regional location of its current source. For this purpose, let us recall the electrical field intensity vector of an oscillating field and its, graphical, spatial presentation of its azimuthal direction as a function of time, presented, in figure **(4.2.12.1).**

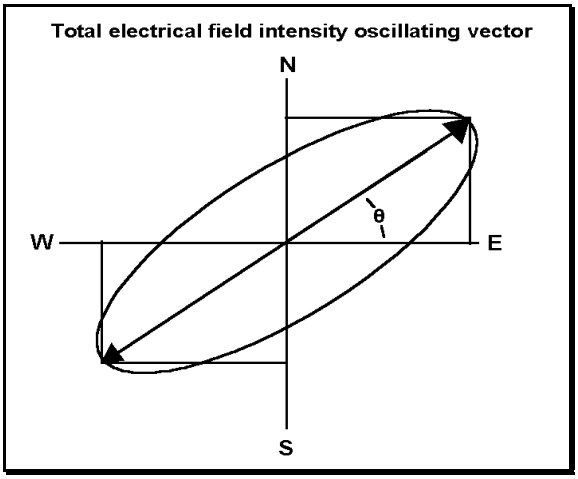

Fig. 4.2.12.1. The oscillating, electric field intensity vector prescribes an ellipse. The angle **(θ),** of its major axis to the EW direction, indicates the azimuthal direction of the location of the current source in relation to the location of the monitoring site.

The major axis of the ellipse indicates the azimuthal direction **(θ)** of the location of the current source in relation to the monitoring site. If a different monitoring site at a different location is used simultaneously, it is obvious that a different ellipse will be produced, but its major axis will point towards the very same current source, too. This is illustrated in the following figure **(4.2.12.2).**

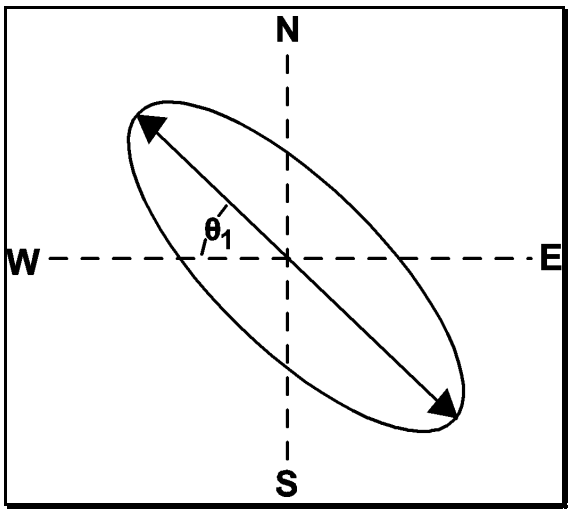

Fig. 4.2.12.2. The oscillating, electric field intensity vector prescribes an ellipse. The angle **(θ1),** of its major axis to the EW direction, indicates the azimuthal direction of the location of the current source, in relation to the location of the monitoring site.

The intersection of these two azimuthal directions **θ** and **θ1,** evidently, indicates the location of the current source that generates the oscillating, electrical field. In other words, it indicates the virtual, epicentral area of the pending earthquake. The latter is illustrated in the following figure **(4.2.12.3).**

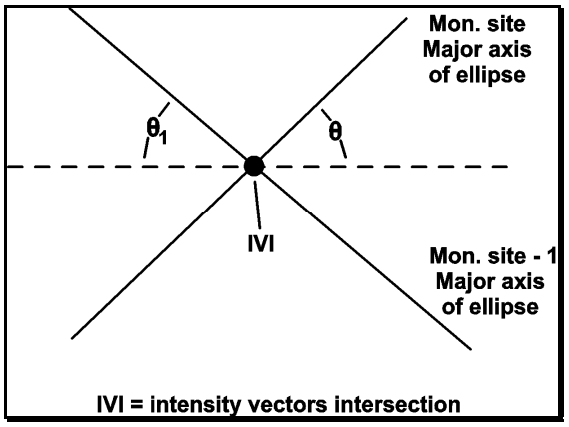

Fig. 4.2.12.3. The two major axis of the ellipses (of azimuthal angles **θ**, **θ1**), observed, at the two monitoring sites, intersect at point **IVI** (Intensity Vector Intersection) which is considered the location of the virtual, epicentral area location.

What actually happens, in practice, is that the intersection of the two intensity vectors, as long as the electrical field oscillates, moves in the plane of oscillation. Consequently, it will prescribe a hyperbolic trace, which asymptotically will coincide with the two major axes of the, observed, ellipses by the two different monitoring sites. The latter is indicated in the following figure **(4.2.12.4).**

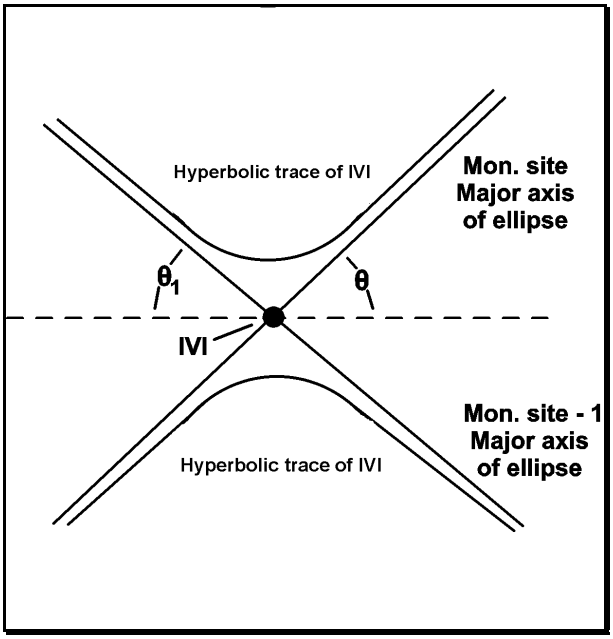

Fig. 4.2.12.4. Hyperbolic traces prescribed, by the intersection of the oscillating, electrical field intensity vector, as a function of time. Intersection (of major ellipse axes) of the hyperbolas asymptotes is indicated by **IVI**.

The intersection of the two intensity vectors follows the hyperbolic paths, just because there is generally an unknown phase shift, between the oscillating fields, as it is evident from figures **(4.2.12.1)** and **(4.2.12.2).** The hyperbolic traces of **IVI** can be easily constructed by the use of the registered, oscillating, electrical fields. Very briefly the procedure is as follows:

a. For each data set, from both monitoring sites, the azimuthal directions are calculated.

b. The location of the **IVI** is determined, from the calculated, azimuthal directions in a plane, as a solution of the linear equations system that corresponds to both azimuthal directions linear equations.

c. The obtained **IVI** locations are plotted, as function of time, on a regional location map.

d. Draw the asymptotes and locate the intersection of the major axes of the two ellipses.

Step **(d)** indicates the virtual epicenter area, identified, which corresponds to the location of the virtual, current source that accounts for the generation of the registered, oscillating, electrical field.

A very similar plot can be generated when the two, recorded, signals, at each monitoring site, are of different origin. Since the asymptotes intersection does not correspond to any seismic, epicentral area, the term “virtual” is used.

In the case that both signals are generated by the same current source, these are closely interrelated and therefore, instead of hyperbolas, ellipses are generated by the **IVI**. Actually, in real conditions, the theoretical intersection of figure **(4.2.12.3)** “explodes” into an ellipse, due to the presence of noisy phase shifts, which are caused by interfering noisy signals.

The calculated intensity vector traces from recordings of the Earth’s electric field, for demonstration purposes of this method, are presented in the following figure **(4.2.12.5).** The used monitoring sites are of **PYR** and **HIO** and the time span of the recording is from 20070401 to 20070406, in yyyymmdd mode.

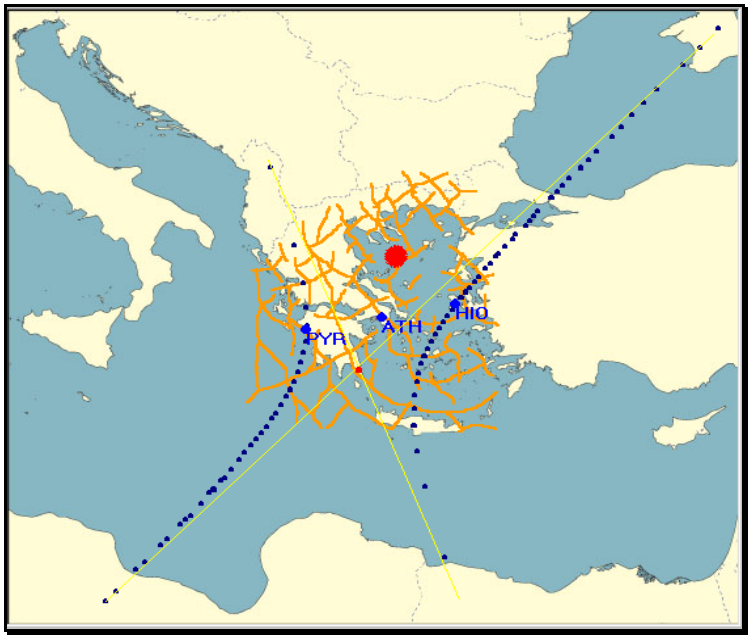

Fig. 4.2.12.5. Typical intensity vector intersections and asymptotes are presented. The red dot indicates the "virtual epicenter" valid for period from 20070401 to 20070406. The large, solid, red circle indicates the location of the earthquake (M=5.4R), that occurred on 19th April 2007.

The calculated traces are depicted by blue dots with a sampling interval of ten (10) minutes. Thin yellow lines represent the corresponding asymptotes. Their intersection is indicated by a small red dot, while a solid, large red circle indicates the location of the earthquake (M=5.4) that occurred on 19th April 2007.

The previous figure **(4.2.12.5)** transforms into the following figure **(4.2.12.6),** gradually, due to the increase of correlation of the recorded signals. The latter indicates that, a hypothetical preseismic signal enters the monitoring network.

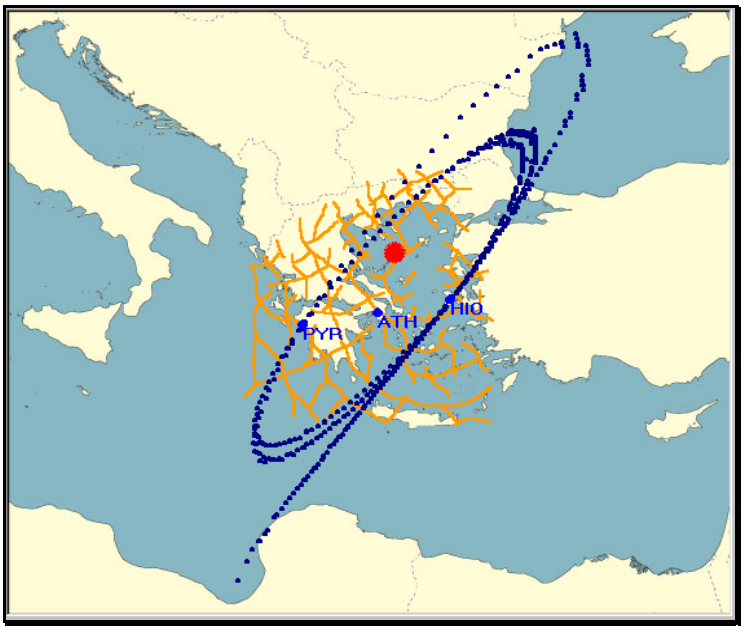

Fig. 4.2.12.6. Ellipses observed, in the period from 20070404 to 20070407. The ellipses suggest the strong interrelationship of the recorded signals. The large, solid, red circle indicates the location of the earthquake (M=5.4R) that occurred on 19th April 2007.

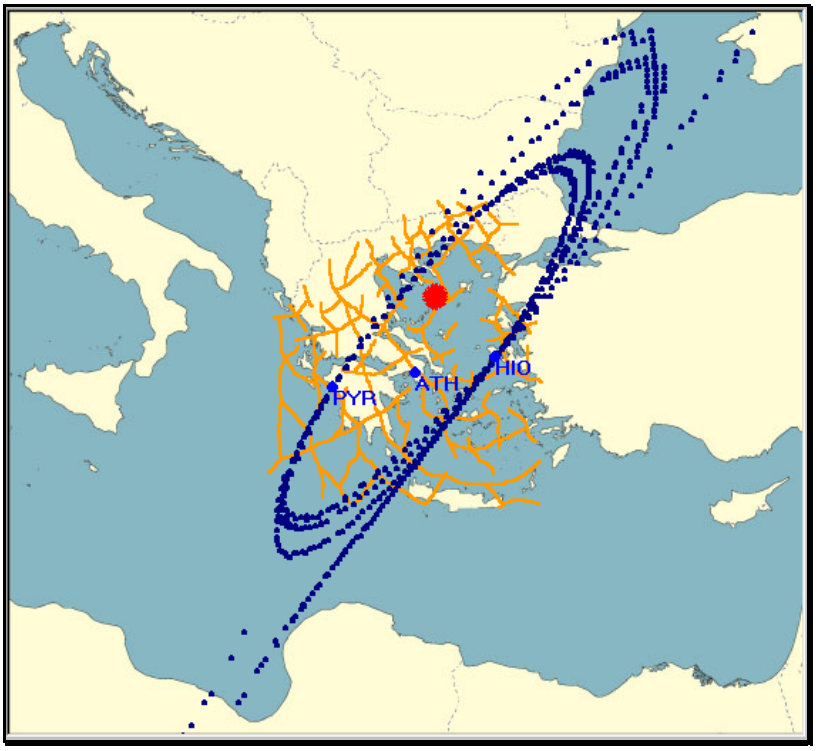

Fig. 4.2.12.7. Ellipses observed, in the period from 20070406 to 20070410. The ellipses suggest the strong correlation of the recorded signals. The large, solid, red circle indicates the location of the earthquake (M=5.4R) that occurred on 19th April 2007.

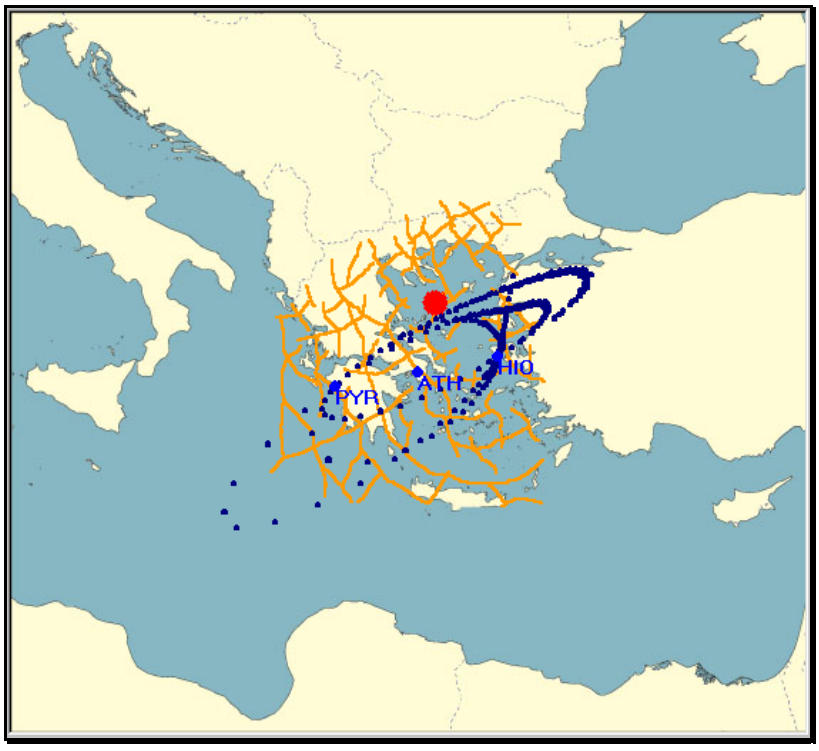

Fig. 4.2.12.8. Ellipses observed, in the period from 20070412 to 20070415. The ellipses suggest the strong correlation of the recorded signals. The large, solid, red circle indicates the location of the earthquake (M=5.4R) that occurred on 19th April 2007.

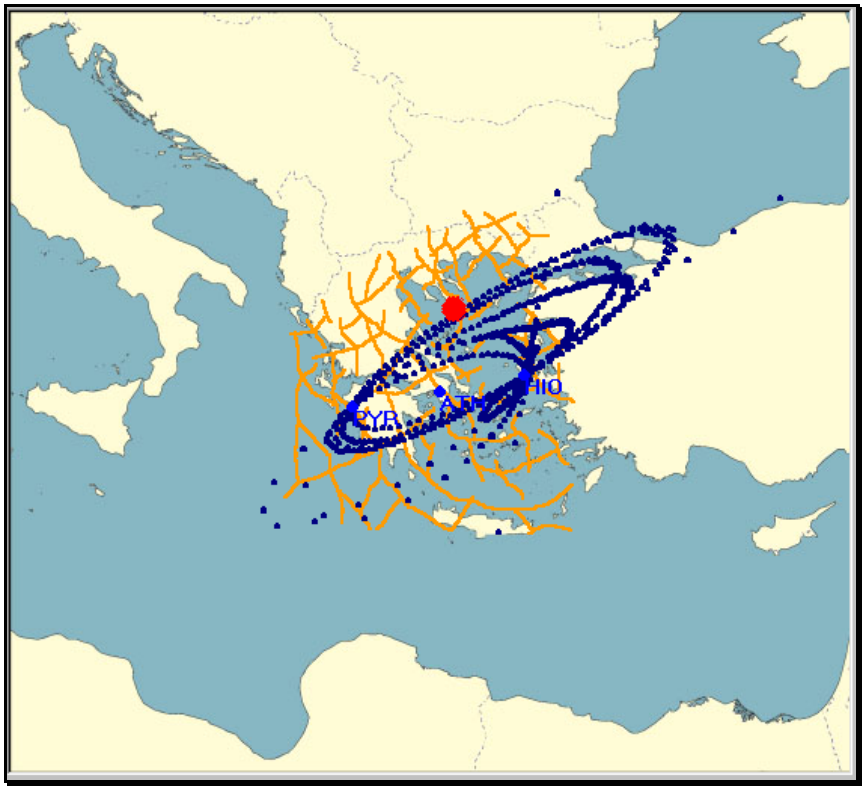

Fig. 4.2.12.9. Ellipses observed, in the period from 20070414 to 20070417. The ellipses suggest the strong correlation of the recorded signals. The large, solid, red circle indicates the location of the earthquake (M=5.4R) that occurred on 19th April 2007.

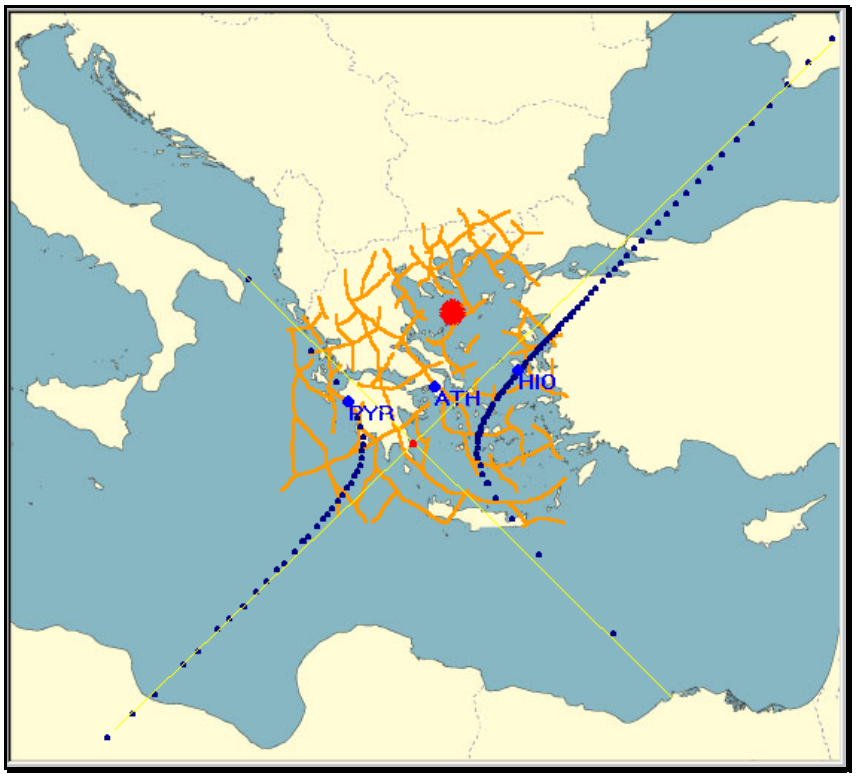

Fig. 4.2.12.10. Hyperbolas observed, in the period from 20070418 to 20070421. It is suggested that the "preseismic signal effect" has disappeared. The large, solid, red circle indicates the location of the earthquake (M=5.4R) that occurred on 19th April 2007.

What can be stated summarizing all the aforementioned results is:

- It is made clear, that a strong correlation of the recorded signals by **PYR** and **HIO** monitoring sites, started after the 4th April 2007 and lasted up to 17th April 2007. That is thirteen (13) days before the occurrence of the pending earthquake.

- During this period the calculated, electrical field intensity vector intersection prescribed ellipses, suggesting that an electrical, preseismic signal was influencing both monitoring sites.

- This signal vanished, in accordance to the piezoelectric model, very short before the occurrence of the earthquake of 19th April 2007, M = 5.4, and on-wards the **(IVI)** traces turned to their normal form.

4.2.13. Application on real earthquakes (epicenter determination).

The next natural step to follow, after the presentation of the theory, is the presentation of some examples, referring to real earthquakes that validate the already postulated methodology.

The first example refers to earlier work from Thanassoulas (1991) that involves data, acquired by the **VAN** team, and after these had been presented in the "International Conference on Measurements and Theoretical Models of the Earth's Electric field Variations Related to Earthquakes", held in Athens, in 1990.

The next six examples refer to data which were obtained through the installed, and still in operation, since 2003, monitoring network, consisting of registration sites, located, at Pyrgos **(PYR)**, Athens **(ATH)** and Hios Island **(HIO)**.

The data are presented in the form of: Raw data, Filtered data, Azimuthal direction of the epicentral area through the calculation of the corresponding, polar diagram, Location map of the calculated, epicentral area correlated to the real, seismological epicenter of the involved strong earthquake.

4.2.13a. Earlier work from Thanassoulas (1991).

This work is, actually, the start for the development of the already presented methodology. The available recorded data, by that time, were in paper analog form and therefore, digital processing was not applicable right from the start. Therefore, the entire analog recordings were digitized manually (!) at a sampling interval of 15 minutes. Consequently the "shorter time period" SES signals vanish completely through this operation. The following figures **(4.2.13a.1, 4.2.13a.2)** refer to Kalamata EQ (13th September, 1986, Ms = 6.2 and 5.5) as the electrical field was recorded by **KER** monitoring site.

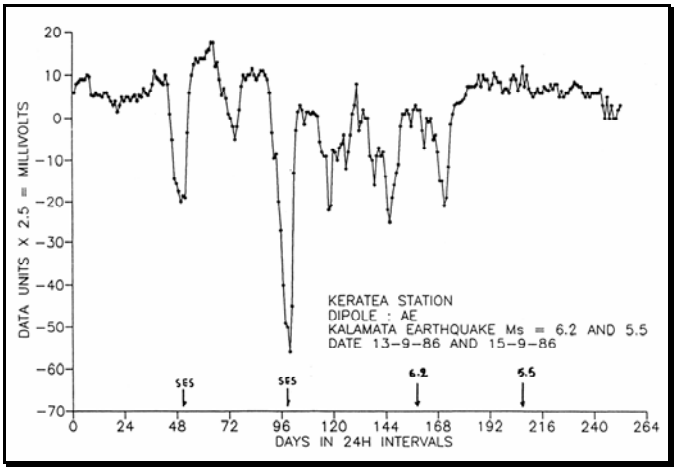

Fig. 4.2.13a.1. **KER** resampled, recording of the dipole **AE** (NW – SE). The arrows show the time of the occurrence of **SES** and main earthquake events (Thanassoulas, 1991).

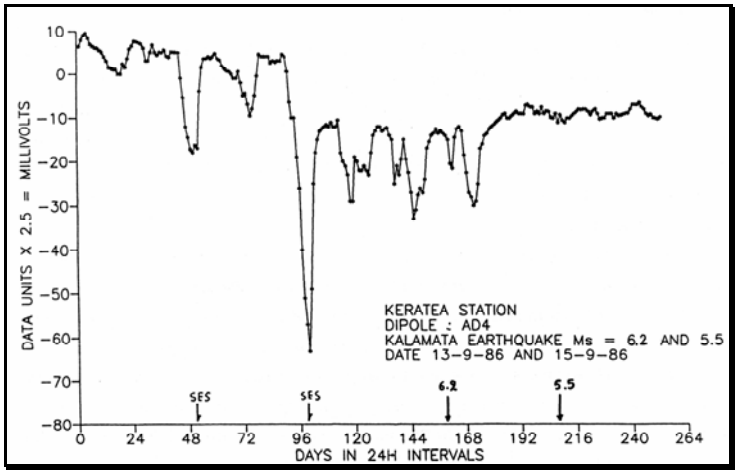

Fig. 4.2.13a.2. **KER** resampled, recording of the dipole **AD4** (N – S). The arrows show the time of the occurrence of **SES** and main earthquakes events (Thanassoulas, 1991).

The recorded, electrical field was smoothed by a "low-pass" filter (figures **4.2.13a.3**, **4.2.13a.4**)

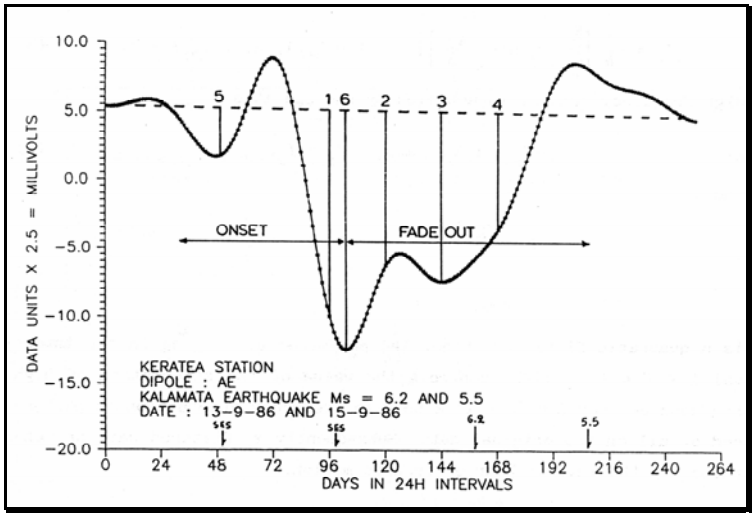

Fig. 4.2.13a.3. Processed observations which correspond to **KER (AE)** station. Sample times for the azimuthal direction calculation are numbered from 1 – 6 (Thanassoulas, 1991).

And discrete signal amplitudes were selected for the calculation of the corresponding azimuthal directions of the Earth's electric field intensity vector.

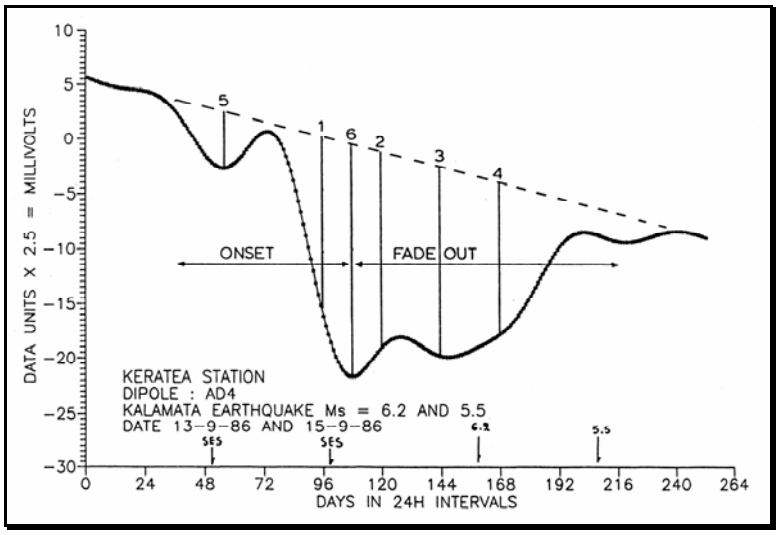

Fig. 4.2.13a.4. Processed observations which correspond to **KER (AD4)** station. Sample times for the azimuthal direction calculation are numbered from 1 – 6 (Thanassoulas, 1991).

At the time when this work was in progress, the entire processing was performed manually and therefore, a graphical presentation was used for the obtained results. The latter are presented in figure **(4.2.13a.5)**.

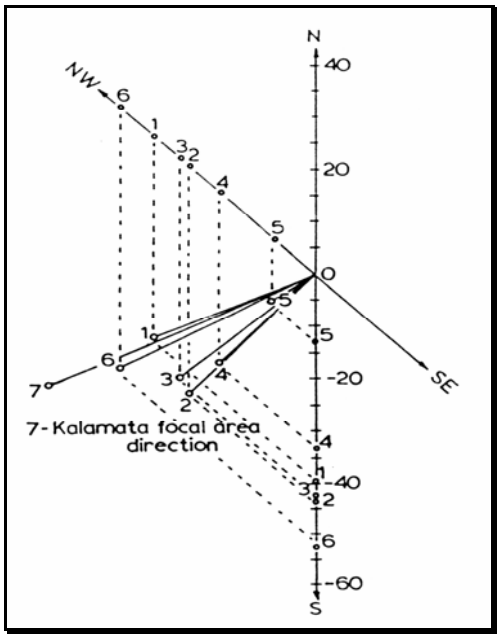

Fig. 4.2.13a.5. Graphical determination of the azimuthal direction of the Earth's electric field intensity vector for samples 1 – 6. Kalamata azimuthal direction, in relation to **KER** station is, represented, by No 7 (Thanassoulas, 1991).

Similar results were obtained through this methodology, applied on recordings, obtained, from different, monitoring sites and related to different strong earthquakes. The latter, are summarized in the following figure **(4.2.13a.6)**.

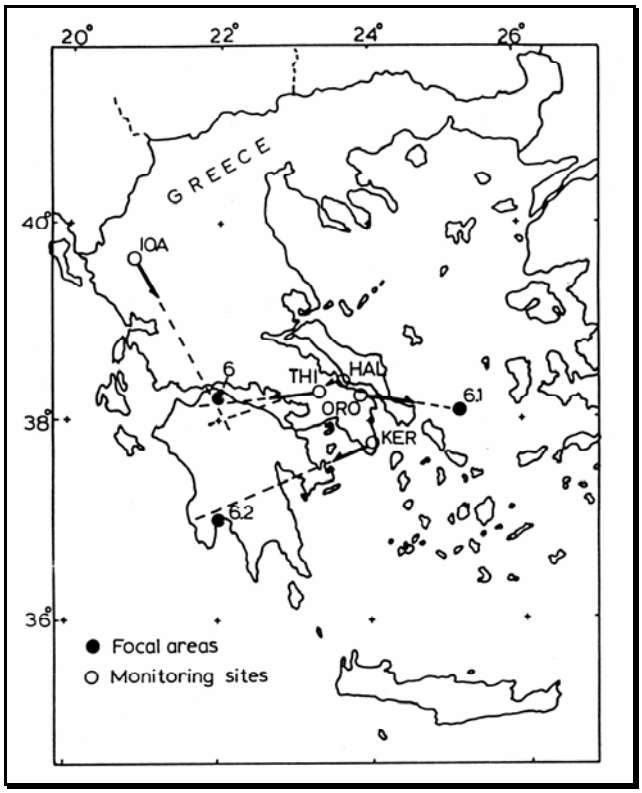

Fig. 4.2.13a.6. Location map of the monitoring sites **KER**, **HAL**, **ORO**, **THI**, **IOA** (open circles) and focal areas of Kalamata (Ms = 6.2R), Patras (Ms = 6.0R), and Aegean Sea (Ms = 6.1R) earthquakes (solid circles). The black arrows indicate the calculated azimuthal directions (Thanassoulas, 1991).

Similar results were presented by Ifantis et al. (1993) and Ifantis (1994). It is worth to notice that, in the case of Patras EQ **(fig. 4.2.13a.6**) there is convergence of three electrical field intensity vectors, calculated, by **THI**, **HAL** and **IOA** monitoring sites. **The probability to consider it as a "by chance" convergence is 1/8000 only.**

4.2.13b. Recent examples from the present in operation network.

The first example to follow, corresponds to registrations obtained by all three **(PYR, ATH, HIO)** monitoring sites that are in operation to date (2007), while the rest of them refer to the monitoring sites of **ATH** and **PYR**. The **HIO** monitoring site was set up in last year (2006).

In the following figures, the thick vertical red line represents the time of occurrence of the considered earthquake. A thin, horizontal red line represents the "reference" level of the anomalous, preseismic signal, while in the polar diagrams the green arrow represents the average value of the calculated azimuths along the anomalous, preseismic signal. It must be pointed out that, each day's recording consists of 1440 samples (1 per minute) and therefore, each polar diagram consists of some thousands of discrete, azimuthal values. Blue lines and arrows indicate the intensity vectors, while blue circles represent their intersection. In the same map, red circles represent the seismological epicenter, provided by the Geodynamic Institute of Athens. Consequently, a comparison of the calculated epicentral area, through the postulated methodology, with the one provided by seismological methods, is facilitated.

The actual examples are as follows:

Zakynthos, Greece, 20060404, Ms = 5.7 EQ.

Athens (ATH) monitoring site.

Raw data, ATH.

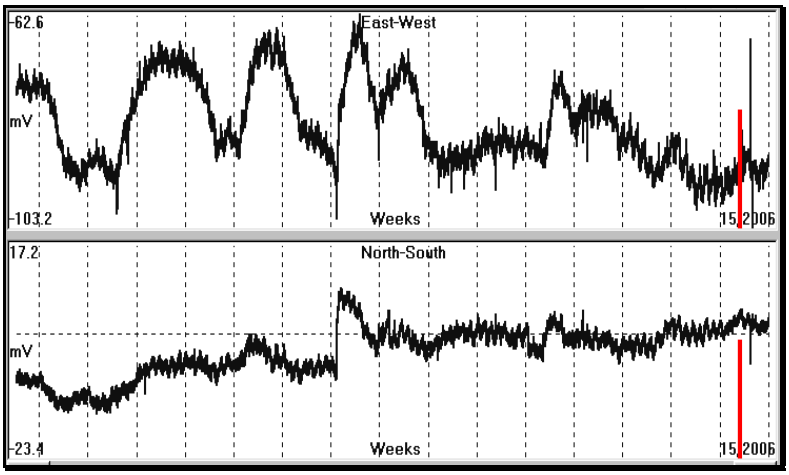

Fig. 4.2.13b.1. Raw data registered, by **ATH** monitoring site.

Filtered data, p = 1.25, ATH.

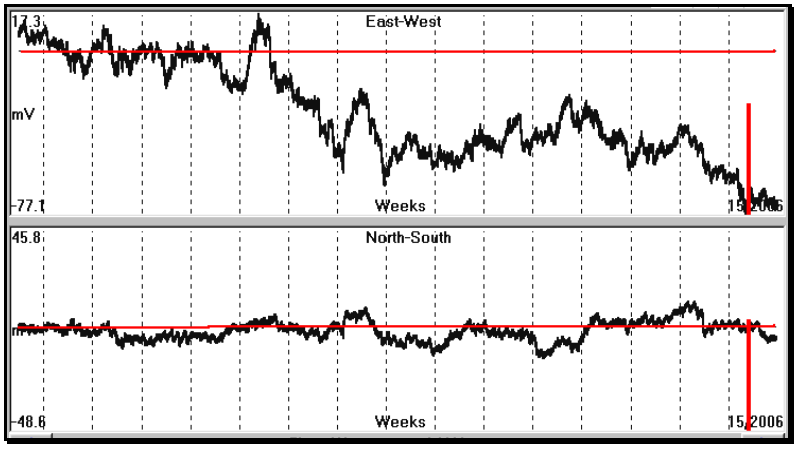

Fig. 4.2.13b.2. Filtered data calculated, for **ATH** monitoring site. Noise injection parameter **p = 1.25**.

Calculated, electrical field intensity vector polar diagram for ATH.

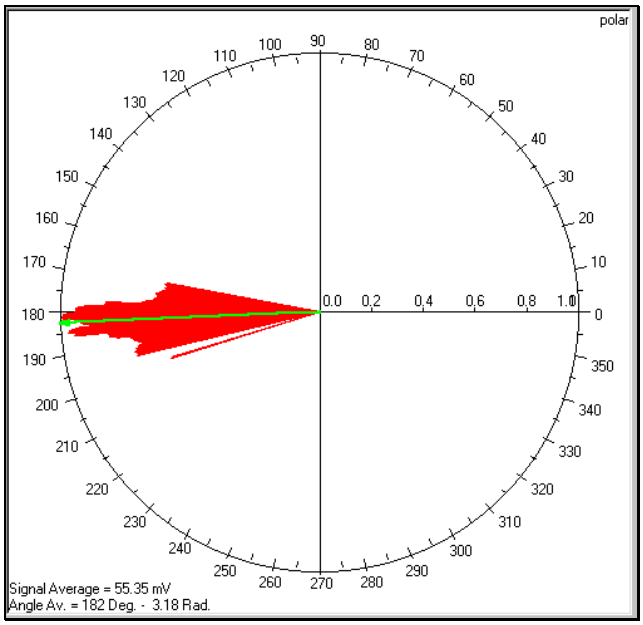

Fig. 4.2.13b.3. Corresponding polar diagram, for **ATH** monitoring site.

<u>Pyrgos (PYR) monitoring site.</u>

Raw data, PYR.

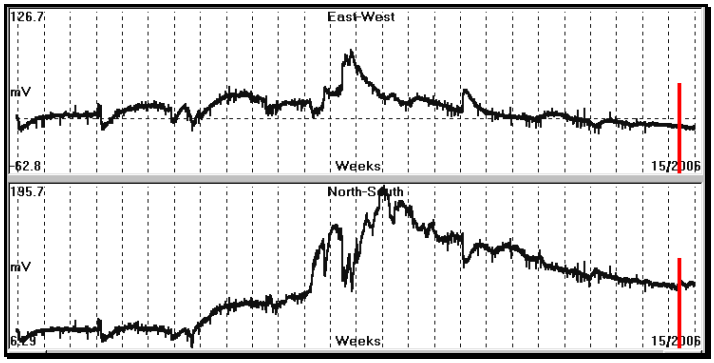

Fig. 4.2.13b.4. Raw data registered, by **PYR** monitoring site.

Filtered data, p = 2.5, PYR.

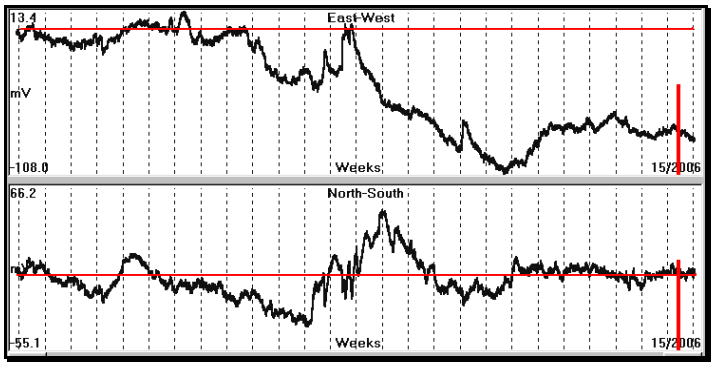

Fig. 4.2.13b.5. Filtered data calculated, for **PYR** monitoring site.

Calculated, electrical field intensity vector polar diagram for PYR.

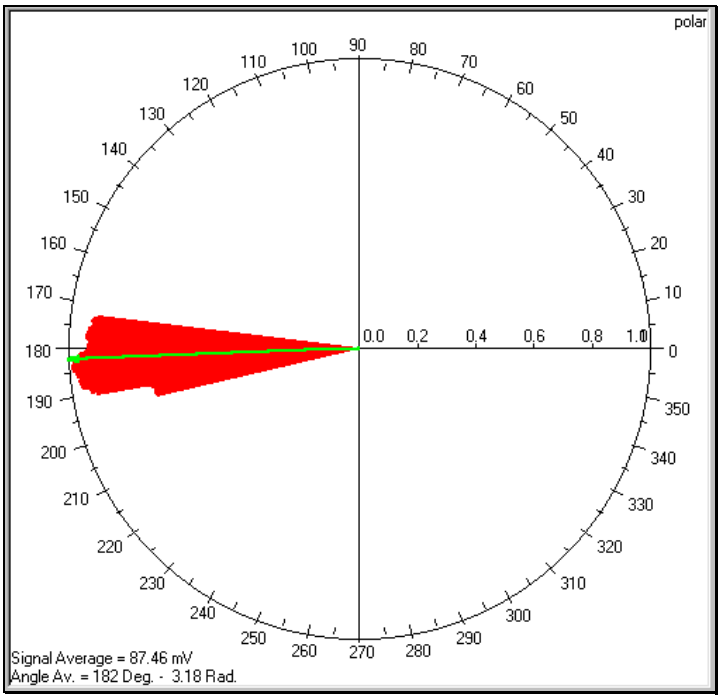

Fig. 4.2.13b.6. Corresponding polar diagram, for **PYR** monitoring site.

<u>Hios (HIO) monitoring site.</u>

Raw data, HIO.

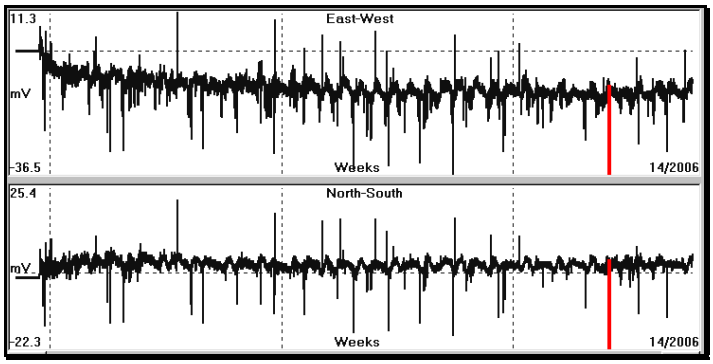

Fig. 4.2.13b.7. Raw data registered, by **HIO** monitoring site.

Filtered data, p = 0.5, HIO.

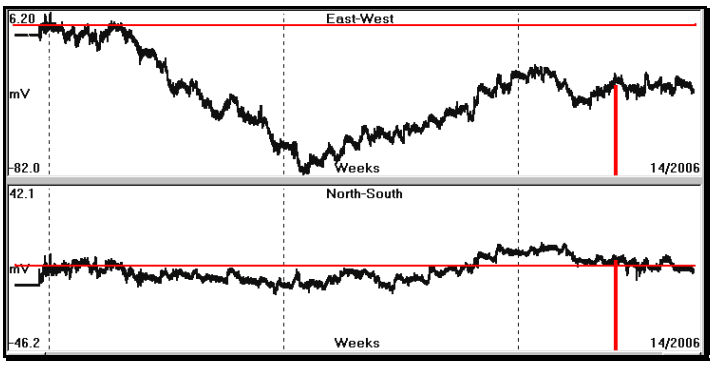

Fig. 4.2.13b.8. Filtered data, calculated, for **HIO** monitoring site. Noise injection parameter **p = .5**

Calculated, electrical field intensity vector polar diagram for HIO.

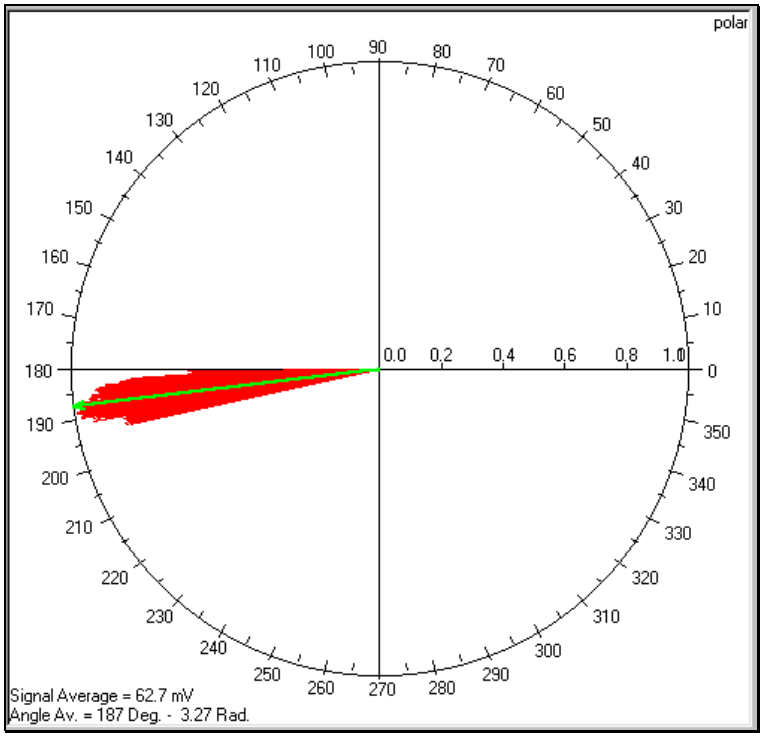

Fig. 4.2.13b.9. Corresponding, polar diagram, for **HIO** monitoring site.

Epicenter location, calculated, for Zakynthos, Greece, 20060404, Ms = 5.7 EQ.

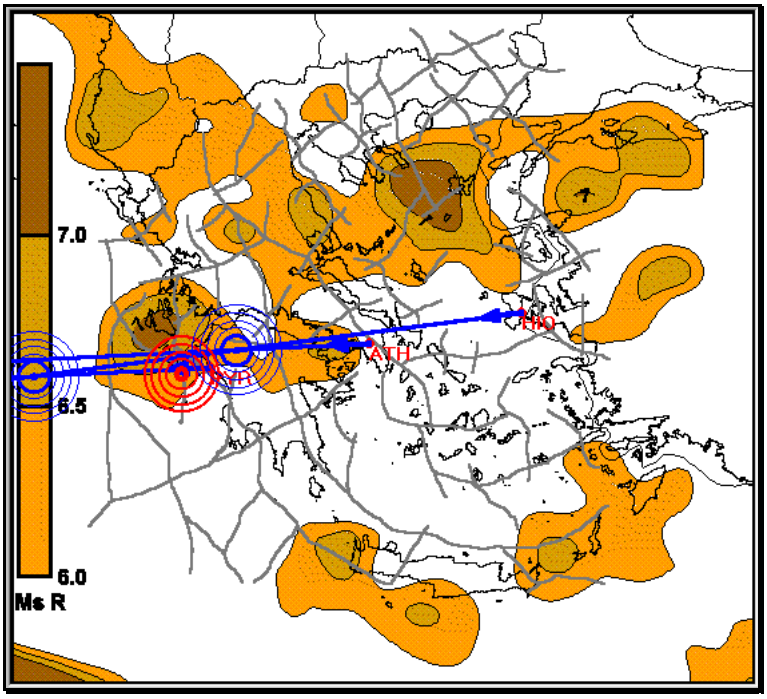

Fig. 4.2.13b.10. Calculated epicenters (blue circles), in relation to the seismological (red circles) one.

The, calculated, electrical field intensity vectors are almost parallel, therefore, the intersections do not coincide. What is interesting, in this case, is the fact that all three monitoring sites “see” the electrical field, arriving from the very same azimuthal direction.

East Kythira, Greece, 20060108, Ms = 6.9 EQ.

Athens (ATH) monitoring site.

Raw data, ATH.

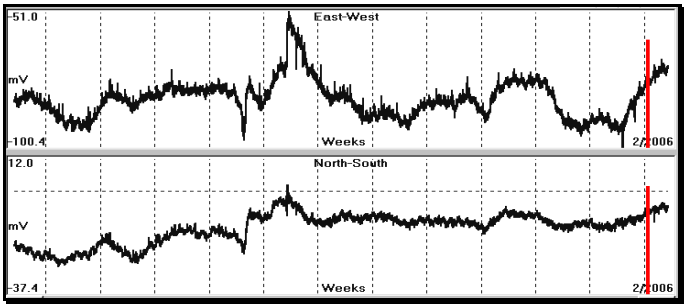

Fig. 4.2.13b.11. Raw data registered, by **ATH** monitoring site.

Filtered data, p =2.5, ATH.

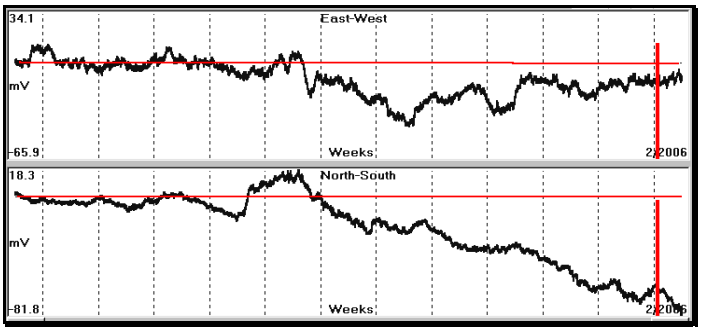

Fig. 4.2.13b.12. Filtered data, calculated, for **ATH** monitoring site. Noise injection parameter **p = 2.5**

Calculated electrical field intensity vector polar diagram for ATH.

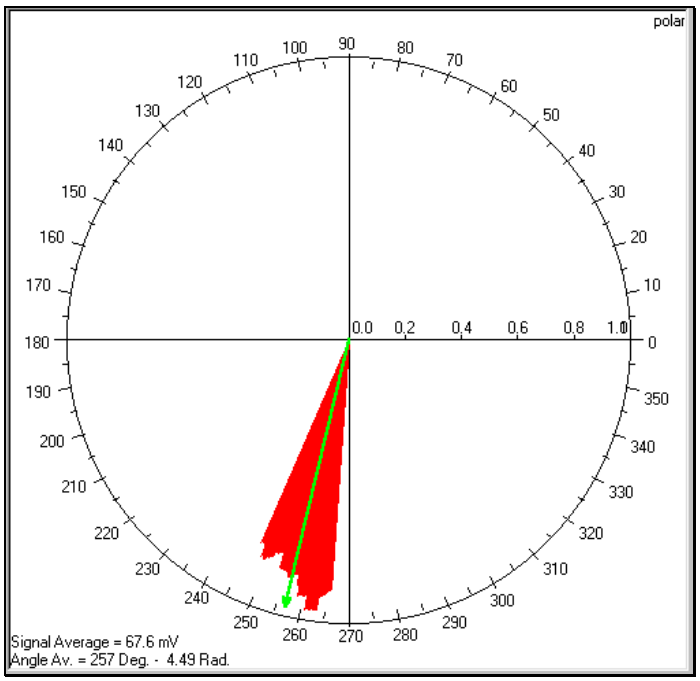

Fig. 4.2.13b.13. Corresponding, polar diagram, for **ATH** monitoring site.

Pyrgos (PYR) monitoring site.

Raw data, PYR.

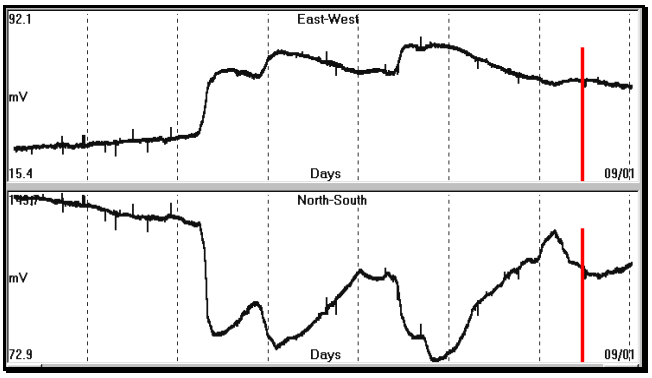

Fig. 4.2.13b.14. Raw data, registered, by **PYR** monitoring site.

Filtered data, p =.0005, PYR.

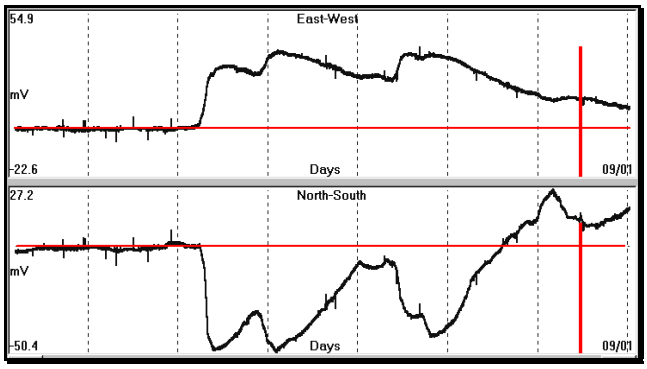

Fig. 4.2.13b.15. Filtered data, calculated, for **PYR** monitoring site. Noise injection parameter **p = .0005**

Calculated electrical field intensity vector polar diagram for PYR.

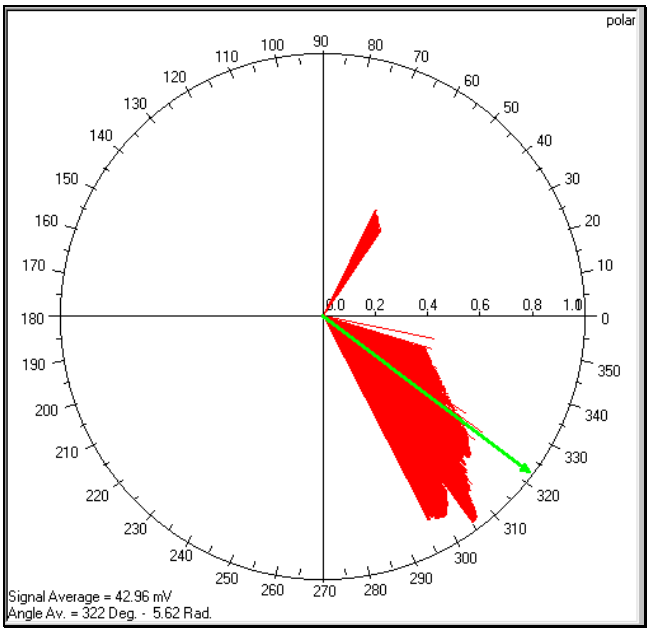

Fig. 4.2.13b.16. Corresponding, polar diagram, for **PYR** monitoring site.

Epicenter location, calculated, for East Kythira, Greece, 20060108, Ms = 6.9 EQ.

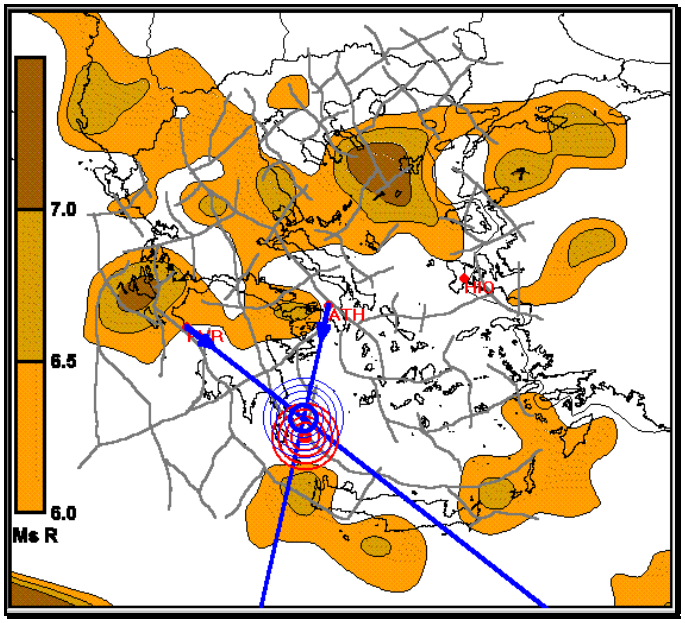

Fig. 4.2.13b.17. Calculated epicenter (blue circles) in relation to the seismological (red circles) one.

West Turkey, 20051017, Ms = 6.0 EQ.

Athens (ATH) monitoring site.

Raw data, ATH.

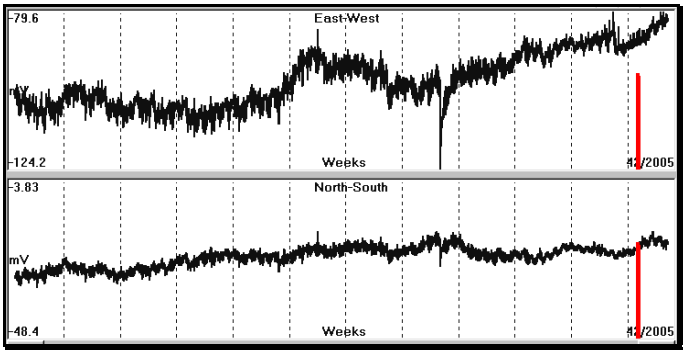

Fig. 4.2.13b.18. Raw data, registered, by **ATH** monitoring site.

Filtered data, p = 40, ATH.

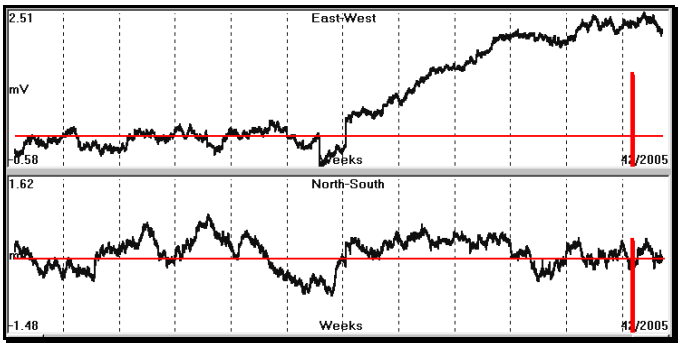

Fig. 4.2.13b.19. Filtered data, calculated, for **ATH** monitoring site. Noise injection parameter **p = 40.**

Calculated, electrical field intensity vector polar diagram for ATH.

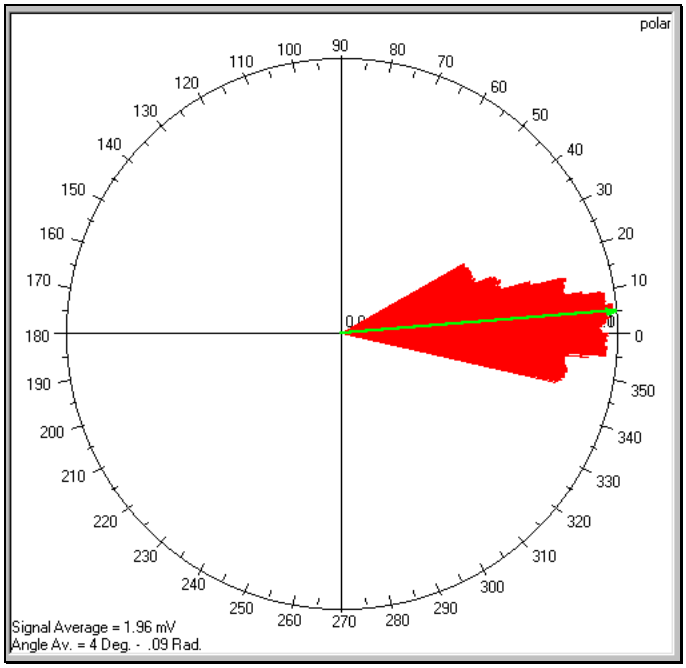

Fig. 4.2.13b.20. Corresponding, polar diagram, for **ATH** monitoring site.

Pyrgos (PYR) monitoring site.

Raw data, PYR.

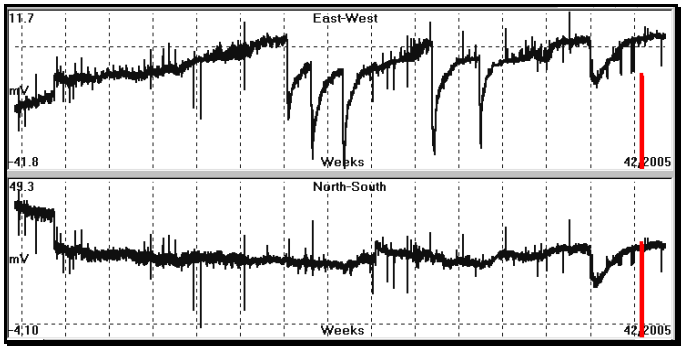

Fig. 4.2.13b.21. Raw data registered, by **PYR** monitoring site.

Filtered data, p = 40, PYR.

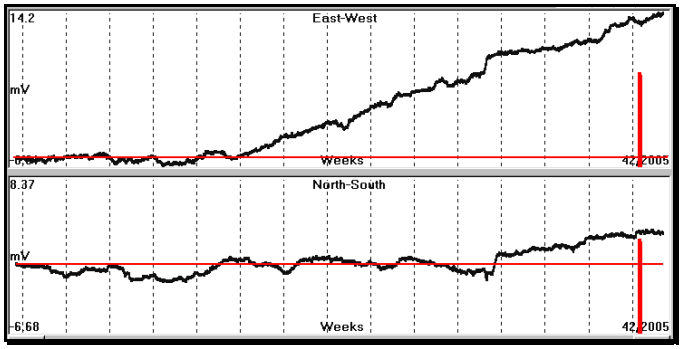

Fig. 4.2.13b.22. Filtered data, calculated, for **PYR** monitoring site. Noise injection parameter **p = 40**.

Calculated, electrical field intensity vector polar diagram for PYR.

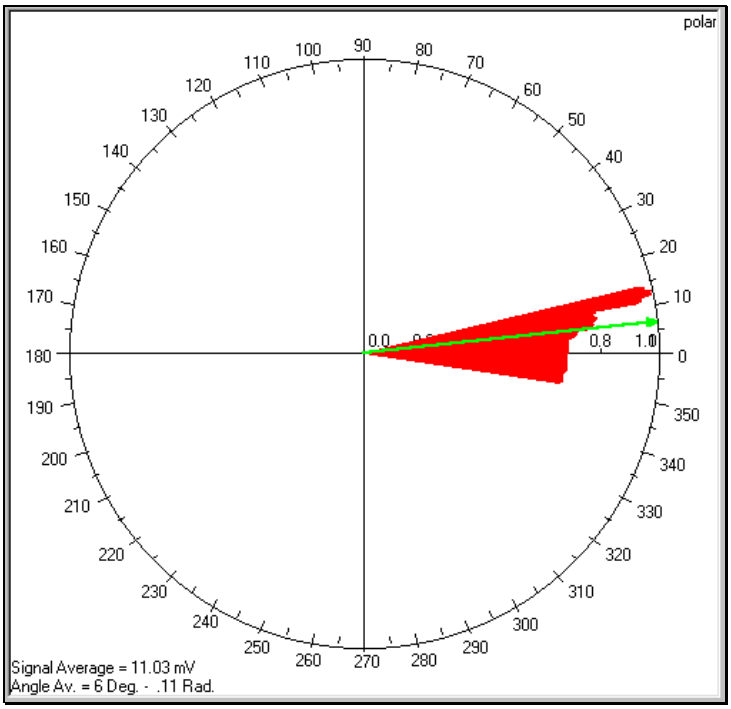

Fig. 4.2.13b.23. Corresponding, polar diagram for **PYR** monitoring site.

Epicenter location calculated for West Turkey, 20051017, Ms = 6.0 EQ.

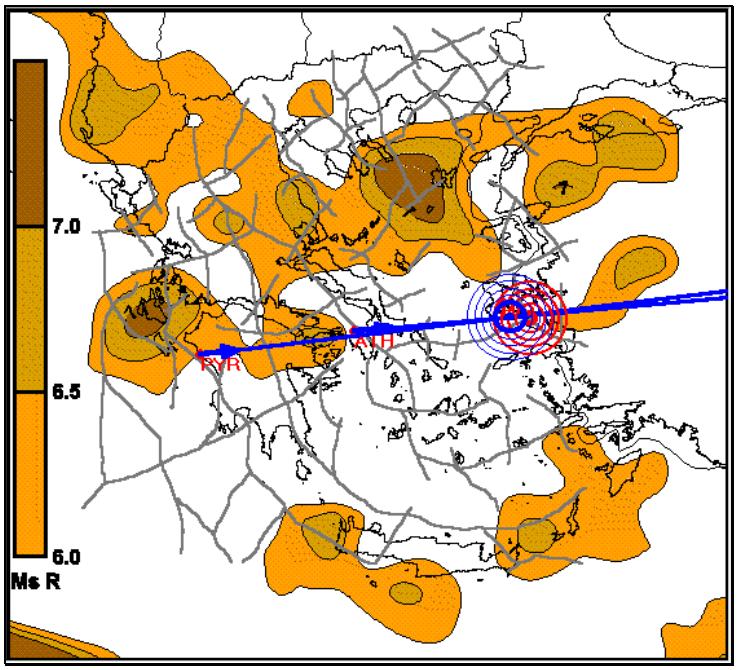

Fig. 4.2.13b.24. Calculated, epicenter (blue circles) in relation to the seismological (red circles) one.

SW Kythira, Greece, 20031017, Ms = 5.8 EQ.

Athens (ATH) monitoring site.

Raw data, ATH.

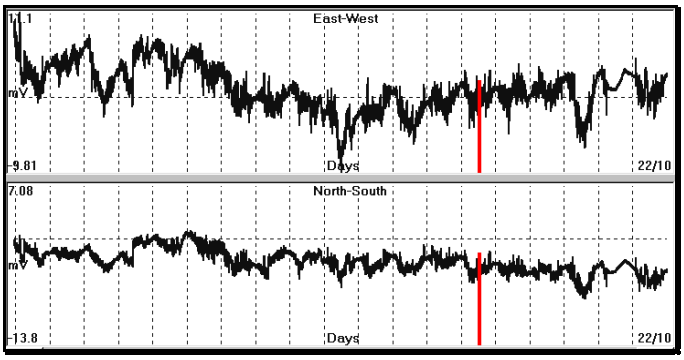

Fig. 4.2.13b.25. Raw data, registered, by **ATH** monitoring site.

Filtered data, p = .0005, ATH.

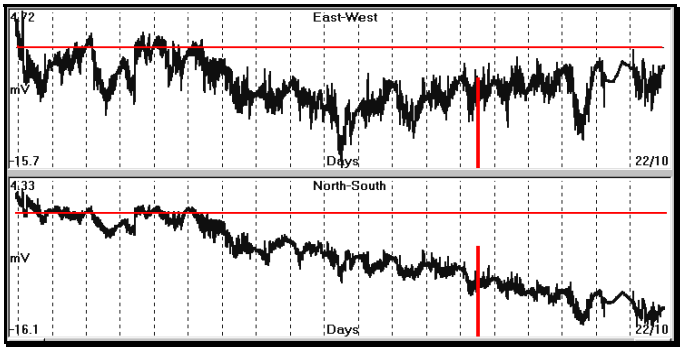

Fig. 4.2.13b.26. Filtered data, calculated, for ATH monitoring site.

Calculated electrical field intensity vector polar diagram for ATH.

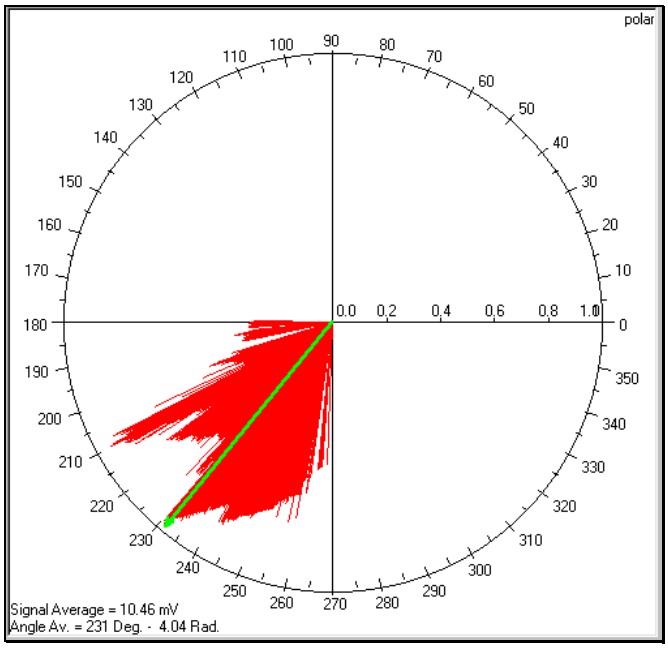

Fig. 4.2.13b.27. Corresponding, polar diagram for **ATH** monitoring site.

Pyrgos (PYR) monitoring site.

Raw data, PYR.

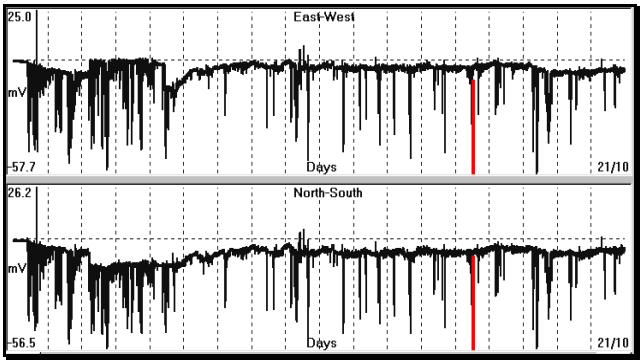

Fig. 4.2.13b.28. Raw data, registered, by **PYR** monitoring site.

Filtered data, p = 0.5, PYR.

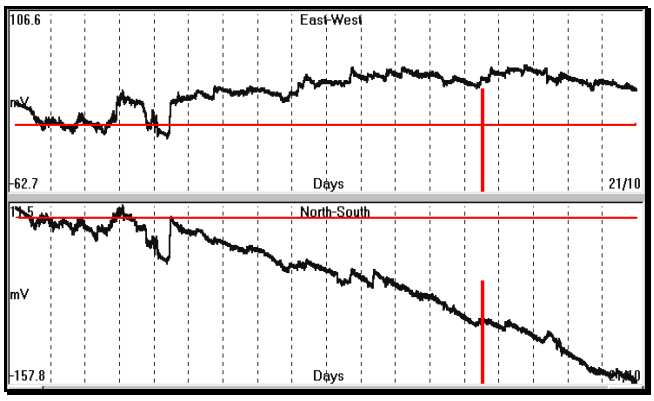

Fig. 4.2.13b.29. Filtered data, calculated, for **PYR** monitoring site. Noise injection parameter **p = 0.5**

Calculated, electrical field intensity vector polar diagram for PYR.

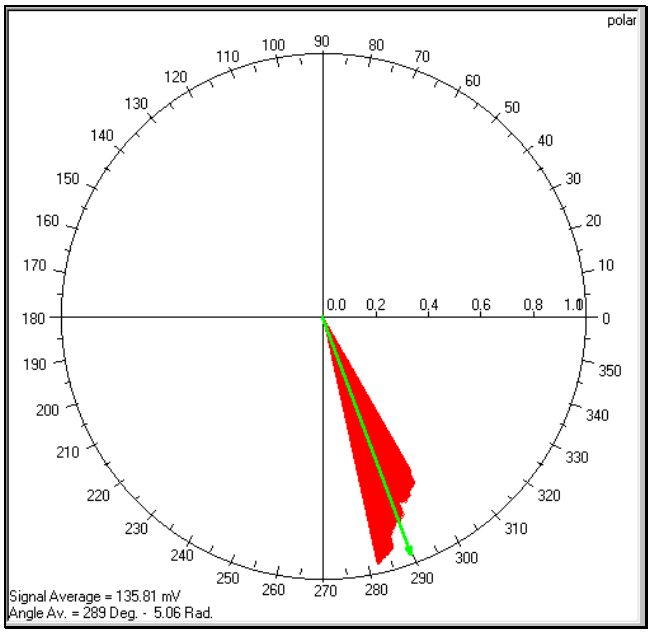

Fig. 4.2.13b.30. Corresponding, polar diagram, for **PYR** monitoring site.

Epicenter location, calculated, for SW Kythira, Greece, 20031017, Ms = 5.8 EQ.

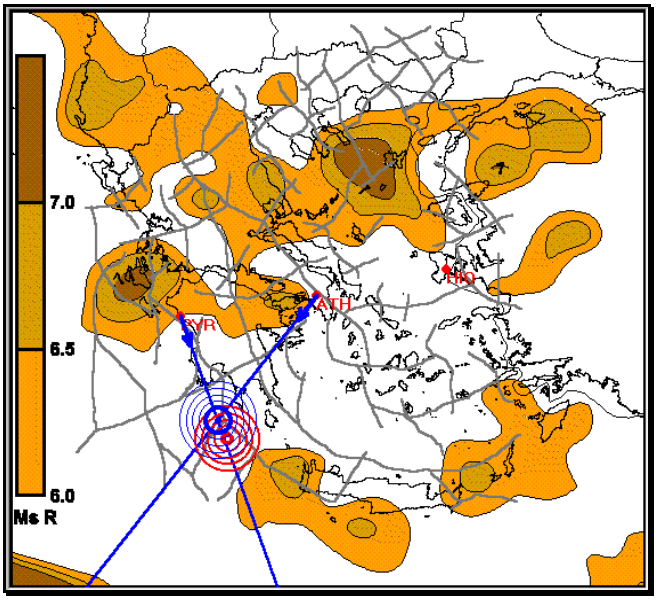

Fig. 4.2.13b.31. Calculated, epicenter (blue circles) in relation to the seismological (red circles) one.

Lefkada, Greece, 20030814, Ms = 6.3 EQ.

Athens (ATH) monitoring site.

Raw data, ATH.

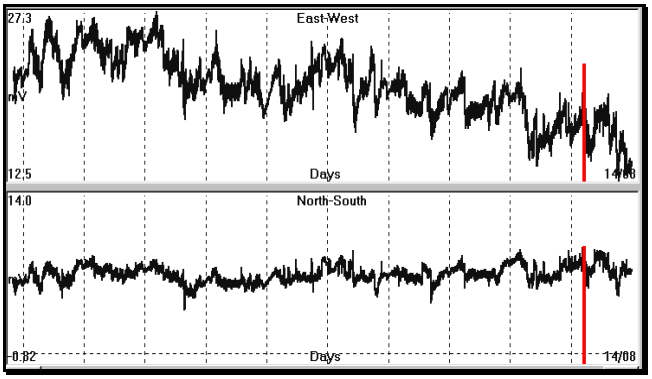

Fig. 4.2.13b.32. Raw data, registered, by **ATH** monitoring site.

Filtered data, p = 0.625, ATH.

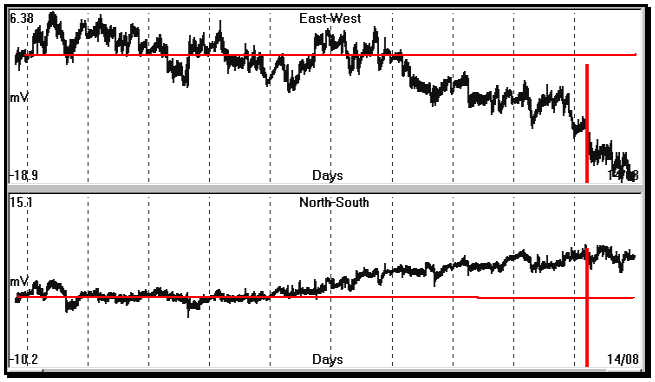

Fig. 4.2.13b.33. Filtered data, calculated, for **ATH** monitoring site. Noise injection parameter **p = 0.625**.

Calculated, electrical field intensity vector polar diagram for ATH.

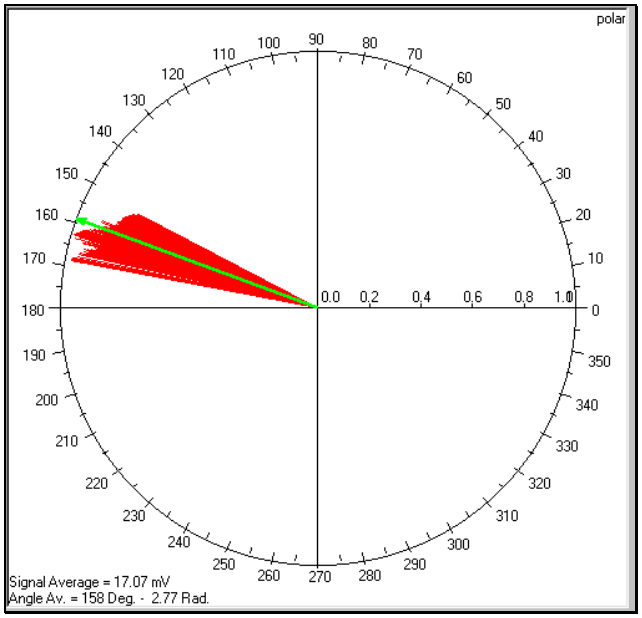

Fig. 4.2.13b.34. Corresponding, polar diagram, for **ATH** monitoring site.

Pyrgos (PYR) monitoring site.

Raw data, PYR.

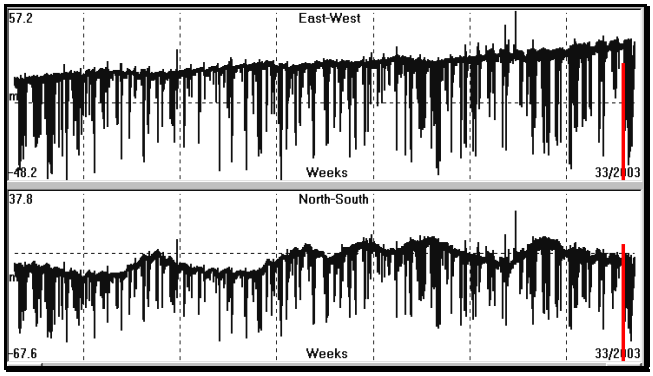

Fig. 4.2.13b.35. Raw data, registered, by **PYR** monitoring site.

Filtered data, p = 0.625, PYR.

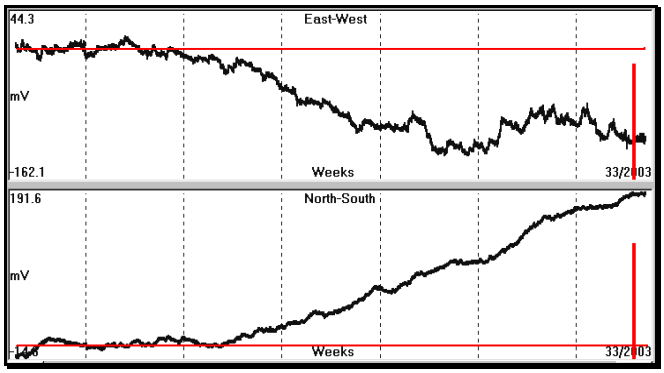

Fig. 4.2.13b.36. Filtered data, calculated, for **PYR** monitoring site. Noise injection parameter **p = 0.625.**

Electrical field intensity vector polar diagram calculated for PYR.

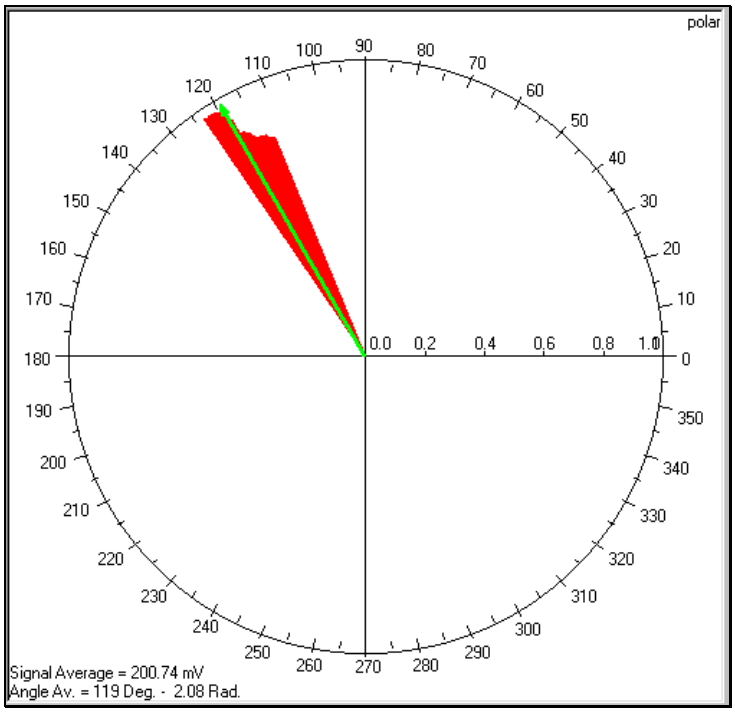

Fig. 4.2.13b.37. Corresponding, polar diagram, for **PYR** monitoring site.

Epicenter location, calculated, for Lefkada, Greece, 20030814, Ms = 6.3 EQ.

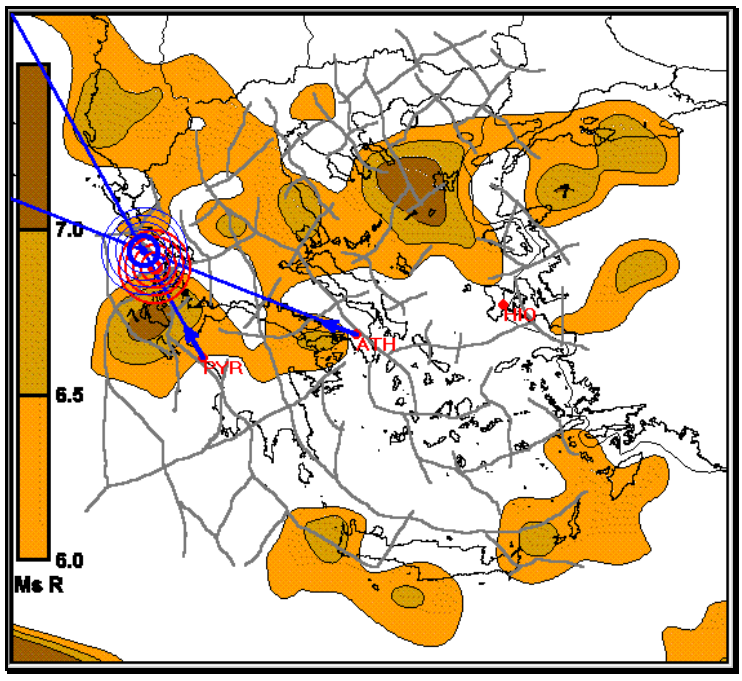

Fig. 4.2.13b.38. Epicenter (blue circles) calculated, in relation to the seismological (red circles) one.

Saros Bay, Turkey, 20030706, Ms = 5.9 EQ.

Athens (ATH) monitoring site.

Raw data, ATH.

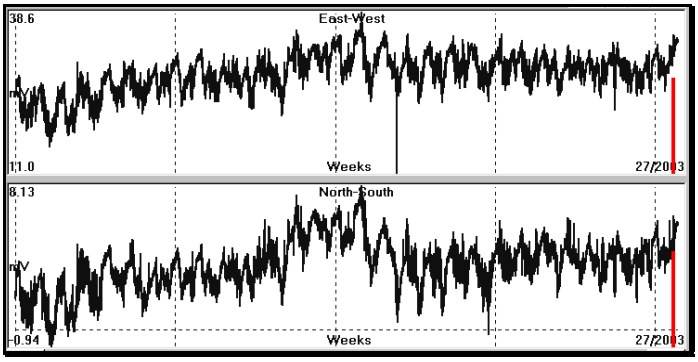

Fig. 4.2.13b.39. Raw data registered, by **ATH** monitoring site.

Filtered data, 10th order polynomial fitting, ATH.

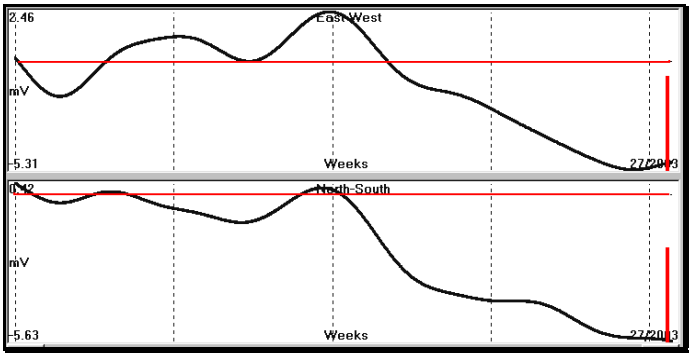

Fig. 4.2.13b.40. Filtered data, calculated, for **ATH** monitoring site. **10th order** polynomial fit.

Electrical field intensity vector polar diagram calculated for ATH.

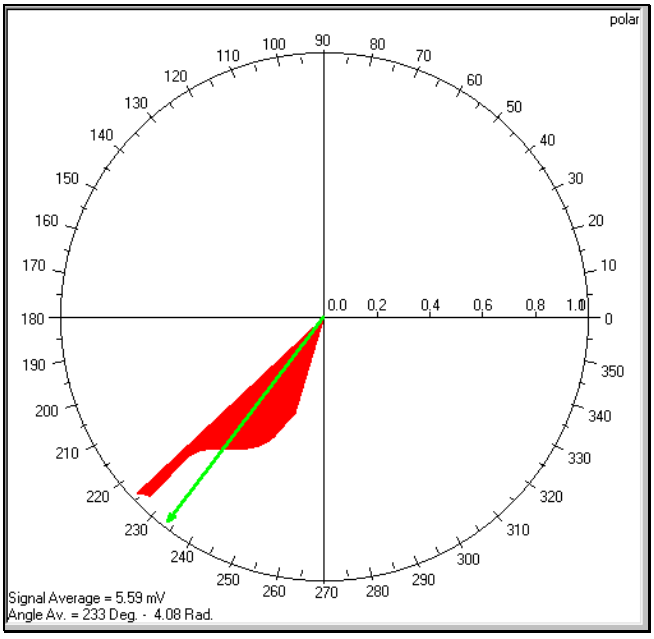

Fig. 4.2.13b.41. Corresponding, polar diagram, for **ATH** monitoring site.

Pyrgos (PYR) monitoring site.

Raw data, PYR.

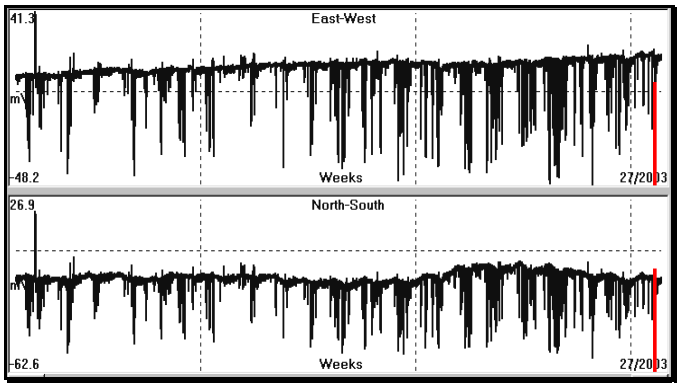

Fig. 4.2.13b.42. Raw data registered, by **PYR** monitoring site.

Filtered data, 10th order polynomial fitting, PYR.

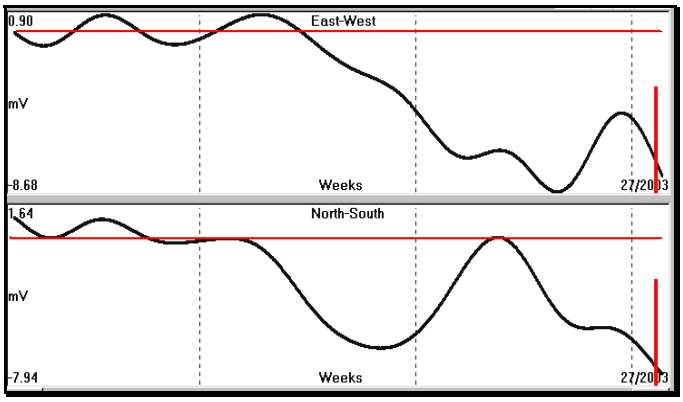

Fig. 4.2.13b.43. Filtered data calculated, for **PYR** monitoring site. **10th order** polynomial fit.

Electrical field intensity vector polar diagram calculated for PYR.

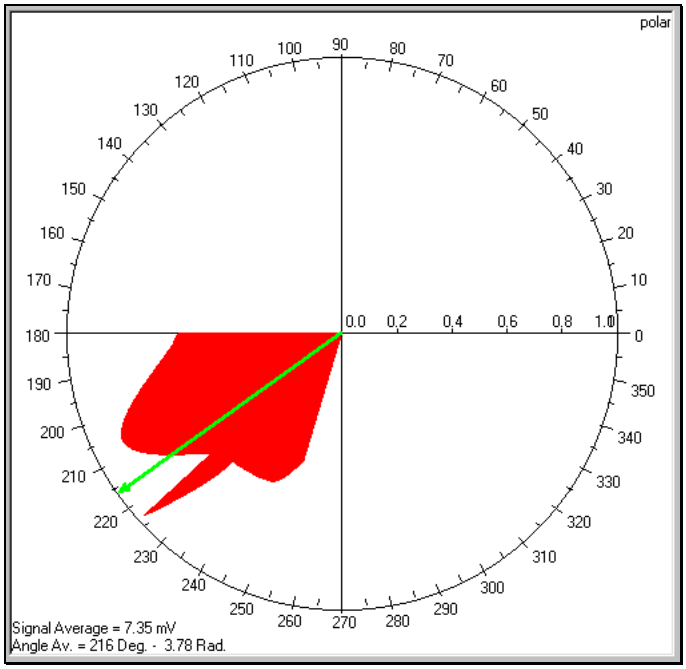

Fig. 4.2.13b.44. Corresponding, polar diagram, for **PYR** monitoring site.

Epicenter location, calculated, for Saros Bay, Turkey, 20030706, Ms = 5.9 EQ.

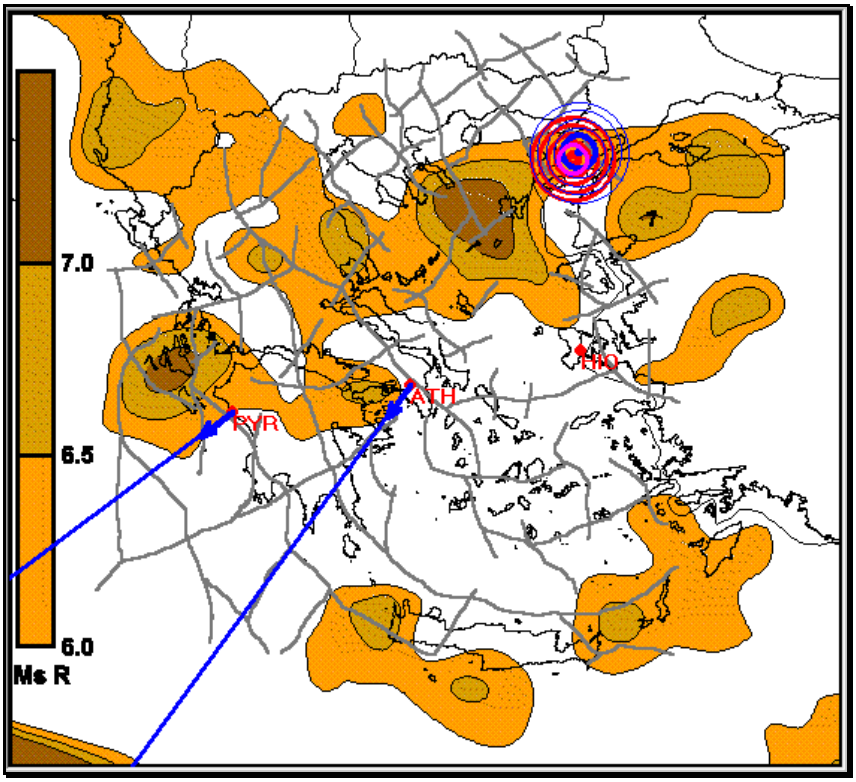

Fig. 4.2.13b.45. Calculated, epicenters (blue circles) in relation to the seismological (red circles) one.

4.2.14. Some more concluding details on epicenter determination.

It had been stated earlier that, the azimuthal direction **(θ)** of the Earth's electric field intensity vector, at a specific time **(t),** is given by the equation:

$$(\theta) = \arctan(V_{NS}/V_{EW}) \qquad (4.2.14.1)$$

where **(V_{NS})** and **(V_{EW})** are the **NS** and **EW** normalized components of the Earth's electric field at time **(t)**.

Spurious potentials, of any origin, interfere with the Earth's electric field, within any given time period. Thus, the angle **(θ),** which is calculated by the equation **(4.2.14.1)**, in the case of a preseismic, electric signal that fluctuates, due to the presence of other preseismic, tectonic, processes which are present in the focal area, will fluctuate, too. This is demonstrated in the following figure **(4.2.14.1)**. The fluctuating azimuths are bounded in an angle (dashed lines), which represents all the azimuths of the discretely, activated, tectonic regions of a regional, seismic area that generates discrete, electrical signals. The calculated **average value of all azimuths** along the entire preseismic signal indicates **the azimuth direction of a single hypothetical epicentral area** that accounts for all the different tectonic regions which are activated in the vicinity of the EQ epicenter.

The latter resembles the notion of "apparent point current source", introduced earlier in the mathematical analysis for the determination of the epicenter.

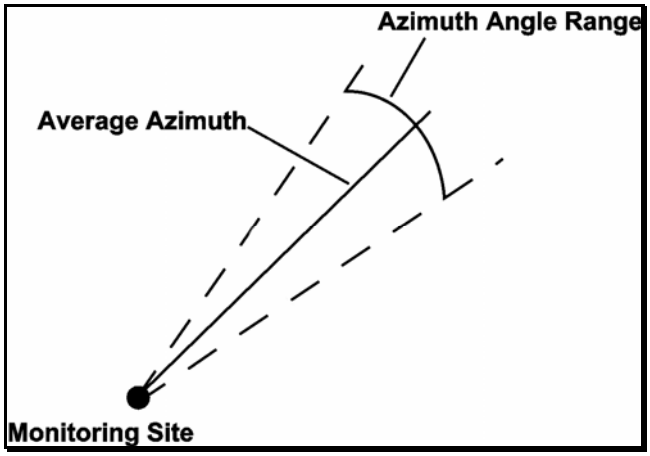

Fig. 4.2.14.1. The calculated azimuth angle range of solutions and average value of azimuths, which correspond to a monitoring site are presented.

The calculated azimuths are affected, too, by the choice of the corresponding reference level. Actually, the issue of ”normal field” and “anomalous field” characterization, depends upon the wavelengths which are used for the corresponding analysis and is similar to the regional - residual separation of any geophysical field, treated, in any, applied geophysical method.

In any case, if we stick to observed azimuth angle ranges from different monitoring sites, the following figure **(4.2.14.2),** shows a direct application of the basic idea of “azimuth angle range”.

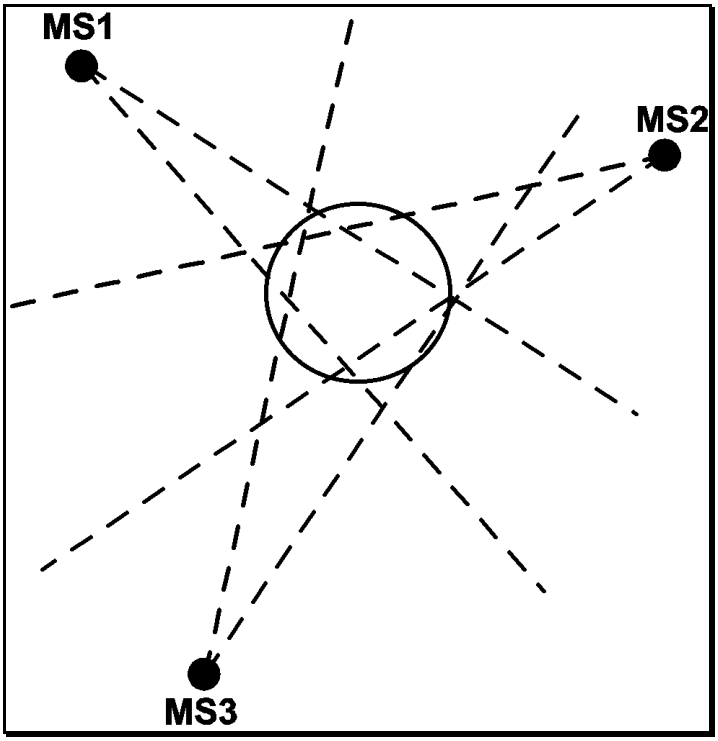

Fig. 4.2.14.2. Intersection of “azimuth angle ranges”, calculated at **MA1, 2, 3** monitoring sites. The solid circle represents the regional, epicentral area.

It is evident that, locations which satisfy the condition of being in the azimuth range of all three monitoring sites (polygon in the solid circle), are the most probable epicenter locations for the pending earthquake **(fig. 4.2.14.3).**

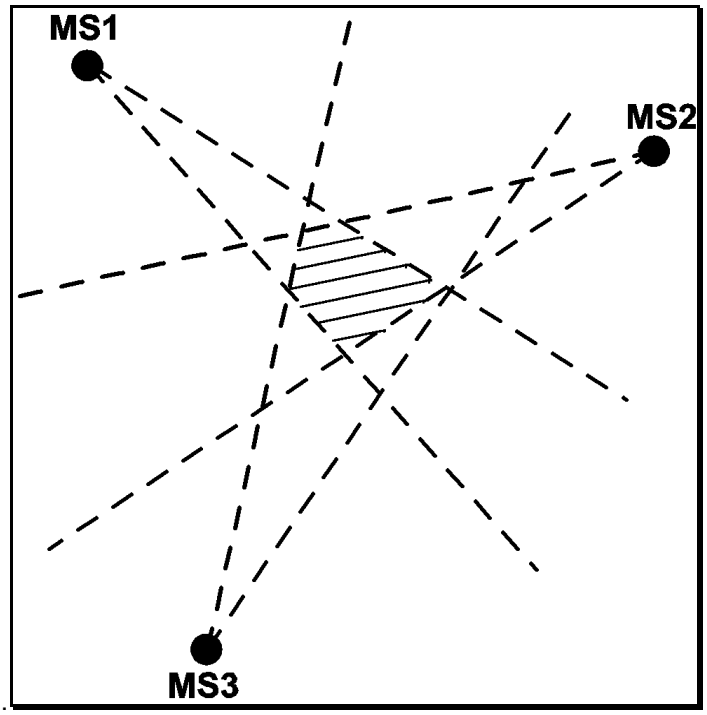

Fig. 4.2.14.3. Probable epicenter locations are represented by the shaded, polygon area (common area of azimuth angle range of all three monitoring sites).

Finally, in terms of average azimuth values and azimuth angle range intersections, the candidate, epicentral area is represented in the following figure **(4.2.14.4)**.

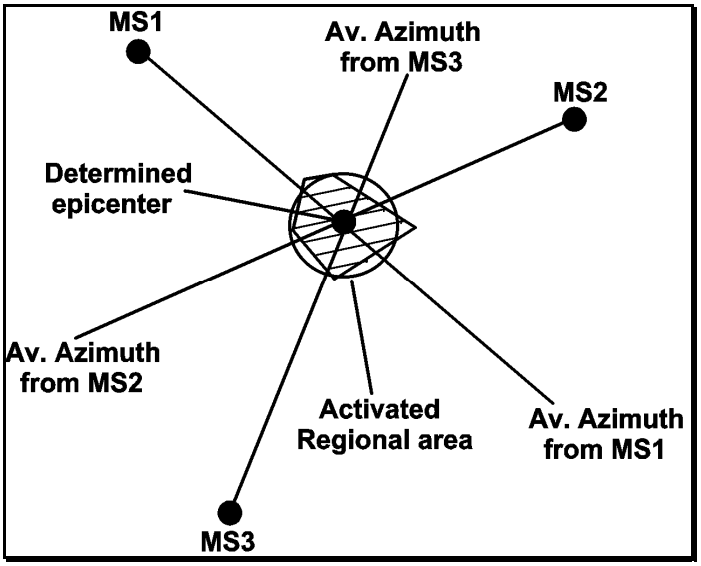

Fig. 4.2.14.4. Calculated epicentral area (solid black circle in the polygon) is presented in relation to the corresponding, regionally, identified (shaded polygon and circle) one by the monitoring sites **MS1, 2, 3**.

The fracturing of the lithosphere and the generation of an earthquake is a dynamic procedure, involving, stress load increase, strain accumulation, lithospheric oscillation and the presence of a weak fracture zone, as well. All these parameters modify, in time, the dynamic conditions, met, along the fracture zone which will be activated seismically. Therefore, these dynamic conditions

affect differently each part of the fault length and the corresponding, preseismic, electric signal generation.

Consequently, what is proposed as an explanation for the fluctuation of the preseismic, electric signals and the corresponding azimuth directions is the following:

Discrete electrical signal, generating mechanisms are triggered in different places in the preseismic period of time along the activated fault. These preseismic signals generate the observed “azimuth angle range”, which could be of some value **to pre-estimate the length of final fracturing of the seismic event to come**. As an overall phenomenon, this corresponds to a single “apparent point current source” and a single, theoretical, epicentral area which is indicated by the intersection of the average azimuth values, observed, at the monitoring sites.

What is concluded from this presentation is the fact that, it is of great importance for the achievement of a successful earthquake prediction, to install and use a wide, regional network, dense enough, for the monitoring of the Earth’s electric field of a seismogenic country.

In conclusion, it has been shown that: the determination of the epicenter area of a strong, pending EQ, is possible (in the case of generation of electrical, preseismic signals), through the use of Physical Laws, concerning the behavior of electrical fields. This is possible if are fulfilled the following prerequisites:

a. Long wavelength electrical signals are taken into account, so that the Earth, as a consequence, will behave as “homogeneous ground”.

b. The postulated “apparent point current source” is applied in the focal area and is used for all subsequent, mathematical analysis.